GEOTECHNICAL IMPACTS OF HURRICANE MARIA IN PUERTO RICO

Event Date: September 20, 2017

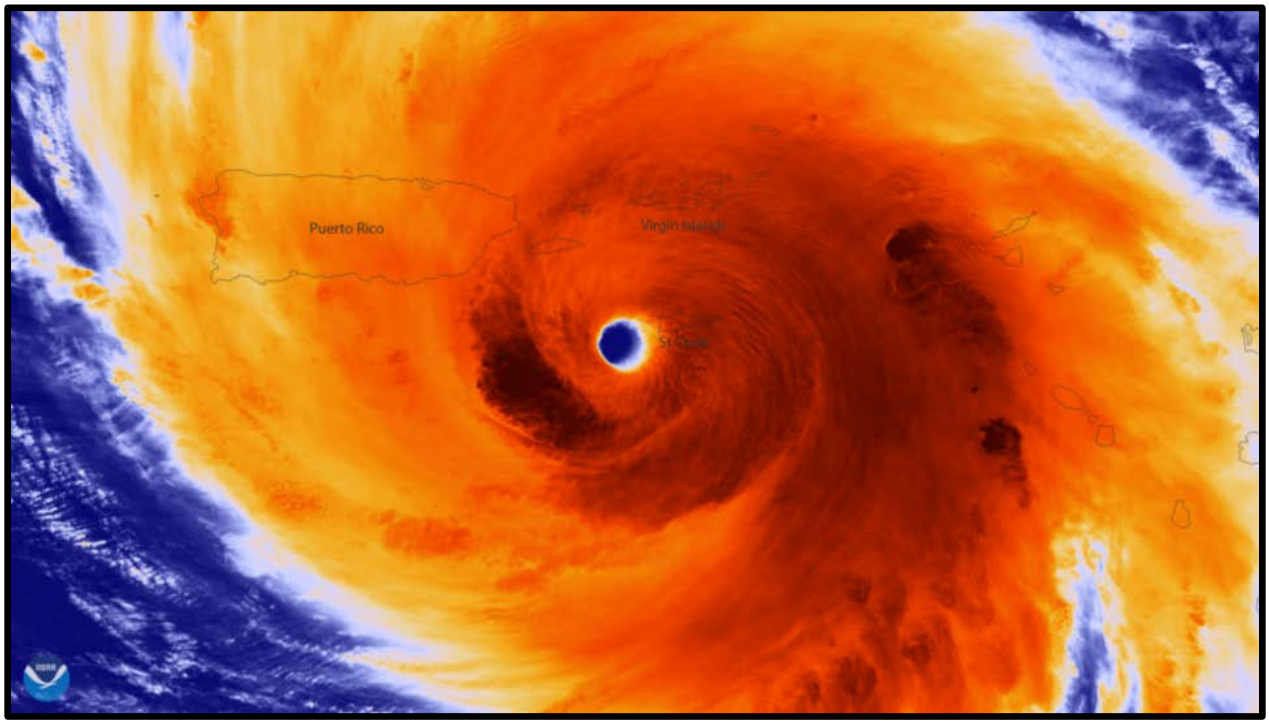

by: Francisco Silva-Tulla (Leader), Miguel A. Pando (Co-Leader), Alejandro E. Soto, Alesandra Morales, Daniel Pradel, Gokhan Inci, Inthuorn Sasanakul, Juan R. Bernal, Robert Kayen, Stephen Hughes, Tiffany Adams, and Youngjin Park

Geotechnical Extreme Events Reconnaissance
Turning Disaster into Knowledge
Sponsored by the National Science Foundation

GEER Association Report No. GEER-057 June 29, 2018

Contents

Acknowledgements ..... **x**

List of Acronyms and Abbreviations ..... **xi**

Summary ..... **xiii**

1 INTRODUCTION **1**

1.1 Hurricane events of September 2017 2

1.2 GEER-PR Team 5

1.3 Topography, Geology, and Climate of Puerto Rico 10

1.3.1 Topography 10

1.3.2 Geology 11

1.3.3 Climate 14

2 LANDSLIDES AND DEBRIS FLOWS **17**

2.1 Introduction and Complementary efforts 17

2.2 Background 18

2.3 Summary of Sites and Main Mechanisms of Failure 23

2.4 Select Landslide Cases 23

2.4.1 Debris Flow on PR-4131, Lares 24

2.4.2 Assessment of preexisting landslide at PR-9 north of City of Ponce 28

3 DAMS **31**

3.1 Introduction 31

3.2 Guajataca Dam 32

3.2.1 History 32

3.2.2 Seepage and Internal Erosion 35

3.2.3 Spillway damage 36

3.2.4 Dam and Other Structures 36

4 COASTAL AND RIVER EROSION AND SCOUR **48**

4.1 Coastal Erosion at Rincón, Puerto Rico 48

4.1.1 Introduction and Background 48

4.2 Coastal Erosion Sites visited by the GEER team 53

4.2.1 Coastal Erosion Site CE1: Punta Cadena 54

4.2.2 Coastal Erosion Site CE2: Calle Bastia Road 56

4.2.3 Coastal Erosion Site CE3: Rincón Ocean Club 59
4.2.4 Coastal Erosion Site CE4: Crash Boat Beach, Aguadilla, PR 67
4.2.5 Coastal Erosion Site CE5: Town center waterfront, Aguadilla 68
4.2.6 Coastal Erosion Site CE6: Playa El Maní, Mayagüez, Puerto Rico 69
4.2.7 Coastal Erosion Site CE7: Playas del Yunque, Rio Grande, PR 72
4.3 River Erosion Sites visited by the GEER team 74
4.3.1 River Erosion Site RE1: Erosion at Highway 52 bridges over the Inabón River 74
4.3.2 River Erosion Site RE2: PR-177 in near Costco of Bayamón, PR 77
4.3.3 River Erosion Site RE3: River bank erosion near Guaynabo, PR 80
5 ROAD AND BRIDGE FAILURES 83
5.1 Introduction 83
5.2 Road failures associated with partial to total culvert blockage 86
5.2.1 Road & Bridge Site 1 86
5.2.2 Road & Bridge Site 2 87
5.3 Road failure sites with downslope slope failures 89
5.3.1 Road & Bridge Site 3 89
5.3.2 Road & Bridge Site 4 90
5.4 Road failure sites with slope failures on the upslope side (road blockage) 92
5.4.1 Road & Bridge Site 5 92
5.4.2 Road & Bridge Site 6 93
5.5 Road failure sites with complete cut-off 95
5.5.1 Road & Bridge Site 7 - Road damage with complete cut-off 95
5.5.2 Road & Bridge Site 8 - complete cut-off of PR-431 96
5.6 Bridge failures 98
5.6.1 Road & Bridge Site 9 – Washed away bridge failure 98
5.6.2 Road & Bridge Site 10 100
6 FOUNDATION FAILURES 102
6.1 Introduction 102
6.2 Cantilevered traffic sign foundation failures 103
6.2.1 Cantilevered Sign Site F1 103
6.2.2 Cantilevered sign Site F2 106
6.2.3 Cantilevered sign Site F3 108
6.3 Foundation failure of a light tower at baseball stadium in Ponce, Site F4 111
7 OTHER IMPACTS 113

REFERENCES..... 117

Appendix A Supplementary Information, Section 2 – Landslides and Debris Flows A-1
Appendix B Supplementary Information, Section 3 – Dams.....B-1
Appendix C Supplementary Information, Section 4 – Coastal Erosion..... C-1
Appendix D Supplementary Information, Section 5 – Roads and Bridges.....D-1
Appendix E Supplementary Information, Section 6 – Foundations..... E-1
Appendix F Supplementary Information, Section 7 – Other Impacts..... F-1
Appendix G LiDAR Data G-1
Appendix H NOAA Graphics and Data.....H-1
Appendix I Index Test Results from UPRM Laboratory I-1
Appendix J GEER – PR Team Resumes.....J-1

List of Tables

Table 1-1: Summarizes the GEER team composition..... 7
Table 4-1: High Water Mark Data, Rincón, PR. 52
Table 4-2: Water elevation measurements during Hurricane Maria..... 52
Table 6-1: Coordinates of foundation failure sites visited by 2017 GEER Team..... 103

List of Figures

Figure 1-1: Path of historical hurricanes that have impacted Puerto Rico (USGS, 2018) (https://www.usgs.gov/media/images/puerto-rico-hurricanes-map). 1
Figure 1-2: Path of Hurricanes Irma and Maria with respect to Puerto Rico (Feng et al., 2018). 2
Figure 1-3: Path of Maria from 9/16/2017 to 10/02/2017 (Landfall in PR September 20, 2017) (NOAA Report AL152017, 2018). 3
Figure 1-4: Wind speed of Maria at Landfall in Puerto Rico (data from NOAA Report AL152017, 2018). 4
Figure 1-5: Daily reconnaissance tracks of GEER mission and location of LiDAR scans..... 9
Figure 1-6: Map of Puerto Rico showing mountainous topography in the central region. 10
Figure 1-7: Slope map showing computed average slope inclinations from 5 m resolution DEM. 11
Figure 1-8: General Seismic Settings and Major Faults of Puerto Rico (Clinton et al. 2006). 12
Figure 1-9: Geology of Puerto Rico adapted from Bawiec (1999). 13

Figure 1-10: Mean Annual Rain Distribution in inches for Puerto Rico (Data 1981-2010). 15
Figure 1-11: Seasonal Distribution of Hurricanes for Puerto Rico (Period 1508 to 1997) (from Boose et al. 2004). 16
Figure 2-1: USGS map showing concentration of landslides attributed to Hurricane Maria (Bessette-Kirton et al., 2017; https://doi.org/10.5066/F7JD4VRF). 17
Figure 2-2: More than 40,000 debris flow sites (shown as red dots) have been identified across Puerto Rico by Hughes and Morales Vélez (2018). 18
Figure 2-3: Map of Puerto Rico showing municipalities most impacted by landslides associated to Hurricane Maria. 18
Figure 2-4: Landslide susceptibility map (adapted from Lepore et al. 2012). 19
Figure 2-5: Location of inventoried rainfall-induced landslides between 1959 and 2003 (Pando et al., 2005). 19
Figure 2-6: Worldwide rainfall-induced landslide threshold by Caine (1980). 20
Figure 2-7: Puerto Rico rainfall-induced landslide threshold by Pando et al. (2005) and estimated rainfall event by Hurricane Maria. 21
Figure 2-8: Rainfall estimates in Puerto Rico during Hurricane Maria (https://www.weather.gov/sju/maria2017; accessed March 2017). 22
Figure 2-9: Variation of slope stability factor of safety during a rainfall event (from Lan et al., 2003). 23
Figure 2-10: Photo taken by the Civil Air Patrol on October 15, 2017 of the PR-4131 debris flow site. 24
Figure 2-11: Large debris flow site on PR-4131 in central Lares along the Rio Blanco. 25
Figure 2-12: Photo taken by GEER team in January 2018 of the PR-4131 debris flow site. 26
Figure 2-13: Photo showing January 2018 TLS survey position. 26
Figure 2-14: Images from LiDAR PR-4131 debris flow site. 27
Figure 2-15: Aerial image showing pre-Maria condition of preexisting landslide at PR-9 north of Ponce 28
Figure 2-16: Post-Maria condition of preexisting landslide site at PR-9 north of Ponce. 29
Figure 2-17: January 2018 TLS survey position at PR-9 landslide site. 29
Figure 2-18: Photo of Toe of PR-9 landslide in January 2018. 30
Figure 3-1: Debris along the upstream face of the gravity dam at Lago Dos Bocas. Compare the dark brown color of the water in the reservoir to the historical blue color (before Maria). 31
Figure 3-2: Photo of Guajataca Dam taken a few decades before Hurricane Maria (date of photo is unknown). 32
Figure 3-3: Cross-section of Guajataca Dam from the 1920's (date of drawing is unknown). 33
Figure 3-4: Landslide and outlet map from 1983. 37

Figure 3-5: Cross-section of Guajataca Dam including 1980's remedial recommendations (date of drawing is unknown). 38
Figure 3-6: Instrumentation of Guajataca Dam (piezometers and slope inclinometers). 39
Figure 3-7: Oblique aerial photo with indication of historical and landslide features. 40
Figure 3-8: Comparison of condition between March and November 2017. 41
Figure 3-9: Sand boils downstream of the dam toe (photographs from the Pennsylvania National Guard). 42
Figure 3-10: Water and debris in piezometer. 43
Figure 3-11: Location of 54-inch water line and siphon structure under the spillway. 43
Figure 3-12: Siphon structure under the spillway 44
Figure 3-13: Damaged spillway. 44
Figure 3-14: Spillway aeration pipes. 45
Figure 3-15: Displaced and damaged spillway. 45
Figure 3-16: Scarp adjacent to the spillway. 46
Figure 3-17: Dam crest. 47
Figure 4-1: General location of town of Rincon. 48
Figure 4-2: Rincon Shoreline Study Area by Thieler et al. (2007). 50
Figure 4-3: USGS Flood Event Viewer for Hurricane Maria. 51
Figure 4-4: Storm Tide Sensor Near San Juan, PR (Lat: +18.4530, Lon: -66.0437). 53
Figure 4-5: Location of coastal erosion sites visited by GEER team 53
Figure 4-6: Erosion Scar at first location of Site CE1. 54
Figure 4-7: Seawall at first location of Site CE1. 55
Figure 4-8: Sinkhole and Road collapse at second location of Site CE1 55
Figure 4-9: Pre-storm aerial image of Site CE2. 56
Figure 4-10: Photos of Residential apartment complex "Pelican Reef" (Building A) at Site CE2. 57
Figure 4-11: Photos of Building B at Site CE2. 58
Figure 4-12: Pre-storm aerial image of Site CE3. 59
Figure 4-13: Pre-storm condition of Rincón Ocean Club I and II (Site CE3). 60
Figure 4-14: Oceanfront damage in Corcega beach area (Site CE3). 61
Figure 4-15: Post-storm condition of Rincón Ocean Club I (Site CE3). 62
Figure 4-16: Post-storm condition of Rincón Ocean Club II (Site CE3). 64
Figure 4-17: Post-storm condition of Building A (Site CE3). 65
Figure 4-18: Pre- and Post-storm damage at the Victoria Del Mar Condominium (Site CE3). 66
Figure 4-19: Coastal erosion at Site CE4 - Crash Boat Beach. 67

Figure 4-20: Coastal erosion Site CE5 – Collapse of sidewalk along coastal avenue in Aguadilla Town Center. 68
Figure 4-21: Coastal erosion at Site CE6 - beachfront house at Playa El Maní, Mayagüez, PR. 69
Figure 4-22: Coastal erosion at Site CE6 - beachfront house at Playa El Maní, Mayagüez, PR. 70
Figure 4-23: Coastal erosion at Site CE6 - Playa El Maní, Mayagüez, PR. 70
Figure 4-24: Coastal erosion at Site CE6 - Playa El Maní, Mayagüez, PR. 71
Figure 4-25: Coastal erosion at Site CE6 - Playa El Maní, Mayagüez, PR. 71
Figure 4-26: Coastal erosion at Site CE7 - Playas del Yunque, Rio Grande, PR. 72
Figure 4-27: Coastal erosion site CE7: Playas del Yunque, Rio Grande, PR. 72
Figure 4-28: Coastal erosion site CE7: Playas del Yunque, Rio Grande, PR. 73
Figure 4-29: Coastal erosion site CE7: Playas del Yunque, Rio Grande, PR. 73
Figure 4-30: Location of river erosion sites documented by the GEER team. 74
Figure 4-31: West abutment of westbound Highway 52 bridge over the Inabón River (October 31, 2017). 75
Figure 4-32: West abutment of westbound Highway 52 bridge over Inabón river (October 31, 2017). Photo shows erosion along this abutment and ongoing emergency repair work. 75
Figure 4-33: Erosion damage at west abutment of westbound Highway 52 bridge over the Inabón River (October 31, 2017). 76
Figure 4-34: Erosion along pier foundation of westbound Highway 52 bridge over the Inabón River (October 31, 2017). 76
Figure 4-35: Erosion along pier foundation of bridges of Highway PR-177 in Bayamón, PR (Photo by Geo-Cim). 77
Figure 4-36: Erosion along pier foundation of bridges of Highway PR-177 in Bayamón, PR (Photo by Geo-Cim). 78
Figure 4-37: Erosion along pier foundation of bridges of Highway PR-177 in Bayamón, PR (Photo by Geo-Cim). 78
Figure 4-38: Erosion along pier foundation of bridges of Highway PR-177 in Bayamón, PR (Photo by Geo-Cim). 79
Figure 4-39: River bank erosion failure of Guaynabo River at Site RE3 (Photo by Geo-Cim). 80
Figure 4-40: River bank erosion failure of Guaynabo River at Site RE3 (Photo by Geo-Cim). 81
Figure 4-41: River bank erosion failure of Guaynabo Riverat Site RE3 (Photo by Geo-Cim). 82
Figure 5-1: Map showing location of ten road and bridge failure sites. 83
Figure 5-2: Schematic failure types for road sections on fill embankments. 84
Figure 5-3: Images showing induced curvature on bridges near Yauco, PR, due to heavy river flows during Hurricane Maria (images from NOAA taken a few days after Maria). 85
Figure 5-4: Photos showing large accumulation of debris under bridge. 86

Figure 5-5: General location of Road & Bridge Site 1. 86
Figure 5-6: Photos of Road and Bridge Site 1 associated to culvert clogging. 87
Figure 5-7: Location of Road & Bridge Site 2 at km 4.2 of PR-555 88
Figure 5-8: Photos of Road & Bridge Site 2 related to culvert clogging at km 4.2 of PR-555. 88
Figure 5-9: Location of Road & Bridge Site 3 at km 50.7 of PR-143 89
Figure 5-10: Select photos of Road & Bridge Site 3 involving primarily road damage associated to downslope slope failure. 90
Figure 5-11: Location of Road & Bridge Site 4. 91
Figure 5-12: Road & Bridge Site 4 - Road Damage by Lower Slope Failure. 91
Figure 5-13: Location of Road & Bridge Site 5. 92
Figure 5-14: Photos of Road & Bridge Site 4 showing upslope side failure and road blockage. 93
Figure 5-15: Location of Road & Bridge Site 6. 94
Figure 5-16: Photos of Road & Bridge Site 4 showing surficial slope failure on the upslope side of the road. 94
Figure 5-17: Location of Road & Bridge Site 7. 95
Figure 5-18: Photos of Road & Bridge Site 7 affecting PR-186. 96
Figure 5-19: Road & Bridge Site 8 - Complete cut-off failure along PR-431 in Lares. 97
Figure 5-20: Photos of Road & Bridge Site 8 - Road damage with complete cut-off at PR-431 in Lares. 98
Figure 5-21: Road & Bridge Site 9 - Washed away bridge failure in Ciales. 99
Figure 5-22: Road & Bridge Site 9 - Failure of Bridge over the Río Grande de Manati river in Ciales. 99
Figure 5-23: Road & Bridge Site 10: PR-123 bridge over Río Grande de Arecibo. 100
Figure 5-24: Road & Bridge Site 10 - Failure of PR 123 Bridge failure. 101
Figure 6-1: Foundation failures visited by 2017 GEER Team. 102
Figure 6-2: Photo of Cantilevered sign foundation failure at Site F1. 104
Figure 6-3: Photo of drilled shaft foundation of traffic sign at Site F1. 105
Figure 6-4: Photo of drilled shaft foundation of traffic sign at Site F1. 106
Figure 6-5: Photo of Cantilevered sign foundation failure at Site F2. 107
Figure 6-6: Photo of drilled shaft foundation of traffic sign at Site F2. 108
Figure 6-7: Photo of cantilevered sign foundation failure at Site F3. 109
Figure 6-8: Photos of foundation pedestal of traffic sign at Site F3. 109
Figure 6-9: Photo showing the rotation of the traffic sign at Site F3. 110
Figure 6-10: Photo of foundation failure of illumination tower at Site F4 in Ponce. 111

Figure 6-11: Photo of failed tower published by El Vocero 9/27/17 (Photo from Bartolomei, 2017). 112
Figure 7-1: Before and after pictures of the NEXTRAD NOAA Doppler radar in Cayey, PR. (photo credit: Dr. Luis Suarez). 113
Figure 7-2: Destroyed wind turbine at Punta Lima Wind Farm, PR. 114
Figure 7-3: Before and after pictures of Ilumina Project Farm in Guayama, PR. 115
Figure 7-4: Before and after pictures of the Humacao's sewage treatment facility solar farm. 116

Acknowledgements

Our visit to Puerto Rico in the aftermath of Hurricane Maria was supported by the National Science Foundation (NSF) through the Geotechnical Engineering Program under Grant No. CMMI-1266418. Any opinions, findings, and conclusions or recommendations expressed in this report are those of the authors and do not necessarily reflect the views of the NSF.

The Geotechnical Extreme Events Reconnaissance (GEER) Association exists thanks to the vision and support of the NSF Geotechnical Engineering Program Directors: Dr. Richard Fragaszy and the late Dr. Cliff Astill. GEER members also donate their time, talent, and resources to collect perishable data and field observations of geotechnical effects of extreme events. The GEER Association web site, http://www.geerassociation.org , contains additional information. The GEER mission to Puerto Rico benefitted greatly from the organizational support provided by GEER members R. Lee Wooten and especially J. David Frost.

Table 1-1 lists the reconnaissance team members and collaborators. Everyone worked hard during the visit to collect as much perishable data as possible throughout the island. All team members helped in some way during the writing of this report, but the report would not have been finished without the steadfast contributions from Dr. Youngjin Park and Prof. Daniel Pradel.

The reconnaissance team leadership would also like to acknowledge the contributions of the following organizations to the success of our mission:

- Federal Emergency Management Agency (FEMA), for supporting the expenses of team member Dr. Gokhan Inci, and for sharing relevant information and data.
- Puerto Rico Department of Transportation and Public Works (DTOP) and its Secretary, Carlos Contreras Aponte and staff – for graciously meeting with part of our team and sharing the wealth of information about landslides, roads, and bridges obtained prior to our arrival in Puerto Rico.
- Puerto Rico Electrical Power Authority, Dams and Irrigation Division – for meeting with part of our team and sharing design, construction, and performance information for dams.
- University of Puerto Rico, Mayagüez Campus – for providing transportation (vans and drivers) at a favorable cost and meeting rooms at no cost.
- U.S. Army Corps of Engineers (Mobile and Jacksonville Districts) – for facilitating the reconnaissance team's visit to Guajataca Dam while emergency operations were still underway.
- United States Geological Survey – for sharing their data about landslide locations derived from satellite photo interpretation.
- AECOM for providing editorial assistance through Ms. Emily Cencula.
- GeoCim for making their offices available to the advance party during the first days of the mission and facilitating project information for some of the sites visited.

List of Acronyms and Abbreviations

Acronym	Definition
AEE	Electric Power Authority (In Spanish, Autoridad de Energia Electrica)
AST	Atlantic Standard Time
C	Celsius
cm	Centimeter
CNN	Cable News Network
CO	Colorado
CRIM	Centro de Recaudación de Impuestos Municipales
DEM	Digital Elevation Model
DTOP	Puerto Rico Department of Transportation and Public Works
E	East
EST	Eastern Standard Time
F	Fahrenheit
FEMA	Federal Emergency Management Agency
ft	Feet
GEER	Geotechnical Extreme Events Reconnaissance
h	Hour
hPa	Hectopascal
in	inch
km	Kilometer
kPa	Kilopascal
kW	Kilowatt
LiDAR	Light Detection And Ranging
LL	Liquid limit
m	Meter
MA	Massachusetts
m/s	Meters per second
m/year	Meters per year
mi	Mile
mm/h	Millimeters per hour
mph	Miles per hour
N	North
NASA	National Aeronautics and Space Administration
NBC	National Broadcasting Corporation
NGVD	National Geodetic Vertical Datum
NID	National Inventory of Dams
NOAA	National Oceanic and Atmospheric Administration
NSF	National Science Foundation
NWS	National Weather Service

Acronym	Definition
PRHTA	Puerto Rico Highway and Transportation Authority
OH	Ohio
PI	Plasticity Index
PL	Plastic limit
PR	Puerto Rico
PRASA	Puerto Rico Aqueduct and Sewer Authority
PREPA	Puerto Rico Electric Power Authority
S	South
SC	South Carolina
TLS	Terrestrial Laser Scanning
UAV	Unmanned Aerial Vehicle
UPRM	University of Puerto Rico at Mayaguez
USA	United States of America
USACE	United States Army Corps of Engineers
USBR	United States Bureau of Reclamation
USGS	United States Geological Survey
UTC	Coordinated Universal Time
VSABR	Volcano Sedimentary Arc Basement Rocks
W	West

Summary

On the morning of Wednesday, September 20, 2017, Hurricane Maria made landfall near the southeastern town of Yabucoa, Puerto Rico as a powerful Category 4 storm. Hurricane Maria moved diagonally across the island with sustained winds of 155 mph – the worst storm to hit Puerto Rico in over 80 years. Hurricane Maria arrived only two weeks after Hurricane Irma passed just north of the island causing heavy rains throughout the island leaving about 1 million residents without power.

The scale of María's destruction was devastating, causing as much as $95 billion in damages according to an estimate released on September 28, 2018 by Moody's Analytics. Electricity was cut off to 100% of the island, and access to clean water and food became limited for most residents. Although the official number of fatalities attributed to Hurricane Maria stands at 64, a study published in the New England Journal of Medicine (2018)[1] attributed 4,645 fatalities to Hurricane Maria (excess deaths from September 20 through December 31, 2017).

The impact of Hurricane Maria was evident everywhere the GEER[2] team went. Hurricane María wind and water related forces wreaked havoc throughout the island. The force from the ferocious winds overwhelmed the foundation resisting forces for many structures resulting in bearing capacity failures. The reduced soil strength due to the heavy rainfall, which increased pore pressures and thus decreased the effective stresses in the foundations, contributed to many of these bearing capacity failures. Decreased effective stresses also resulted in over 2,000 landslides and debris flows throughout the island. The erosive power of the storm surge and river floods destroyed or damaged coastal infrastructure (e.g., piers, seawalls, roads, buildings, houses, utilities) and inland facilities (e.g., bridges, houses, highway embankments, pipelines). Facilities with geotechnical impacts from Hurricane Maria inspected by the team included the following:

1. **Dams –** Except for the well-publicized failure of a 100-year-old section of the Guajataca Dam spillway due to erosion and scour, dams throughout the island performed remarkably well. None of the 38 dams listed in the National Performance of Dams Program (NPDP) failed. The team did not encounter any failed dams during the Puerto Rico reconnaissance mission. Malfunctions were limited to loss of capacity due to sediment transport and minor landslides or rock falls near the abutments of several dams.

[1] Nishant Kishore, Domingo Marqués, Ayesha Mahmud, Mathew V. Kiang, Irmary Rodriguez, Arlan Fuller, Peggy Ebner, Cecilia Sorensen, Fabio Racy, Jay Lemery, Leslie Maas, Jennifer Leaning, Rafael A. Irizarry, Satchit Balsari, and Caroline O. Buckee (2018). *Mortality in Puerto Rico after Hurricane Maria*, The New England Journal of Medicine, Special Article, downloaded from https://www.nejm.org/doi/full/10.1056/NEJMsa1803972 June 9 2018.

[2] GEER stands for Geotechnical Extreme Events Reconnaissance

2. **Slopes and embankments –** The hurricane triggered a large number of landslides, over 2,000 by an early USGS count using satellite photographs. These landslides occurred throughout the island and impacted roads, power transmission, water supply, sewer systems, and housing. Three deaths were attributed directly to one of the landslides in the town of Utuado. A common failure mode encountered by the team consisted of erosion of highway embankments from overtopping water after debris plugged the pipes and culverts design to allow the streams to flow underneath. This failure mode involved both wind and water forces. Wind toppled trees and other vegetation creating vast amounts of debris and water carried the debris to the upstream toe of the embankment where it plugged the drainage facilities.
3. **Coastal and River Erosion and Scour –** Storm waves destroyed or damaged facilities built near the shoreline, many of which were in close proximity to the waterline. Flooded rivers damaged or destroyed bridges, bridge abutments and other constructed facilities along the river bank.
4. **Road and Bridge Failures –** Many of the road and bridge failures were caused by the mechanisms mentioned above, e.g., erosion and scour, landslides and debris flows triggered by low effective stresses. Numerous landslides in the mountainous central part of the island cut off terrestrial transportation for many residents. If the landslide occurred above the road, covering the pavement with soil and rock, the remedy consisted of partial or total removal of the landslide debris, a time consuming and costly task but generally within the capabilities of the municipal governments. If the landslide included the road, often the water, sewer, electricity, and telecommunications infrastructure was destroyed along with the road. This situation presented a much more complicated recovery challenge.
5. **Foundations –** Foundation failures observed by the team included those for lighting towers, electrical transmission poles, and many road sign failures. Some of the road signs simply rotated about the axis of their circular foundation while others rotated and also experienced bearing capacity failures. Although some electrical transmission poles failed from bearing capacity failures, the large number of reinforced concrete poles snapped at mid height provided graphic evidence of the storm power.

Hurricane Maria overwhelmed the natural and constructed facilities in Puerto Rico with strong winds and intense rainfall. Perhaps the best demonstration of its unstoppable destructive power came when the National Oceanographic and Atmospheric Administration NEXRAD Doppler radar, a structure designed to monitor — and thus presumably resist – extreme weather events, failed shortly after Hurricane Maria made landfall in Puerto Rico.

Cover Photograph – Eye of Hurricane Maria Approaches Puerto Rico: In this colorized infrared image from the NOAA/NASA Suomi NPP satellite, taken on September 20, 2017 at 6:15 UTC, the well-defined eye of Hurricane Maria can be seen as it skirts the island of St Croix. Approximately three hours later, the storm made landfall in Puerto Rico as a Category 4 hurricane, with maximum sustained winds of around 150 mph. (https://www.nnvl.noaa.gov/MediaDetail2.php?MediaID=2108&MediaTypeID=1)

STATEMENT OF GENERAL LIABILITY LIMITATION – DISCLAIMER

The team who performed this reconnaissance mission is comprised of individual volunteers. The findings and observations presented in this report are based on the conditions of the observed features at the time of the inspection and our experience with other similar structures. This report is not an assessment of condition or safety of the structures observed. No warranty or guarantee regarding the performance or safety of the observed structures is included or intended. Any use of or reliance on this report is at the sole risk of the party using or relying on the report.

1 INTRODUCTION

The island of Puerto Rico (PR), the easternmost and smallest of the Greater Antilles, is a United States territory bounded to the north by the Atlantic Ocean and to the south by the Caribbean Sea (Figure 1.1). The island measures approximately 160 km (100 mi) in the east to west direction and 55 kilometers (km) (34 miles [mi]) in the north to south direction (Figure 1-1).

Centered at latitude 18.2°N, and longitude 66.4°W, Puerto Rico lies in the commonly designated *Caribbean Hurricane Alley*, thus making it very vulnerable to hurricane impacts. Figure 1-1 shows a United States Geological Survey (USGS) map with historical hurricanes that have impacted Puerto Rico. Recent hurricanes that made landfall in Puerto Rico include: Hugo (Category 3 to 4; September 18, 1989), Hortense (Category 1; September 9-10, 1996), and Georges (Category 3; September 21-22 1998).

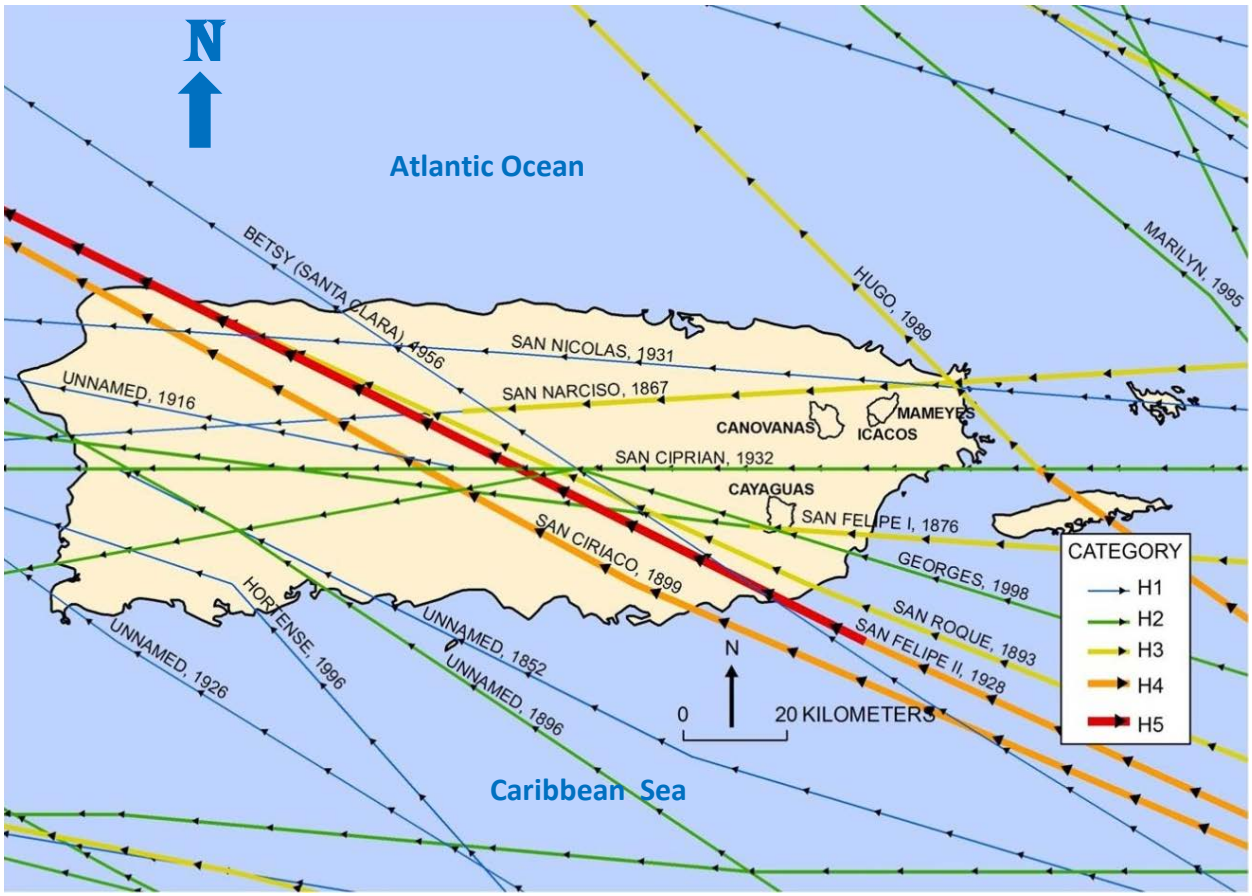

Figure 1-1: Path of historical hurricanes that have impacted Puerto Rico (USGS, 2018) (https://www.usgs.gov/media/images/puerto-rico-hurricanes-map).

1.1 Hurricane events of September 2017

The two hurricanes that impacted Puerto Rico in September 2017 were Irma and Maria. Irma was a Category 5 hurricane when it passed just north of Puerto Rico on Tuesday, September 5, 2017. The trajectory of the eye of this hurricane is shown on Figure 1-2. Despite not making landfall in PR, hurricane strength winds extended about 80 miles (~129 kilometers [kms]) from its center[3], and it left over 1 million people without power (NBC, 2018). Maria was also a major hurricane, classified as a strong Category 4 hurricane on the Saffir-Simpson hurricane wind scale before making landfall in Yabucoa, PR on September 20, 2017. The path of the eye of this powerful hurricane took a northwesterly direction as shown on Figure 1-3. Hurricane force winds extended 50 to 60 miles (~80 to 97 kms) from its center[4].

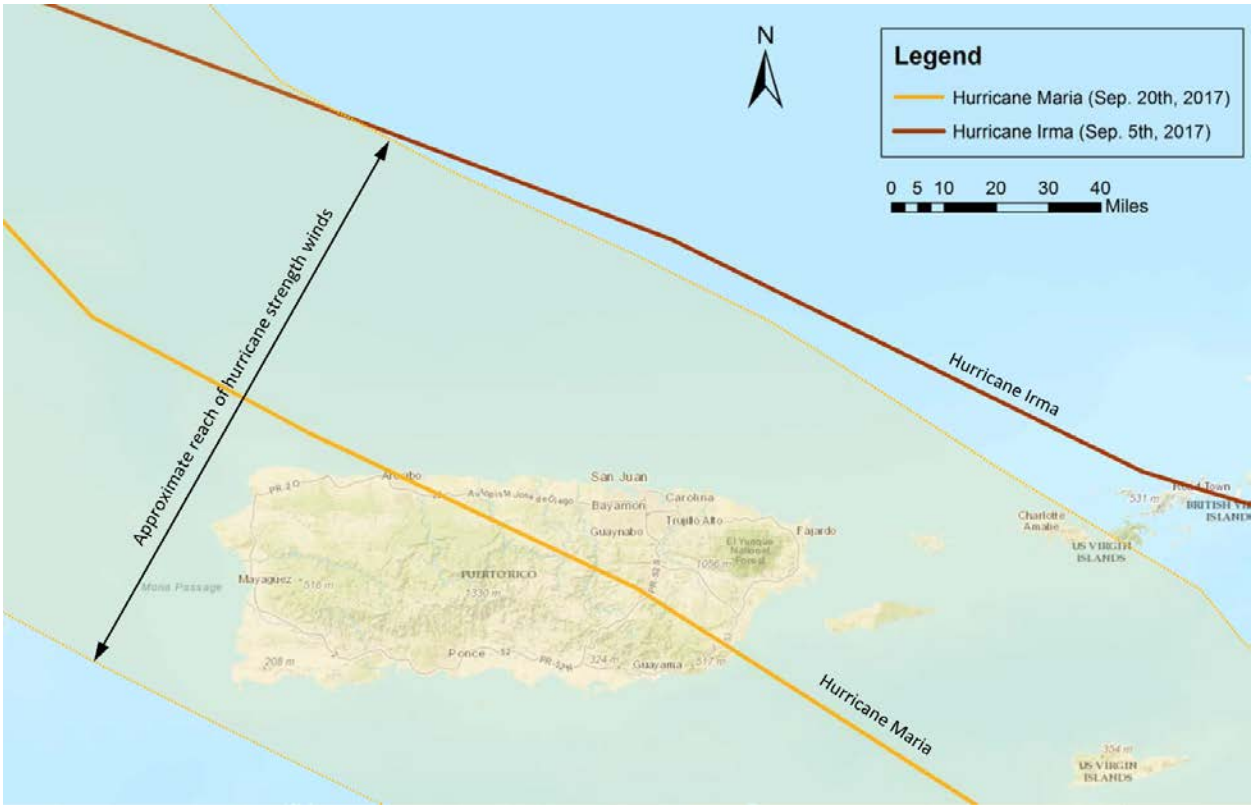

Figure 1-2: Path of Hurricanes Irma and Maria with respect to Puerto Rico (Feng et al., 2018).

[3] https://www.vox.com/science-and-health/2017/9/21/16345176/hurricane-maria-2017-puerto-rico-san-juan-meteorology-wind-rain-power

[4] https://www.vox.com/science-and-health/2017/9/21/16345176/hurricane-maria-2017-puerto-rico-san-juan-meteorology-wind-rain-power

The extended path of this hurricane from September 16 to October 3, 2017, is shown on Figure 1-3. A plot showing variations in wind speed and pressure at the eye of the hurricane is shown on Figure 1-4. At landfall, the wind speed was about 75 meters per second (~167 mph). Maria is considered the most devastating hurricane to hit Puerto Rico in almost a century. Many lives were lost; at least 64 people killed according to CNN (2018), homes and businesses suffered immense damage, and large parts of the Island's infrastructure and about 80% of the agricultural crops were destroyed. The aftermath of Hurricane Maria included numerous geotechnical failures related to the intense rainfall and strong winds associated with this extreme event. Nearly immediately after landfall, Maria rendered the island's power grid, cellphone towers, banking system, and even the National Oceanic and Atmospheric Administration's (NOAA) San Juan WSR-88D Weather Radar inoperable. Puerto Rico's power outage was, by far, the most severe in United States history in terms of total customer-hours lost, and in March 2018 (6 months after the event), many areas of central Puerto Rico were still without power and water.

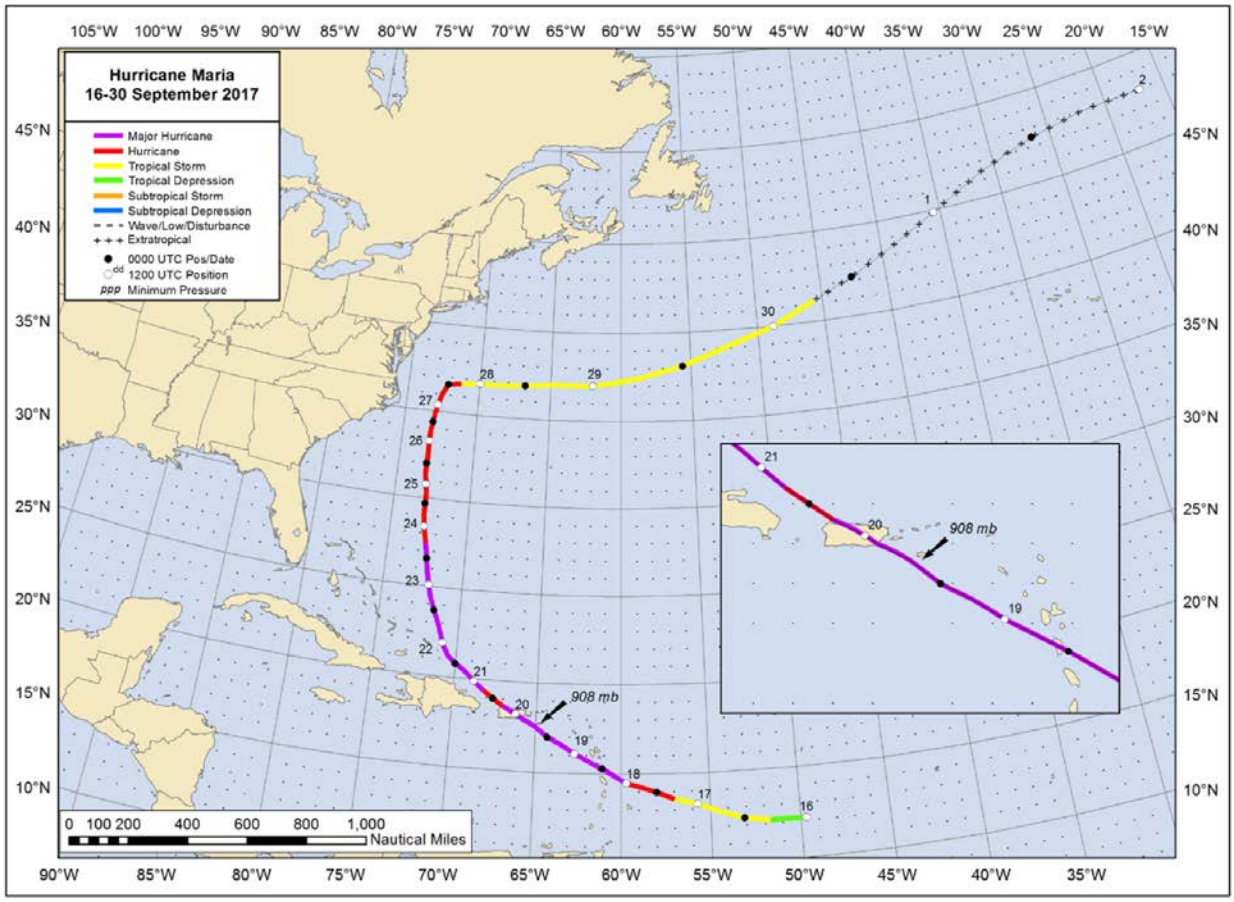

Figure 1-3: Path of Maria from 9/16/2017 to 10/02/2017 (Landfall in PR September 20, 2017) (NOAA Report AL152017, 2018).

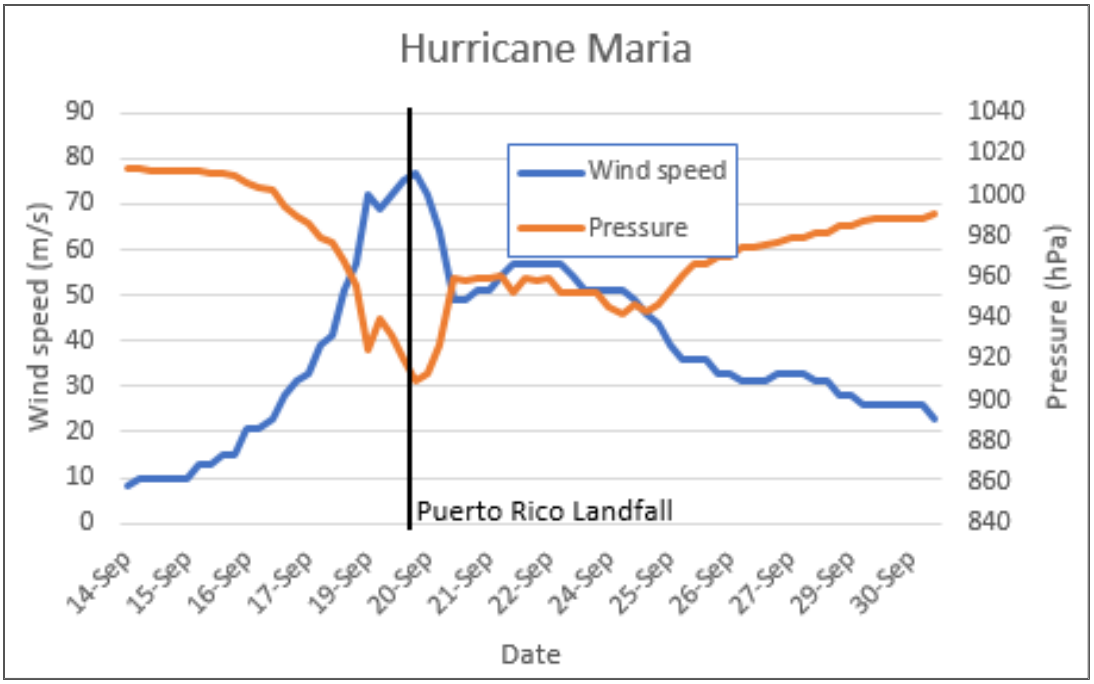

Figure 1-4: Wind speed of Maria at Landfall in Puerto Rico (data from NOAA Report AL152017, 2018).

This report summarizes the event timeline and the geotechnical impacts of Maria's path across Puerto Rico. The impacts of Hurricane Maria on infrastructure and geomorphology are documented through the data and observations of the engineers and geologists that participated as members of the Geotechnical Extreme Events Reconnaissance (GEER) team. The main component of the reconnaissance mission took place between October 25 and November 6, 2017, a second component involving an unmanned aerial vehicle (UAV) and LiDAR scanning took place from January 8-11, 2018. Observations of geotechnical impacts such as the Guajataca Dam spillway failure; coastal erosion events, including foundation failures due to coastal erosion in Córcega, Rincón; bridge abutment scour failures; over 2,000 landslides along the PR highway system (e.g., along the PR-10, region of Lares, Barranquitas and Utuado); foundation failures; and other failures related to this destructive hurricane were also investigated.

Rainfall-induced landslides in Puerto Rico have been a serious recurring problem (e.g., Jibson, 1987; Larsen and Simon, 1993; Larsen and Santiago-Roman, 2001; Pando et al., 2005) and have been observed in the different physiographic regions of the island as result of Maria and other hurricanes such as Hortense (September 10, 1996), Georges (September 21-22, 1998), and Debby (August 22, 1999). Hurricane Maria triggered thousands of landslides as discussed in Section 2. The most common type of failure mode consisted of shallow debris flows, but many deeper-seated failures were also observed, typically at sites with road fill and blocked drainage culverts. The geotechnical failures presented in this report provide insight to help identify typical failure modes and help the engineering community adapt and improve design and construction practices to increase the resiliency of our infrastructure and lifelines.

1.2 GEER-PR Team

On September 27, 2017, seven days after the passage of Hurricane Maria through Puerto Rico, Francisco Silva received a call from GEER's Lee Wooten with a request to lead a GEER-sponsored team on a reconnaissance mission to observe and document the geotechnical impacts of Hurricane Maria throughout the island. The planning process moved fairly rapidly with David Frost taking over as the main GEER point of contact and Miguel Pando agreeing to co-lead the team.

In order to organize an effective and balanced team, these team leaders considered the following during the team member identification process:

- Participation of individuals from academic, government, and private sectors
- Representation of the different relevant geo-engineering disciplines, including:
    - Geology;
    - Earth structures (e.g., dams, dam safety, embankments);
    - Mass movements (e.g., landslides, debris flows);
    - Coastal erosion and scour;
    - Bridge foundation erosion and scour;
    - Foundations;
    - Retaining structures; and
    - Pavements.
- Participation by individuals with knowledge of the island and the predominant Spanish language.
- Participation by individuals with local relationships that could facilitate gathering of information and access to field sites.

Table 1-1 summarizes the team composition and Appendix A presents resumes of the GEER-PR Team participants.

Although the intent was to travel to Puerto Rico as soon after the hurricane as possible, difficult living conditions on the island, resource focus on emergency operations, and unavailability of return flights and reasonably priced hotel rooms delayed the start of the mission until Wednesday, October 25, 2017. The team leaders flew to Puerto Rico that day to finalize the advance coordination efforts completed by University of PR (Mayagüez campus) professors and team members Dr. Stephen Hughes and Dr. Alesandra Morales-Velez, who had negotiated arrangements including affordable hotel rooms at the Mayagüez Resort and Casino Hotel in Mayagüez, a city on the western coast of the island, and transportation in University of Puerto Rico vans at-cost (driver and fuel). The hotel was equipped with its own emergency power generator, potable water well, and a fully functioning restaurant.

By the time the team leaders arrived on the island, conditions in Puerto Rico had improved somewhat during the four weeks since the hurricane made landfall, but still remained very difficult. Most of the island lacked electricity or potable water; team members were advised to bring enough drinking water for the duration as well as provisions for meals while traveling), traffic in the urban areas without traffic signals moved slowly, and telephone communications proved difficult and unreliable. Team members Luis and Carlos García offered the use of their company office as base of operations. The office had an emergency power generator, fully functioning internet service, and air conditioning, among other amenities.

On Thursday and Friday October 26 and 27, reconnaissance was performed throughout the island to investigate the numerous geotechnical failures that had occurred. Through Luis and Carlos García's personal contacts, the team was able to meet with Puerto Rico's Secretary of Transportation and Public Works and his engineering advisors to go over the main landslide locations identified by this agency that affected road infrastructure. During that meeting, the team learned that more than 2,000 landslides had been recorded to that point. Through team collaborator, Puerto Rico's Dam Safety Official José Miguel Bermudez, we were able to arrange for escorted visits to Guajataca Dam, the site of a well-documented spillway failure, as well as several other affected dams. Concurrent with Miguel and Francisco's meetings in San Juan, Drs. Hughes and Morales-Velez were developing possible reconnaissance routes for the team based on intelligence obtained from their Mayagüez base and making final transportation arrangements.

Table 1-1: Summarizes the GEER team composition

First Name	Last Name	Team Role	Organization	Expertise	Home Base
Francisco	Silva-Tulla	Leader*	Consulting Civil Engineer	Geotechnical engineering, earth structures	MA
Miguel A.	Pando	Co-Leader*	University of North Carolina (NC), Charlotte	Geotechnical engineering	NC
Tiffany	Adams	Member*	AECOM	Geotechnical engineering	CO
Juan R.	Bernal Vera	Member*	University of PR, Mayagüez	Geotechnical engineering	PR
Luis Oscar	García	Member	GeoCim	Geotechnical engineering	PR
Carlos	García Echevarría	Member	GeoCim	Geotechnical engineering	PR
Stephen	Hughes	Member*	University of PR, Mayagüez	Geology of PR, unmanned aerial vehicle (UAV)	PR
Gokhan	Inci	Member*	Federal Emergency Management Agency (FEMA)	Civil engineer, FEMA National Dam Safety Program	Washington, DC
Robert	Kayen	Member*	USGS	Geometry determination, UAV, LiDAR	CA
Alesandra Cristina	Morales Velez	Member*	University of PR, Mayagüez	Geotechnical engineering	PR
Youngjin	Park	Member*	University of NC, Charlotte	Geotechnical engineering	NC
Daniel	Pradel	Member*	The Ohio State University	Geotechnical engineering	OH
Inthuorn	Sasanakul	Member*	University of South Carolina (SC)	Geotechnical engineering, erosion and scour	SC
Alex	Soto	Member*	GeoCim	Geology of PR, landslides	PR
José Miguel	Bermudez	Collaborator	Puerto Rico Electric Power Authority (PREPA), Dams and Irrigation Division	PR State Dam Safety Official	PR
Ruben	Estremera	Collaborator	PRASA	Dam safety	PR
Jaime	Lopez	Collaborator	PRASA	Dam Safety	PR
Aurelio	Mercado-Irizarry	Collaborator	University of PR, Mayagüez	Oceanography	PR

* Indicates report co-author

The reconnaissance activities were started on Saturday, October 28, 2017; the team leaders began with a visit to the easternmost region of the island. On Sunday, October 29, Professor Juan Bernal led reconnaissance in Aguadilla and Moca during a trip from San Juan to Mayagüez. The U.S. mainland-based team members arrived in Mayagüez on Sunday, October 29, and the bulk of reconnaissance took place from Monday, October 30 to Friday, November 3. Although the initial plan was to split the team into several sub-teams to increase coverage, the team leaders decided to keep the group generally together after further assessing the situation, traveling in a 15-passenger University of PR van. This decision was primarily based on safety considerations, given that communications and transportation were logistically difficult, and the team only had one satellite telephone. The team experienced communications and operational efficiency difficulties on the two occasions it split into smaller groups.

The mainland-based team members began to return to their respective home bases on Saturday, November 4, 2017, although Miguel, Youngjin, and Francisco completed a full day of reconnaissance that day while returning to San Juan. Youngjin and Francisco similarly were able to visit landslide-affected areas in northeast PR for about a half-day on Sunday, November 6. Figure 1-5 shows the tracks of the team's daily reconnaissance activities.

A second field component involving LiDAR surveys using a UAV, led by Robert Kayen, was performed from January 8 to January 11, 2018. Alesandra and Stephen assisted Robert with the LiDAR field activities, focusing primarily on the Guajataca Dam spillway (January 9, 2018) and two landslide sites described in Chapter 2.

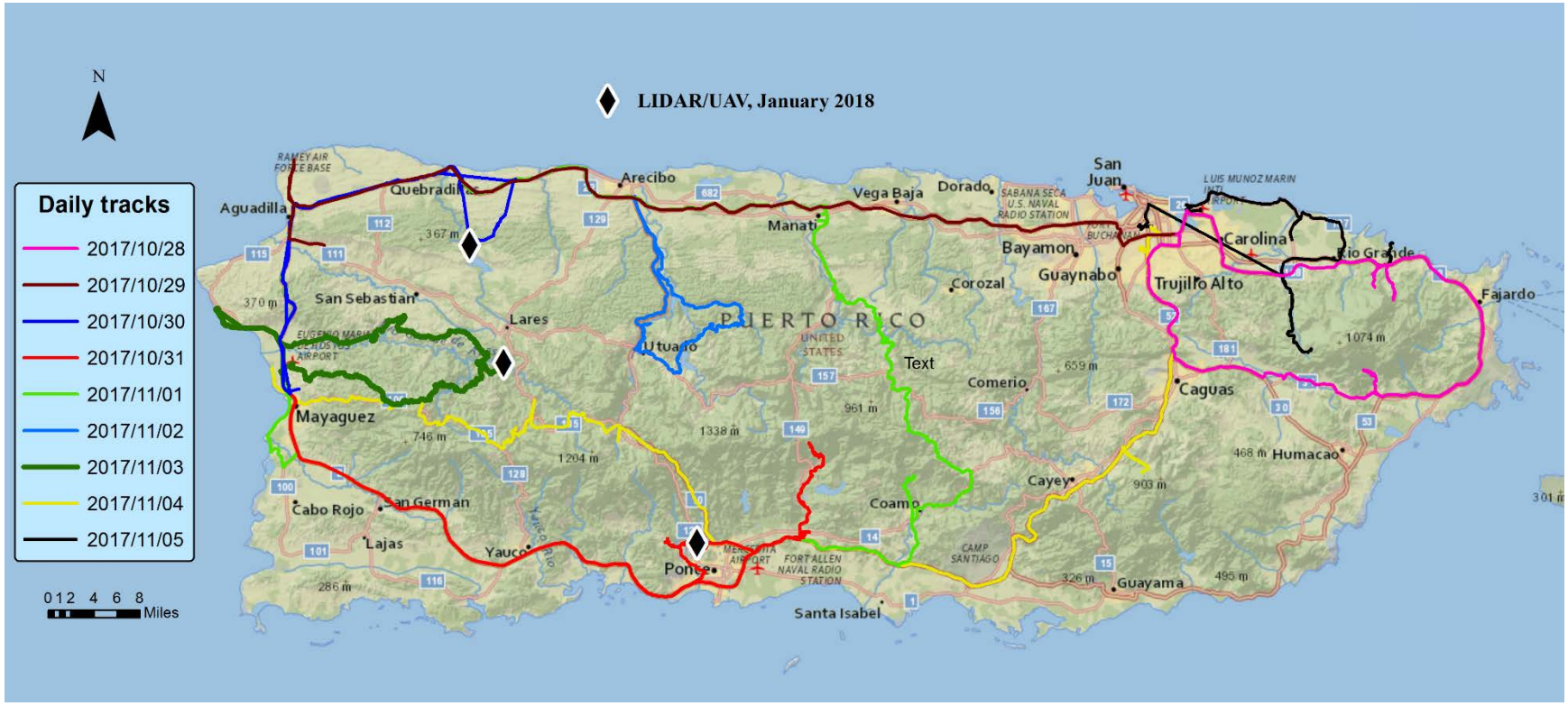

Figure 1-5: Daily reconnaissance tracks of GEER mission and location of LiDAR scans.

1.3 Topography, Geology, and Climate of Puerto Rico

The following subsections provide background information for the topography, geology, and climate of Puerto Rico as it is relevant to many of the observed geotechnical impacts, particularly the rainfall-induced landslides.

1.3.1 Topography

Most of the island of Puerto Rico is mountainous, as shown in Figure 1-6. The mountain ranges include a central mountain range (the Cordillera Central) that extends across the island from west to southeast with average elevations between 330 to 600 meters (m) above sea level, and a maximum peak with an elevation of 1,338 m above sea level, as well as the Luquillo Mountains (Sierra de Luquillo), which are located in the northeast portion of the island with a maximum elevation of 1,074 m. A relatively flat coastal plain, which is 8 to 16 km wide, is located around most of the perimeter of the island.

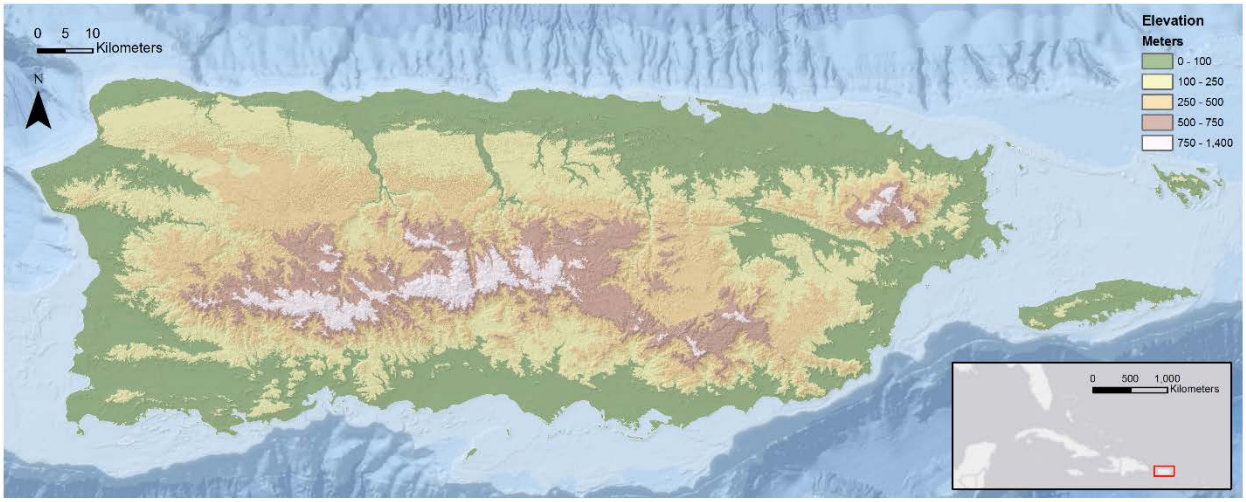

Figure 1-6: Map of Puerto Rico showing mountainous topography in the central region.

The rugged and steep nature of the topography of the interior of the island is illustrated on Figure 1-7, a slope map created from a 5 m resolution digital elevation model (DEM) from Puerto Rico's Real Estate Tax Collection Center, or, *Centro de Recaudación de Ingresos Municipales* (CRIM), in Spanish. This map shows the majority of the central region has average slope inclinations from 20 to 30 degrees, with many locations (more than 10% of this region) with slope angles between 30 and 40 degrees, or higher than 40 degrees' inclination with respect to the horizontal.

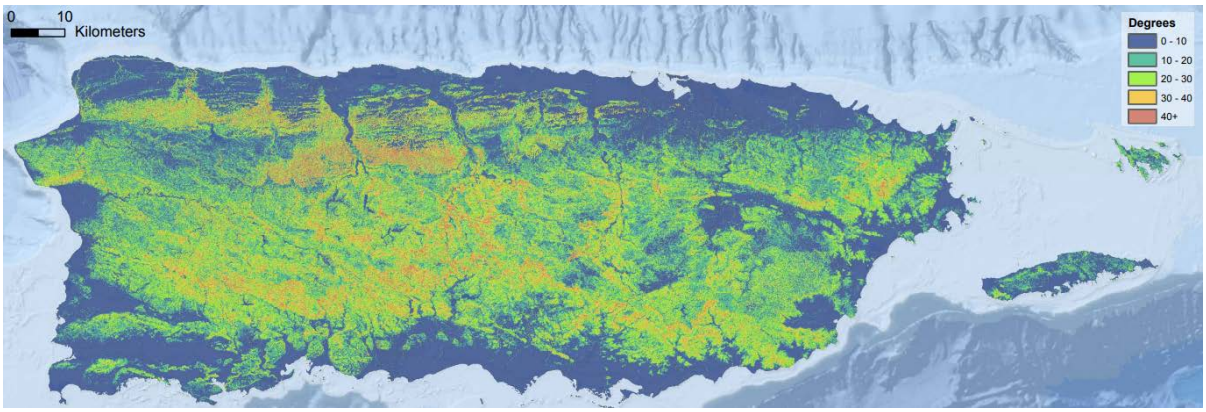

Figure 1-7: Slope map showing computed average slope inclinations from 5 m resolution DEM.

1.3.2 Geology

Puerto Rico sits along the northeast corner of the seismically active boundary between the Caribbean and the North American tectonic plates. At present, Puerto Rico and the northern Virgin Islands to the east occupy the crest of what has been called the Puerto Rico-Virgin Islands (PRVI) platelet, or microplate, a small crustal block wedged between the Caribbean and North American plates, and subject to the stresses generated by their interplay, here dominated by left-lateral faulting with a component of oblique subduction along the Puerto Rico Trench north and northeast of the island (Figure 1-8). The interplate stresses cause the PRVI microplate to rotate in a counterclockwise direction, creating prominent submarine features that mark the remaining microplate boundaries: extensional basins to the west (Mona Canyon) and east (Anegada Trough), and underthrusting of Caribbean crust at the Muertos Trough to the south. Active tectonics extend into southwest to south-central Puerto Rico where Quaternary faulting has been documented (Geomatrix, 1988; Prentice and Mann, 2005; Redwine et al., 2013).

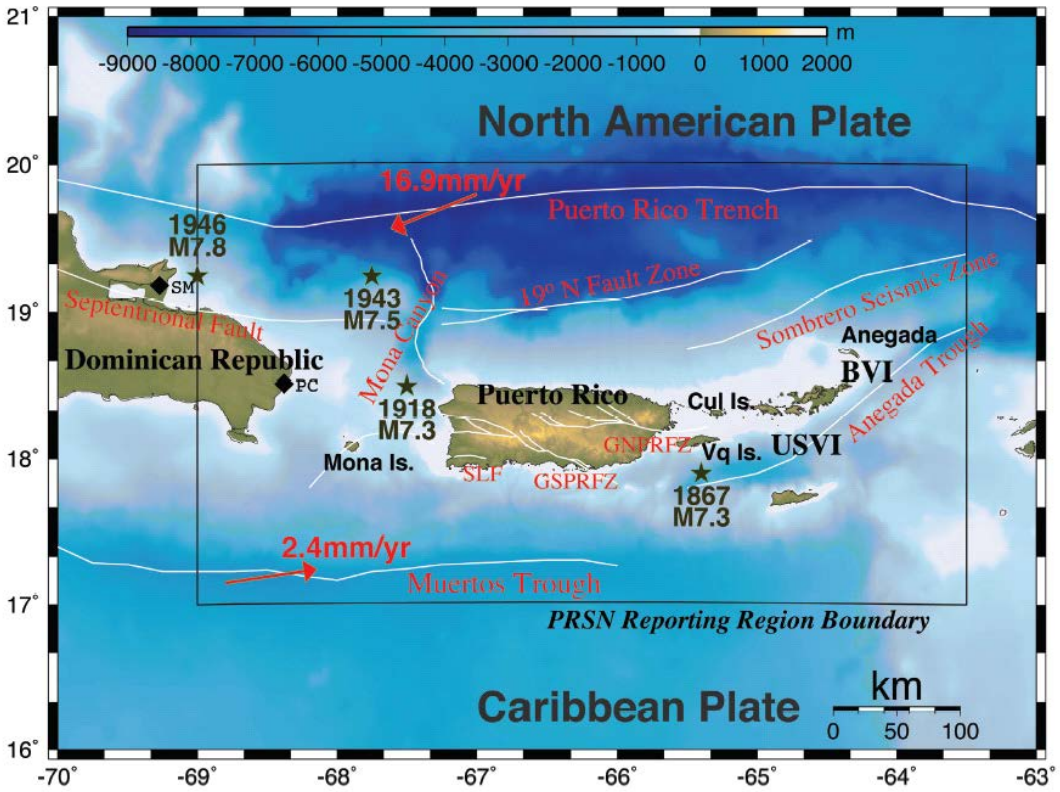

Figure 1-8: General Seismic Settings and Major Faults of Puerto Rico (Clinton et al. 2006).

The island's landscape contains an array of landforms that reflect its varied geology and climate, and landsliding has been an ever-present factor shaping the topography, with overall incidence increasing since the arrival of Europeans five centuries ago. As described in Section 1.3.1, with a high proportion of its land surface in slopes of 20° or steeper, and a host of geologic settings typically associated with landsliding, all failure modes described in landslide classification schemes occur, including slow to fast-moving earth slumps, slides, and flows occurring in residual and transported soils, and all types of rock failure occurring in the steep rocky slopes that are common along coastal cliffs and the dryer southern cordillera slopes.

The USGS has published preliminary or final 1:20,000-scale geologic maps for 61 of the island's 64 7.5-minute topographic quadrangles. Bawiec (1999) combined the USGS map units into 12 geologic terranes that group units on the basis of similarities in "lithologic rock type, depositional environment, and (or) age of deposition", as shown on Figure 1-9. The island consists of thick sequences of late Cretaceous to Eocene island arc rocks of volcanic, intrusive, and sedimentary origin, with a slice of Jurassic ocean crust that came together as the Caribbean plate migrated to its present position from the eastern Pacific Ocean. The rocks of this older complex are folded, faulted, and cut by predominantly felsic intrusive rocks that include two small plutons, the San Lorenzo and Utuado Batholiths (Figure 1-9). They outcrop throughout the island's mountainous backbone that makes up close to 60% of the island's surface. Elsewhere, they are covered by up to 1,400 meters of Oligocene to Miocene carbonate

platform sediment and/or up to about 100 meters of a variety of Quaternary alluvial, eolic, and coastal sediment.

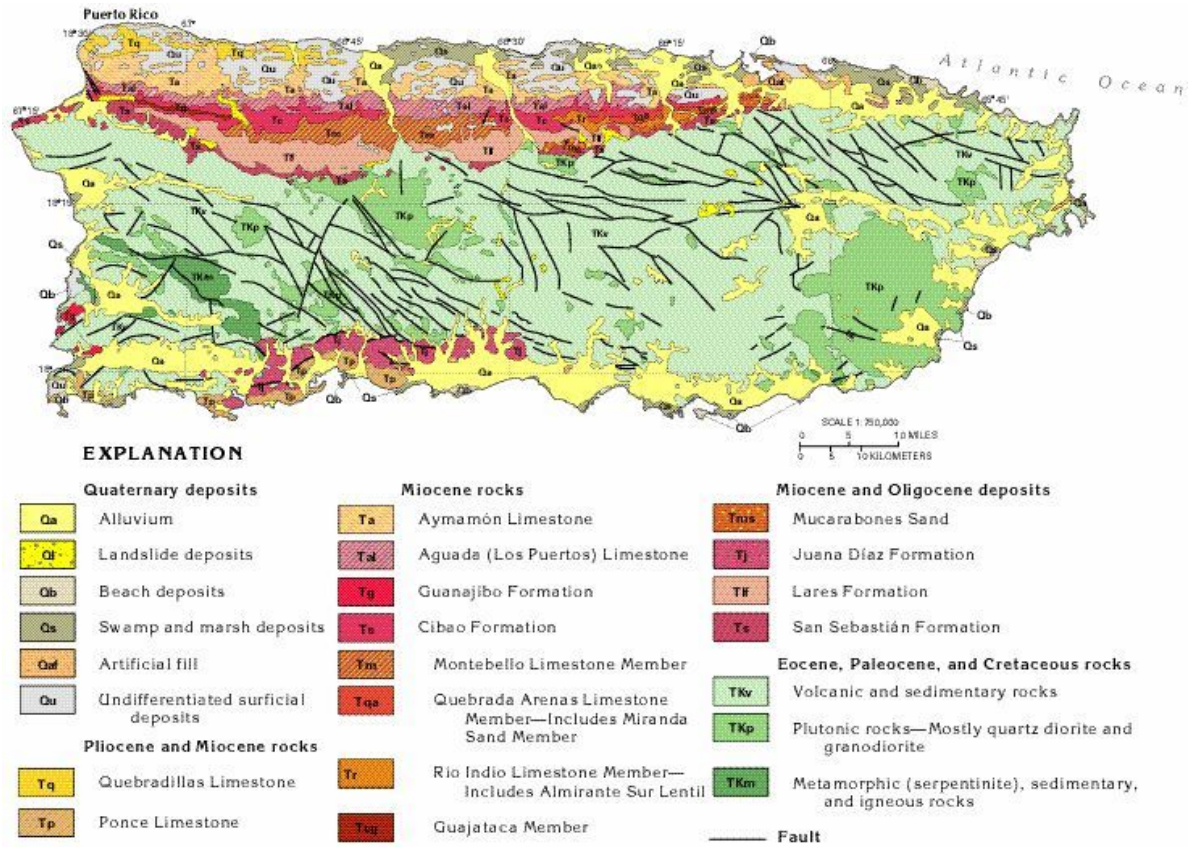

Figure 1-9: Geology of Puerto Rico adapted from Bawiec (1999).

The Volcano Sedimentary Arc Basement Rocks (VSABR) unit is the most extensive terrane, forming most of the island's central highland. The highland itself is subdivided into three principal ranges: the Cordillera Central that extends eastward from the rocky headlands of the west coast to about the longitude of San Juan; here it splits into the northeast-trending Sierra de Luquillo and the southeast trending Sierra de Cayey, which are separated by hilly terrain of lower elevation that coincides with the outcrop of the island's largest Intrusive terrane, the San Lorenzo Batholith (Figure 1-9). The VSABR terrane consists primarily of a variety of predominantly submarine volcanic and volcaniclastic rocks with a patchwork of ultramafic igneous and metamorphic rocks outcropping in the island's southwest corner. Topographically, the VSABR outcrop is characterized by deep entrenched valleys bordered by rugged peaks and foothills with sharp ridges and steep slopes, or low, rolling ranges with moderate slopes and relatively flat, accordant crests, with many of these features exhibiting northwesterly trends that mirror the orientation of major faults and folds in the older complex rocks.

In addition to the San Lorenzo Batholith, the highland contains one other moderate-sized and several smaller Intrusive terranes and a number of small areas of Carbonate and Quaternary terranes. As at San Lorenzo, the coarse-grained intrusive rocks tend to weather more rapidly than the bulk of the VSABR rocks, such that Intrusive terranes typically exhibit a more subdued, lower elevation topography. The Carbonate terranes are small areas of Cretaceous to Eocene

reefs that formed around volcanic islands and that typically exhibit a variety of karst features. The Quaternary terranes consist of a number of small intermontane valleys, in which the older complex terranes are buried by up to tens of meters of alluvial sediment.

The remainder of the island consists of Carbonate and Quaternary terranes. The former occurs as two east-west trending belts that flank a portion of the northern and southern cordillera foothills. The northern terrane coincides with the northern Puerto Rico karst, a well-developed karstic terrain dominated by thick to massive beds of Middle Tertiary limestone that dip gently northward. The karst drains underground and exhibits a variety of karstic landforms that include some of the island's roughest terrain, exemplified by many deep sinkholes surrounded by steep-sided mogote hills and by the Lares Escarpment, a steep, south-facing limestone bluff between Aguadilla and Toa Alta that overlooks the contact between the older complex rock and the limestone strata. The southern Carbonate terrane is underlain by a thick sequence of clastic and carbonate soil and rock units of Oligocene to Pliocene age that experienced syn- and post-depositional normal faulting and now exhibit gentle to moderate southerly dips.

The Quaternary terranes include the extensive alluvial deposits of the northern and southern Puerto Rico coastal plains, the Lajas Valley, and several smaller alluvial valleys that occupy the low land between rocky headlands where the older complex rocks reach the island's east and west coasts. Near the coasts, the alluvial plain soils merge with a variety of coastal swamps and lagoons interspersed with sections of beach and dune sand that on the north and west coasts include sections of cemented beach and dune sand. Lajas Valley is a west-trending, poorly-drained, sediment-filled fault basin that during the Pleistocene age was occasionally a strait separating the Cordillera foothills from the islands that are today the Hills of Parguera and the Sierra Bermeja, home to the island's oldest rocks.

From Figure 1-9, it can be seen that the central mountain range is composed predominantly of volcanic and sedimentary rocks of Early Cretaceous to Eocene age (Briggs and Akers, 1965). The rocks of the Upper Cretaceous age are comprised of a great variety of pyroclastic, sedimentary, extrusive, and intrusive igneous rocks (Deere, 1955). Because of high moisture and warm temperatures, the bedrock in the Cordillera Central is highly weathered and overlain with an average of 5 to 10 m of saprolite (St. John et al., 1969; Deere and Patton, 1971; Sowers, 1971). The central mountain range is surrounded to the north and south by a belt of middle Tertiary age limestones, siltstones, and claystones (Briggs and Akers, 1965; Jibson, 1987). Rock falls from steep cliffs and road cuts originating in colluvial deposits are common in the foothills of the mountains in these sedimentary rocks (Monroe, 1979; Jibson, 1987). The coastal plains are mainly depositional environments composed of sand, gravel, and clay, which form Quaternary beach deposits, swamps, dunes, alluvial plains, and fan deposits (Briggs and Akers, 1965).

1.3.3 Climate

The climate of Puerto Rico has considerable variation due to its topography and the prevailing north-easterly winds (Boose et al., 2004). The climate is humid-tropical in the central mountain range and northern coast and seasonal dry (dry winters, wet summers) in the southern coastal plain (Larsen and Simon, 1993). Annual precipitation is between 1,500 to 2,000 mm in the northeast part of the island, about 750 mm in the southwest, and more than 4,000 mm in the

Luquillo Mountains (Boose et al., 2004). Much of the yearly rainfall is delivered by tropical waves, depressions, storms, and hurricanes approaching from the east and southeast (Calvesbert, 1970). The rainy season is typically between the months of May and December. The levels of mean annual rain range from about 30 to 40 inches (762 – 1016 mm) in the south of the island to 70 to 100 inches (1,778 – 2,540 mm) in the central cordillera of Puerto Rico as shown on Figure 1-10.

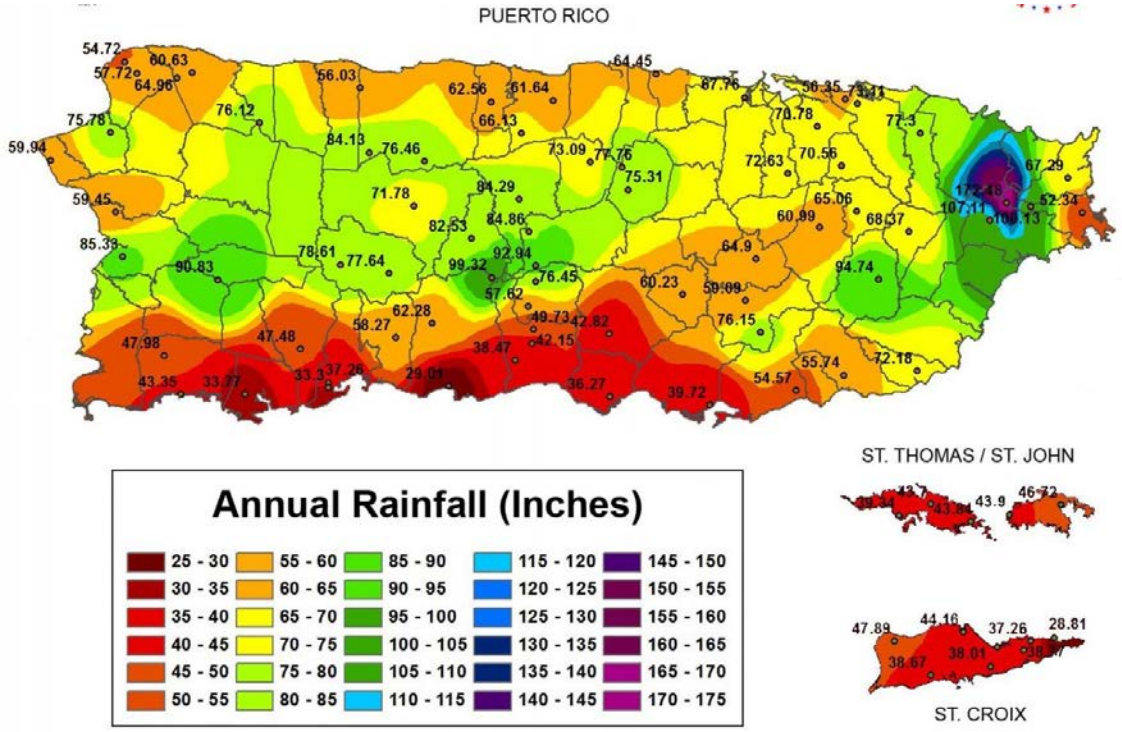

Figure 1-10: Mean Annual Rain Distribution in inches for Puerto Rico (Data 1981-2010).

Hurricane frequency in PR is among the highest in North America (Neumann et al., 1987). Reviewing historical records since European settlement, Boose et al. (2004) documented 85 hurricanes that affected PR for the period from 1508 to 1997. The seasonal distribution of these hurricanes (considering only the ones with sustained wind speeds above 26 m/s) is shown on Figure 1-11. The hurricane season runs from June through October, with 84% of the hurricanes occurring during the months of August and September.

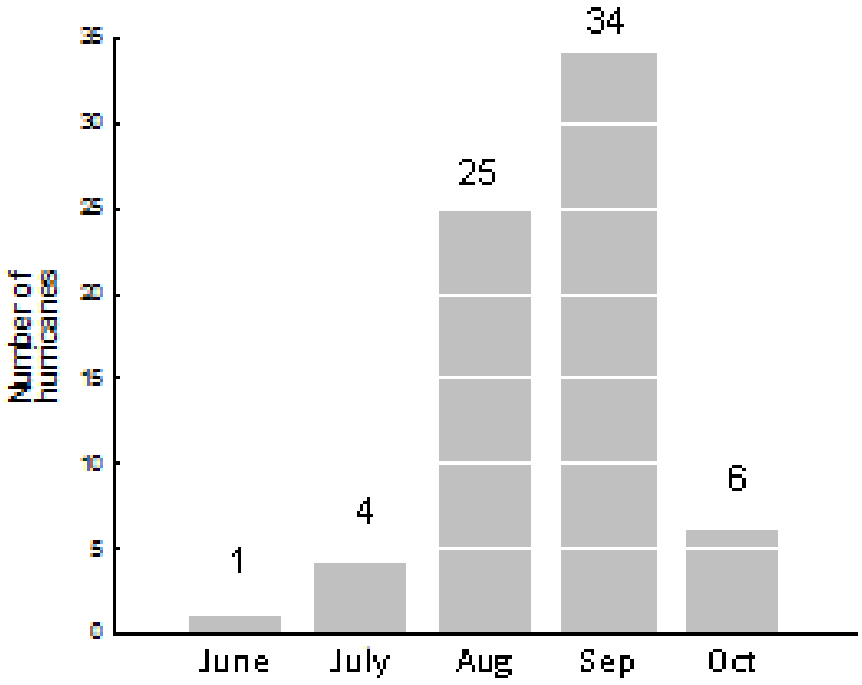

Note: plot includes only hurricanes with sustained wind speeds above 26 m/s

Figure 1-11: Seasonal Distribution of Hurricanes for Puerto Rico (Period 1508 to 1997) (from Boose et al. 2004).

The mean annual temperatures vary with the elevation and range from 23° to 27° Celsius (C) (74° to 81° Fahrenheit [F]) in the foothills and along the coastal plains, and 19° to 23° C (66° to 74° F) in the mountains and highest peaks (Deere, 1955; Calvesbert, 1970).

2 LANDSLIDES AND DEBRIS FLOWS

2.1 Introduction and Complementary efforts

Heavy rainfall associated with Hurricane Maria caused thousands of landslides throughout Puerto Rico. A rapid identification of landslide density across the island was performed by the USGS (Bessette-Kirton et al., 2017) by examining post-hurricane satellite and aerial images (Figure 2-1). The map was generated analyzing FEMA and DigitalGlobe images collected between September 26, 2017 and October 8, 2017, to estimate the number of landslides inside 2 km x 2 km square cells. The authors warn of limitations of the study related to poor visibility associated with clouds, vegetation, or shadows. Further, the authors assumed that the majority of landslides detected were triggered by rainfall from Hurricane Maria, but the effects of antecedent rainfall from Hurricane Irma (September 6, 2017) and heavy rainfall reported in the days after Hurricane Maria may have also triggered landslides. Despite these constraints, this map is useful in helping to identify the most critical areas of the island affected by landslides and in aiding response and recovery efforts. The map in Figure 2-2 shows results of an ongoing investigation at UPRM by Hughes and Morales Vélez (2018) in which more than 40,000 debris flows sites have been identified across Puerto Rico. Based on results from these two studies, the municipalities most severely impacted by landslides are Añasco, Mayagüez, Las Marías, Maricao, Lares, Utuado, Adjuntas, Jayuya, Ciales, and Orocovis (Figure 2-3).

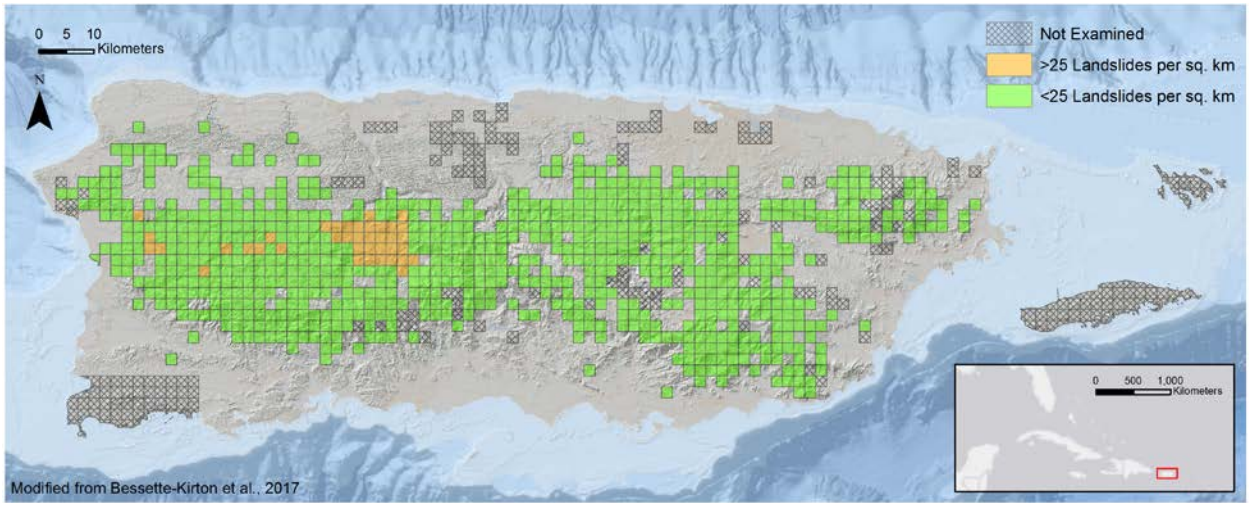

Figure 2-1: USGS map showing concentration of landslides attributed to Hurricane Maria (Bessette-Kirton et al., 2017; https://doi.org/10.5066/F7JD4VRF).

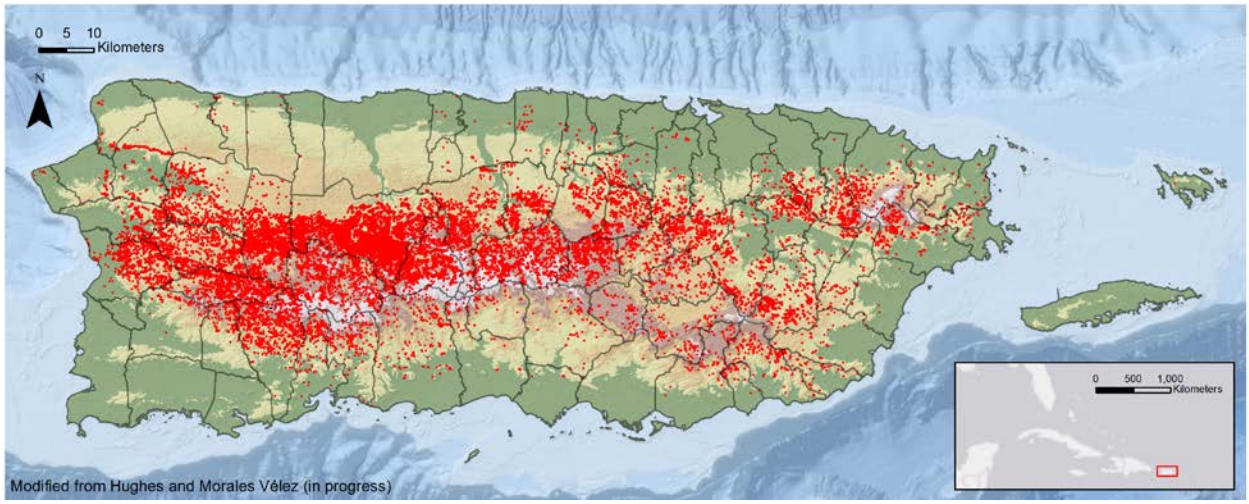

Figure 2-2: More than 40,000 debris flow sites (shown as red dots) have been identified across Puerto Rico by Hughes and Morales Vélez (2018).

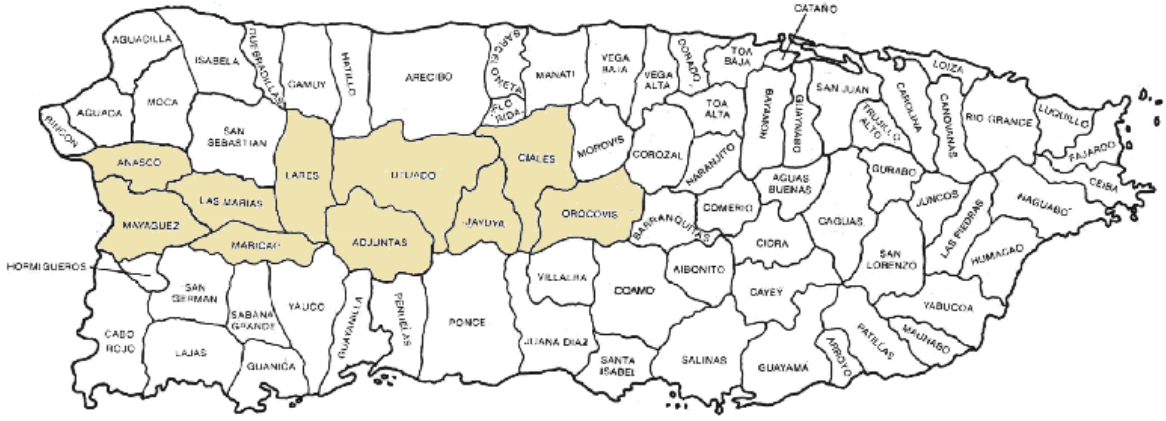

Figure 2-3: Map of Puerto Rico showing municipalities most impacted by landslides associated to Hurricane Maria.

2.2 Background

The geology, topography, and climate of Puerto Rico were described in Section 1.3 of this report. Rainfall-induced landslides are common in Puerto Rico due to high-relief mountainous topography in the central region coupled with deeply weathered soils and high frequency of intense rainfall (Monroe, 1979; Larsen and Simon, 1993; Pando et al., 2005; Lepore et al., 2012; Hughes and Morales Vélez, 2017). Hurricanes Hortense (1996) and Georges (1998) are examples of recent hurricanes that caused large numbers of debris flows and flooding in the central mountains (Larsen and Santiago-Román, 2001). All physiographic provinces of the island have experienced landslides. Monroe (1979) published a map of landslides and zones of susceptibility to landslides for PR. A more recent map of landslide susceptibility for PR by Lepore et al. (2012) is shown in Figure 2-4.

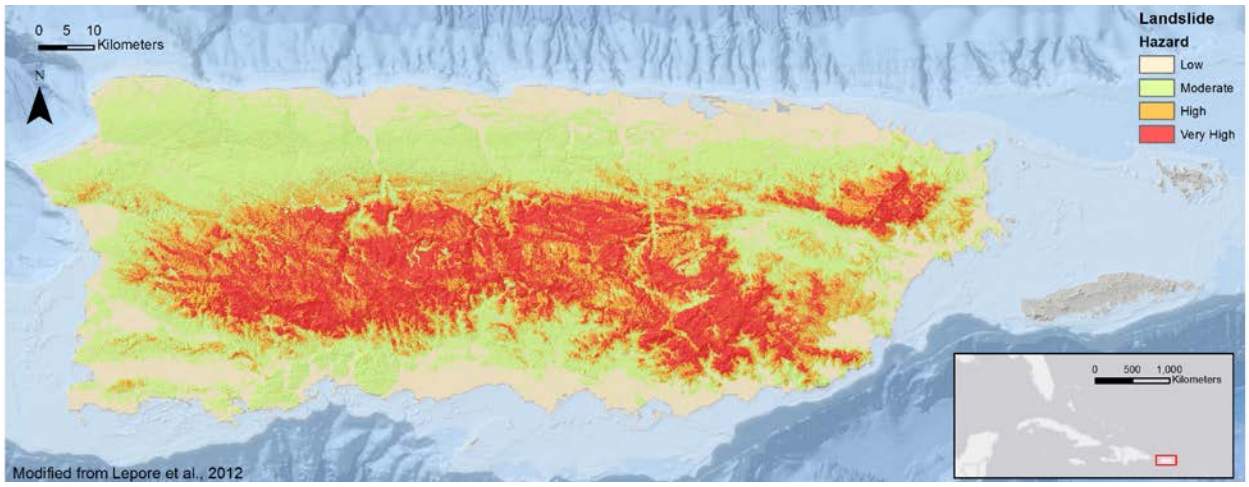

Figure 2-4: Landslide susceptibility map (adapted from Lepore et al. 2012).

All major types of landslides affect PR, but rainfall-induced debris flows are by far the most abundant (Jibson, 1987; Larsen and Simon, 1993; Larsen and Torres-Sánchez, 1995; Larsen and Santiago-Román, 2001; Hughes and Morales Vélez, 2017). Rainfall-induced landslides have resulted in substantial property damage as well as the loss human life. At least 147 deaths caused by landslides have been reported in PR for events between 1960 and 1985 (Jibson, 1986; Jibson, 1989; Larsen and Simon, 1993). The Mameyes landslide triggered during the system that became Tropical Storm Isabel in October 1985 is the deadliest mass wasting disaster in United States history and claimed at least 129 lives (Jibson, 1986, 1989; Silva-Tulla, 1986). Economic loss due to landslide damage in PR is difficult to assess, but has been estimated, on the basis of NOAA records to be in the tens of millions of dollars during the 20th century.

A compilation of 75 rainfall-induced landslides between 1959 and 2003 compiled by Larsen and Simon (1993) and Pando et al. (2005) can be seen on Figure 2-5.

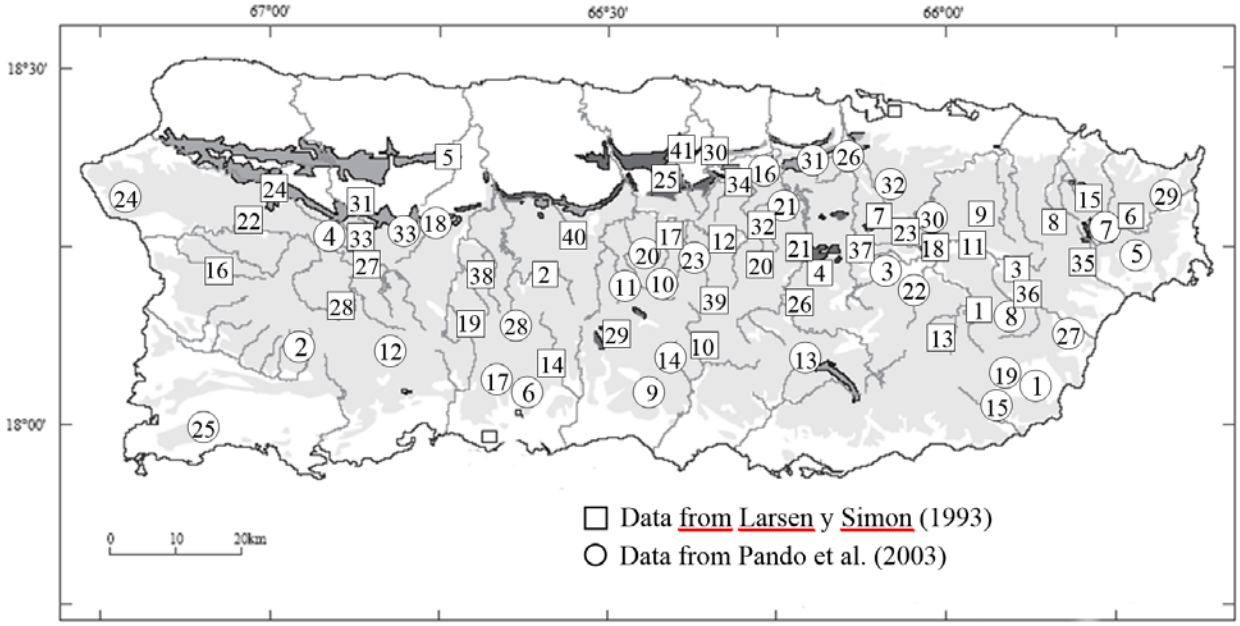

Figure 2-5: Location of inventoried rainfall-induced landslides between 1959 and 2003 (Pando et al., 2005).

The use of rainfall intensity thresholds for landslide occurrence and as a tool in landslide warning systems is popular worldwide (e.g., Wieczorek and Glade, 2005; Segoni et al., 2018). They are used to define the rainfall event conditions that when reached or exceeded are likely to trigger landslides. The landslide triggering rainfall threshold concept at a global level was first proposed by Caine (1980), where he hypothesized an empirical relation between rainfall characteristics in terms of duration and intensity and the occurrence of landslides to define a landslide triggering threshold. He developed the rainfall threshold in terms of a power-law that defined the lower boundary of 73 rainfall storm events (in terms of intensity versus duration) that triggered landslides in a variety of locations around the world. The dashed line and equation shown in Figure 2-6 represents the lower bound of the scattered data and defines the landslide rainfall-intensity duration threshold proposed by Caine (1980). Recognizing the global nature of these 73 storm locations included varying geologic and climatic characteristics, and despite limitations, rainfall thresholds have been widely used. Applicable to the study area of this GEER report, a regional rainfall threshold was proposed by Pando et al. (2005). The authors used a similar approach to Caine (1980) and, with a database of the 75 rainfall induced landslides shown in Figure 2-5, developed the preliminary landslide rainfall threshold for Puerto Rico shown in Figure 2-7. This rainfall threshold for landslide occurrence is a generalized regional threshold that is a reasonable first approximation for the general conditions of Puerto Rico, but no differentiation is made regarding important site-specific factors such as geologic and topographic settings, failure type and mechanism, human activity or land use, etc. Inclusion of these factors is very important for investigating site-specific landslides and their triggering mechanisms. Thus, it must be used with caution and for preliminary purposes.

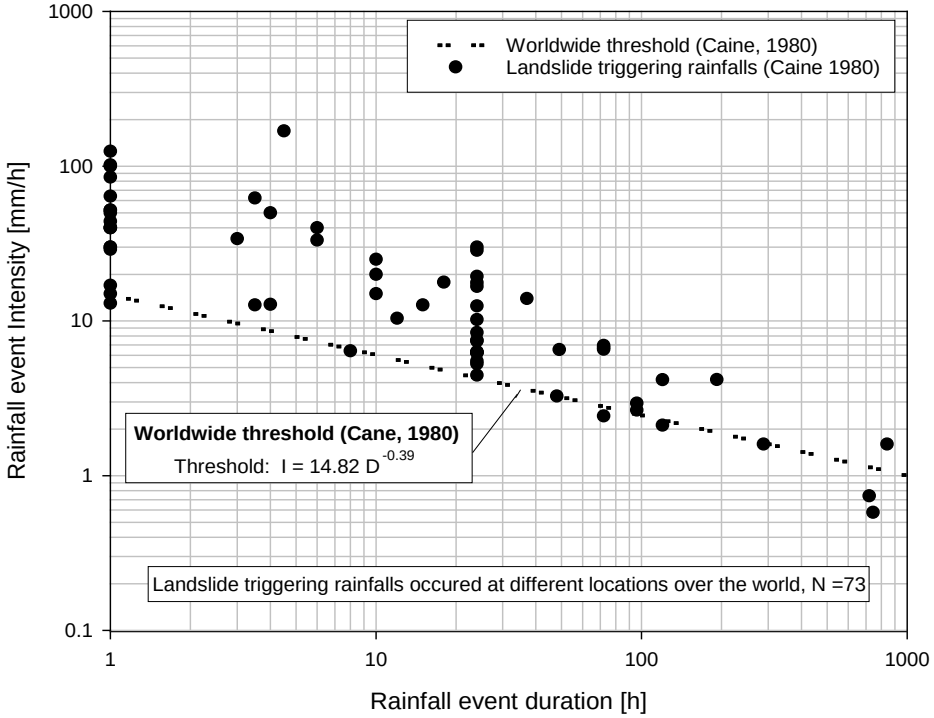

Figure 2-6: Worldwide rainfall-induced landslide threshold by Caine (1980).

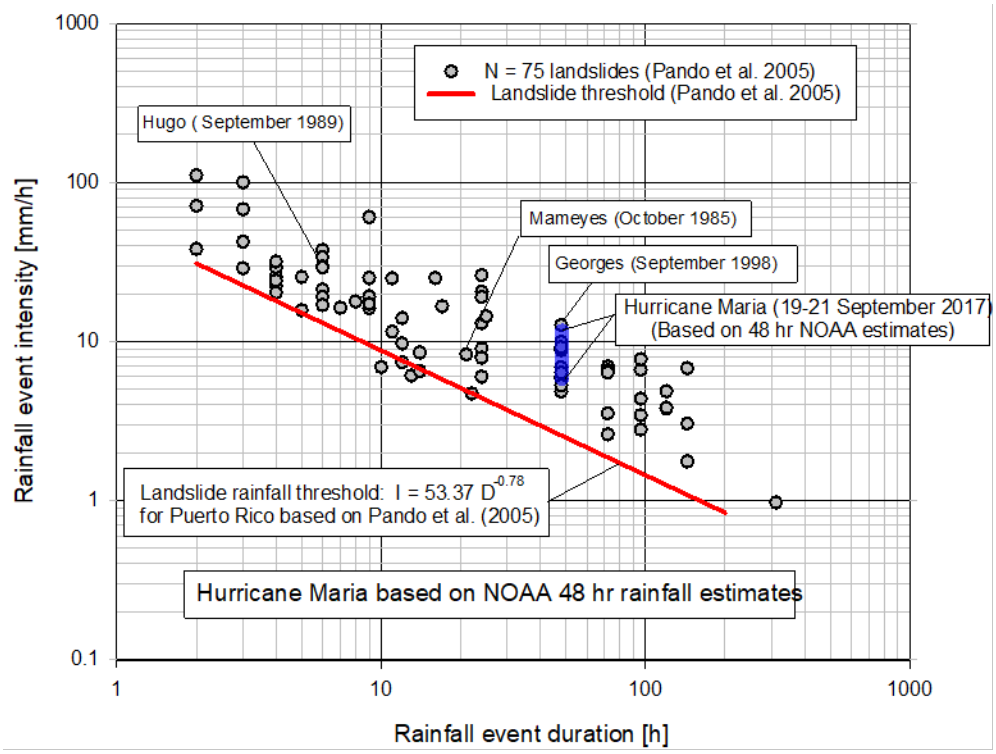

Figure 2-7: Puerto Rico rainfall-induced landslide threshold by Pando et al. (2005) and estimated rainfall event by Hurricane Maria.

The passing of Hurricane Maria destroyed most rainfall gauges; however, preliminary estimates by NOAA and the National Weather Service (NWS) are available for the period of 8:00 AM on September 19, 2017, to 8:00 AM on September 21, 2017, as shown in Figure 2-8. Based on the reported range of about 11 to 22 inches of rainfall for the municipalities most affected by landslides (see Figure 2-3), the 48-hour average rainfall intensity would range approximately from about 5.8 to 11.6 mm/hr. This range of rainfall intensity for Hurricane Maria, assuming a 48-hour duration, is shown on Figure 2-7 as a thick blue line. This estimated rainfall intensity and duration for Hurricane Maria falls above the preliminary landslide rainfall threshold, consistent with the many documented landslides recorded.

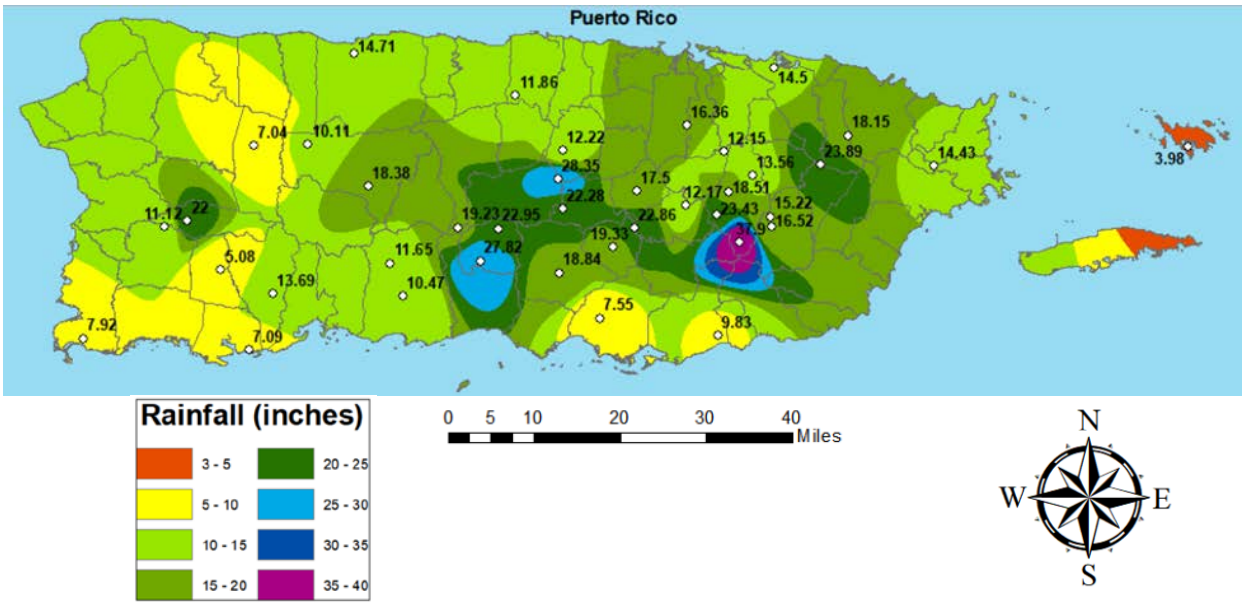

Note: NOAA and NWS Hurricane Maria estimated 48-hour rainfall from 8 AM AST Sep 19, 2017 to 8 AM AST Sep 21, 2017 [values in inches].

Figure 2-8: Rainfall estimates in Puerto Rico during Hurricane Maria (https://www.weather.gov/sju/maria2017; accessed March 2017).

A brief description of the failure mechanism usually involved in these types of failures is included, given the abundance of shallow rainfall-induced landslides following Hurricane Maria. Many of the pre-failure geometries of the landslide sites indicate the presence of steep slope angles that are often well beyond the anticipated shear strength of these soils. The suction-related effective stresses in unsaturated residual soils explain why slopes in these types of soils may be steep, and why failures occur in these slopes during intense rainfall as the degree of saturation of the soil increases (Terzaghi et al., 1996). Slope vegetation cover also plays an important role in the resulting amount of infiltration versus surface runoff during a rainfall event and can also contribute toward increased stability for extremely shallow failure mechanisms through the root systems (Wu et al., 1979). The failure mechanism is primarily associated with rainfall infiltration that increases the driving force through increased weight of the soil mass, and through a gradual decrease of the shear strength due to the loss of the suction-related effective stresses. Soil/water retention relationships show that important matric suction levels can be present within the structure of fine-grained residual soils when they have low moisture contents. The suction in the soil matrix translates into significant effective stress values, which explain the stable condition of many very steep slopes present in the topography of Puerto Rico. The factor of safety of a slope prior to a rainfall event is usually well above unity, indicating a stable condition from a deterministic perspective. Figure 2-9 shows site-specific rainfall data and the variation of the factor of safety for a landslide event in Hong Kong reported by Lan et al. (2003). As previously covered, at a particular site, the rainfall on the slope will infiltrate or become runoff depending on many factors such as slope geometry, geotechnical conditions, vegetation cover, wind, etc. The authors used hydrogeology and geotechnical models to predict infiltration and the slope stability factor of safety during the rainfall event. Figure 2-9 shows how the factor of safety decreases with time in relation to the rainfall intensity event. The decrease of the factor of safety is related to

increase of in-situ moisture content values, thus increasing the driving forces, and decrease in the available shear strength of the soils within the slope due to loss of suction and the associated effective stresses. In summary, for most residual soil slope sites, it is possible to find a rainfall event of sufficient duration and intensity that can decrease the factor of safety to unity.

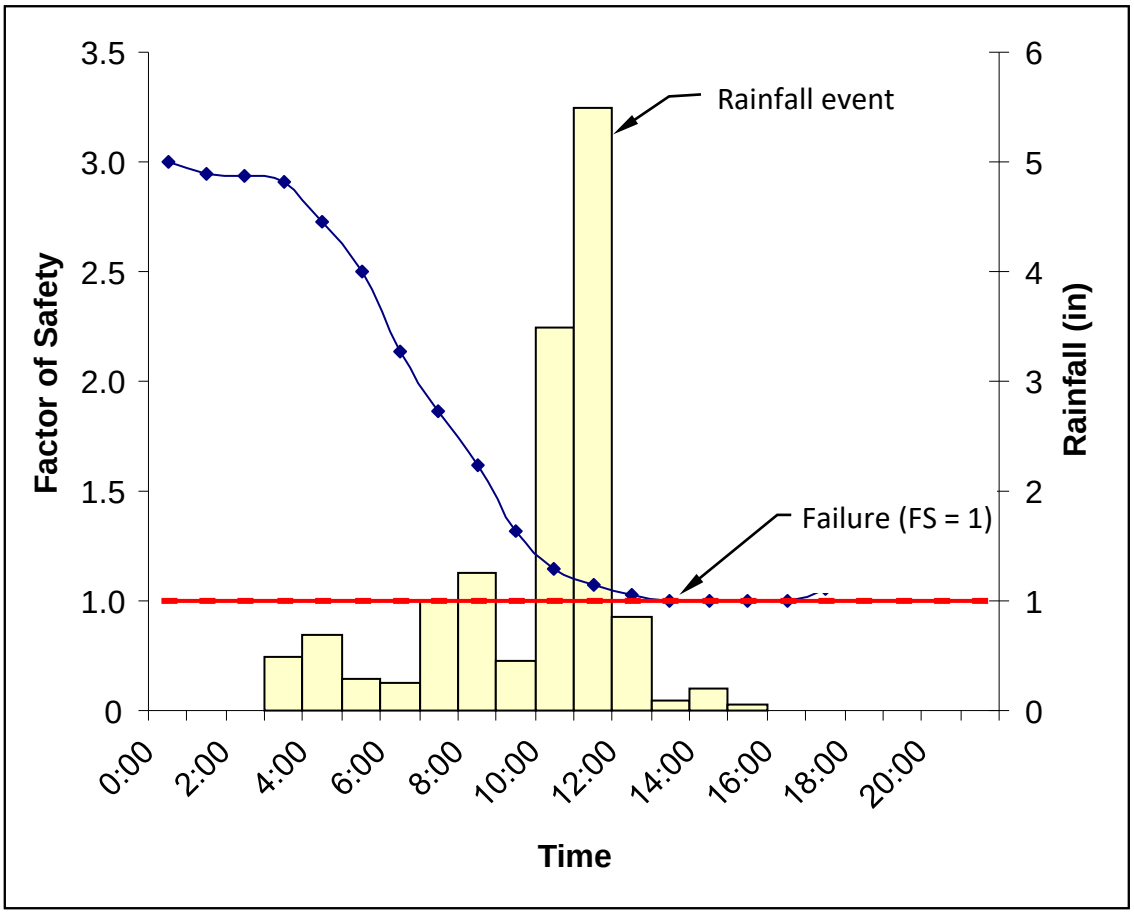

Figure 2-9: Variation of slope stability factor of safety during a rainfall event (from Lan et al., 2003).

2.3 Summary of Sites and Main Mechanisms of Failure

The majority of the slides shown on Figure 2-2 were shallow debris flows. Appendix A includes photos of landslides visited by the GEER team. The following sections describe select landslide sites visited by the GEER team. It should be noted that this section does not include failures involving mechanisms associated with road design or culvert blockage, as this is discussed in Section 5.

2.4 Select Landslide Cases

In addition to the Guajataca Dam spillway, two additional sites were targeted with the Terrestrial LiDAR Scanner: one of the largest debris flow sites caused by Hurricane Maria located along Puerto Rico State Road 4131 (PR-4131) near the Rio Blanco River in the

municipality of Lares and a pre-existing deep-seated failure along new construction of PR-9 in the municipality of Ponce that did not appear to re-activate during Hurricane Maria. These two landslide sites are described in the following sections.

2.4.1 Debris Flow on PR-4131, Lares

To our understanding, this site is the third largest failure after two other debris flows caused by Hurricane Maria on PR-143 in Barranquitas and PR-191 in Naguabo, respectively. All three sites were noted as points of emphasis by FEMA as recently as March 2018 (Beauchamp, 2018). According to eyewitness accounts, this debris flow (Figure 2-10) is responsible for destroying three houses. Witnesses indicated that the inhabitants of those homes were not present during the hurricane. The site lies on the steep northern bluff of the Rio Blanco River in Barrio Pezuela in the central area of the municipality of Lares. The Rio Blanco River joins the Rio Prieto River a few kilometers west, and they collectively form the Rio Grande de Añasco River that empties into the Bahia de Mayagüez. The Rio Blanco and Rio Grande de Añasco rivers are marked by very steep and short northern tributaries, and both follow the general trace of the Cerro Goden Fault, a part of the much larger Great Southern Puerto Rico Fault Zone.

Figure 2-10: Photo taken by the Civil Air Patrol on October 15, 2017 of the PR-4131 debris flow site (Lat: +18.247885, Lon: -66.882794).

The failure initiated just above the highest road cut on a switchback along PR-4131 (not PR-431 as often erroneously referenced by other reports; the road was recently re-designated as PR-4131 before Hurricane Maria's landfall). The upper area is the primary area of volume loss; in fact, the lower portion of the road was not lost, only covered by debris from above. The

liberated hillslope material was delivered directly to the fluvial system below. Much of the small- to medium-sized sediment was carried downstream by the river on September 20, 2017, and in the following days; however, a toe of large boulders remained at the site. Aerial imagery of the landslide site before and after Hurricane Maria are shown on Figure 2-11.

Note: Upper image from before Hurricane Maria. Lower photo captured by FEMA on October 12, 2017. The location of our January 2018 TLS scan position (Lat: +18.247885, Lon: -66.882794) is shown as a white circle with black center dot on the south bluff of the river.

Figure 2-11: Large debris flow site on PR-4131 in central Lares along the Rio Blanco.

In January 2018, members of the GEER team conducted both TLS and drone photogrammetry surveys at this site (Figure 2-12 and Figure 2-13). The purpose of these surveys is to provide DEMs that can be used for volume change detection (Figure 2-14).

Note: Notice a new primitive access road that has been developed by local residents with 4-wheel drive vehicles. Other detours around the site add an additional half hour to a normally 15-minute drive to essential services available in the small city of Lares. Notice the toe of the debris flow that has re-routed the flow of the Rio Blanco River.

Figure 2-12: Photo taken by GEER team in January 2018 of the PR-4131 debris flow site (Lat: +18.247885, Lon: -66.882794).

Figure 2-13: Photo showing January 2018 TLS survey position (Lat: +18.247885, Lon: -66.882794).

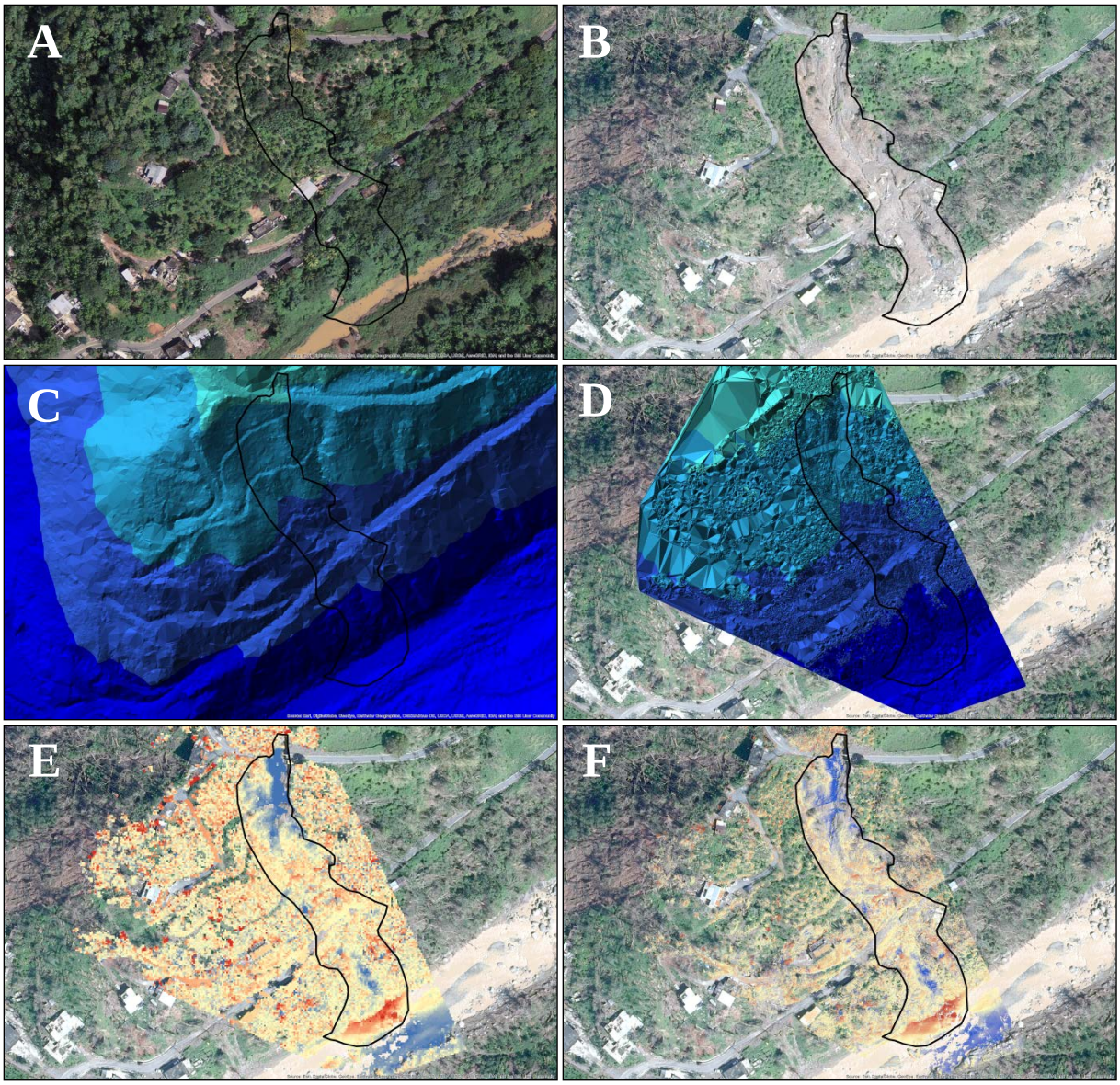

A) PR-4131 debris flow site before Hurricane Maria. **B)** PR-4131 debris flow site on October 12, 2017. **C)** Shaded relief map of the same area created with classified ground point data from a 2016 airborne LiDAR survey. **D)** Digital surface model of the site created with data from Terrestrial LiDAR Scan survey in January 2018. Compare the footprint of the model with the position of the scanner shown in Figure 2-13. **E)** One-meter resolution change raster from 2016 to January 2018; blue areas indicate volume loss, red areas indicate volume addition, and beige areas show no major change. Point clouds were aligned using Cloud Compare software. **F)** Ten-centimeter resolution change raster for the same time span. Key features to note are the loss primarily in the head scarp, a small zone of loss in the center-west of the site that reflects a house that was destroyed by the debris flow, a scour channel in the lower center of the site, a toe area of large boulders, and a zone of loss on the southern bank of the river, likely the result of a forced shift in the river's course around the toe.

Figure 2-14: Images from LiDAR PR-4131 debris flow site.

2.4.2 Assessment of preexisting landslide at PR-9 north of City of Ponce

To the north of the city of Ponce and along PR-9 is a large deep-seated block failure (Lat: +18.032, Lon: -66.636), that initially failed well before Hurricane Maria. This site is important because it is located in the Juana Diaz Formation, the same unit that failed during the nearby Mameyes landslide disaster of 1985. Drs. Hughes and Morales Vélez visited this site in June of 2017 (Figure 2-15).

Note: Photo taken June 2017. Shaded areas are netting features originally intended to prevent surficial erosion.

Figure 2-15: Aerial image showing pre-Maria condition of preexisting landslide at PR-9 north of Ponce(Lat: +18.033145, Lon: -66.637579).

As part of the GEER mission, this pre-exiting landslide site was visited to by the GEER team on October 31, 2017. No observable changes were noticed with respect to the pre-hurricane condition in June 2017. To further confirm this, the GEER mission performed TLS and drone surveys in January 2018. These surveys were performed to generate data, which will be available for updated DEMs that can be used to confirm that no additional ground displacements have occurred at this site after Hurricane Maria. A photo from FEMA, taken in October 2017, is shown on Figure 2-16. This photo shows the location of the TLS instrument used during the January 2018 survey. The TLS instrument is shown in Figure 2-17.

Note: Position of TLS survey in January, 2018 (Lat: +18.033145, Lon: -66.637579) shown as white circle with center black dot. Shaded areas are netting features originally intended to prevent surficial erosion. FEMA photo from October 9, 2017.

Figure 2-16: Post-Maria condition of preexisting landslide site at PR-9 north of Ponce.

Figure 2-17: January 2018 TLS survey position at PR-9 landslide site (Lat: +18.033145, Lon: -66.637579).

A photo of the toe of the landslide is shown in Figure 2-18. In summary, at this site field observations and measurements by the GEER team did not reveal any movement or activation of this preexisting landslide. However, surface erosion is evident, which could lead to altered geometry that could change the stability of the site.

Figure 2-18: Photo of Toe of PR-9 landslide in January 2018 (Lat: +18.033145, Lon: -66.637579).

3 DAMS

3.1 Introduction

The GEER team visited five dam sites during the reconnaissance visit, namely Guajataca, Prieto, Dos Bocas, Caonillas, and Guayabal Dams. All were concrete dams, except Guajataca which is an earth dam. Generally, the dams and their auxiliary structures performed satisfactorily, with the exception of the spillway at Guajataca, which was severely damaged. Concerns about Guajataca Dam prompted the evacuation of about 70,000 people downstream.

Since Hurricane Maria was preceded about 10 days earlier by Hurricane Irma, the degree of saturation of many slopes had increased when Maria made landfall. Hence, the soil around tree roots was generally wet and soft in the hillsides, when the strong winds of Hurricane Maria affected the island. The high degree of saturation facilitated tree uprooting and enhanced erosion, surficial failures, debris flows, and scour. As a result, the dam reservoirs received large volumes of sediments and debris, as evidenced by the dark brown color of the water and debris along the shore in Figure 3-1.

Figure 3-1: Debris along the upstream face of the gravity dam at Lago Dos Bocas. Compare the dark brown color of the water in the reservoir to the historical blue color (before Maria) (Lat: +18.27691, Lon: -66.6561).

3.2 Guajataca Dam

3.2.1 History

Guajataca dam is an earthfill dam built in the 1920's, mostly by hydraulic fill methods, and modified in the 1980's. According to the National Inventory of Dams (USACE, 2016) it was designed for and owned by the Puerto Rico Electric Power Authority (Figure 3-2). A report by the United States Department of Interior Bureau of Reclamation (USBR) dated June 2002 provides a detailed description of the history and construction of the dam, as well as some of its plans and cross-sections (e.g., Figure 3-3).

Figure 3-2: Photo of Guajataca Dam taken a few decades before Hurricane Maria (date of photo is unknown).

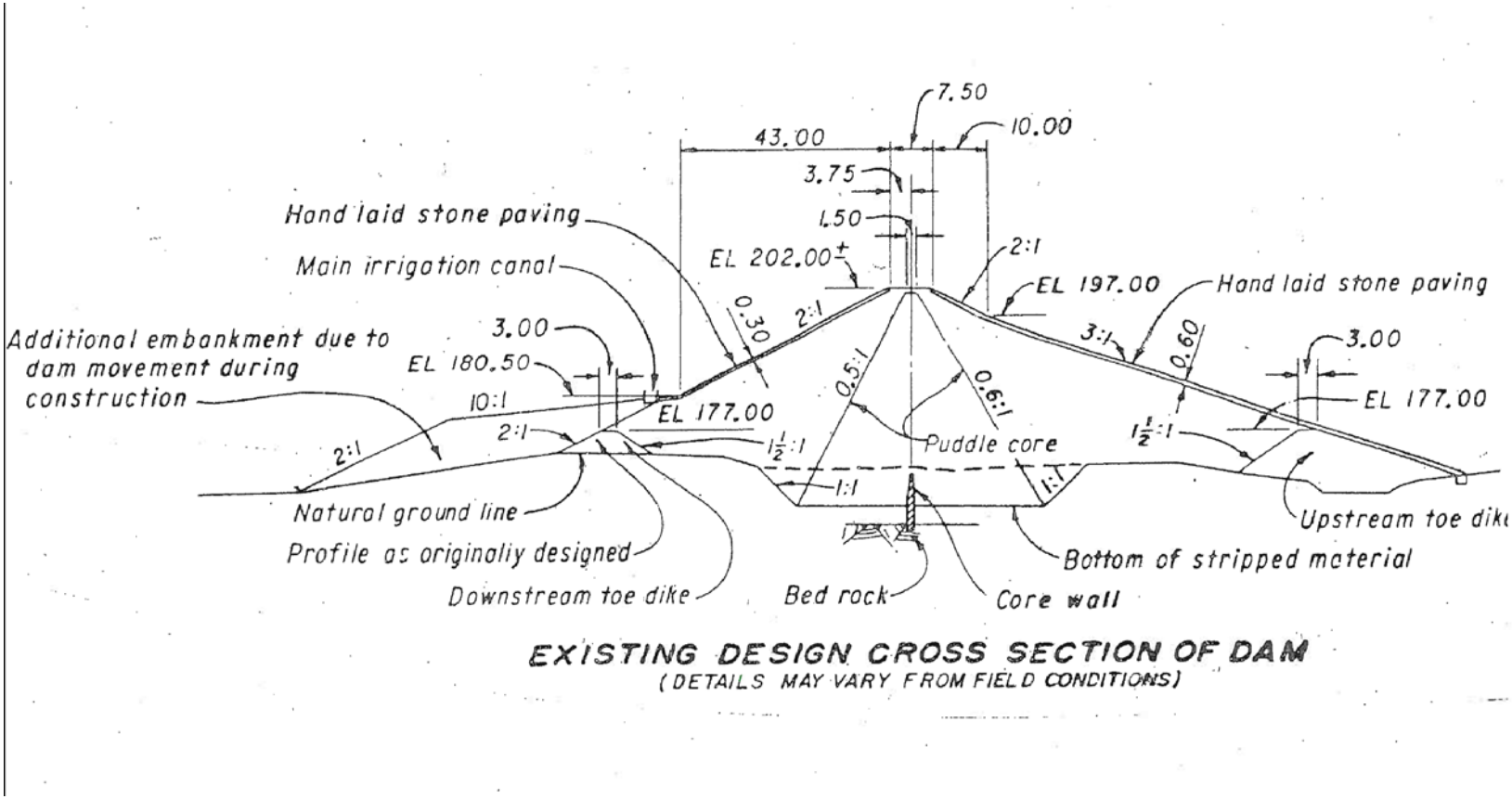

Figure 3-3: Cross-section of Guajataca Dam from the 1920's (date of drawing is unknown).

The dam is reportedly about 37 m (121 feet) high (along the original streambed) and has a crest 316 m (1,037 feet) long and 9.5 m (31.2 feet) wide. Its upstream and downstream faces slope at ratios of 2:1 (horizontal to vertical [H:V]) or flatter. The dam normally operates with a minimum freeboard of 5.5 m (15 feet).

The dam was reportedly authorized under the Isabela Public Irrigation Law on June 19, 1919, by the Government of Puerto Rico and built between 1924 and 1929. A cross-section from the 1920's (Figure 3-3) shows the following features:

- A "puddle clay" core sloping at ratios of 0.5 to 0.6 to 1 H:V;
- A small concrete core wall (cutoff) was built in 1926 and appears to have only minor embedment into the bedrock; and
- Hand-laid stone paving on both upstream and downstream faces.

Records suggest that a large part of the dam consists of hydraulic fill, but its limits are unclear. For example, Figure 3-3 describes the center of the dam as a "puddle core", but a June 2002 USBR report suggests that the hydraulic fill process left the coarsest fill materials near the dam faces and the finest in the core area; the same report indicates that fill placement was changed to "dry" roller compaction in 1927.

In February 1927, during the initial construction of the dam, a crack as well as slippage was observed on the downstream side of the dam. In the ensuing days, additional cracks (5 cm [2-inches] or wider) and signs of movement (including bulging and settlement of the cofferdams) were observed. Reportedly, movements were noted in many locations on both the dam and the downstream natural ground, and maximum movements included a 0.96 m (3.2 feet) downstream deflection and 1.44 m (4.7 feet) of vertical settlement. In an attempt to stabilize the dam, which was experiencing sliding in a downstream direction, the reservoir was drained, a remedial berm was constructed on the downstream side of the dam (as shown in Figure 3-3), numerous drain holes were installed, and the fill placement was changed to "dry" roller compaction. As construction proceeded, new movements of up to 35cm (14 inches) were reported on the upstream face and a heel was installed (location unknown). In November 1927, as the dam was nearing completion, movements were observed and reported as "creep-type". To enhance stability, fill was placed at the toe of the dam.

Crest movements were measured during the years following completion. Movement varied from about 35 cm/year (1.1 feet/year) between 1927 and 1929 to about 1cm/year (0.4 inches/year) between 1942 and 1951. In 1954 about 2,000 m^3 were added to the crest to restore its original elevation.

In 1971, the USBR was requested to evaluate the dam and, in 1977, it recommended various remedial measures including rebuilding the crest and replacing part of the spillway. As an excavation near the toe of the spillway was being performed in 1981, movement of the spillway occurred. The excavation revealed a plastic layer with slickensides, and a more detailed investigation was performed, which resulted in landslides being mapped under the spillway and dam. To increase the stability, it was recommended to limit the elevation of the downstream face berm (Figure 3-3) and to fill, or buttress, the river channel area. The work included the placement of a 2.44-m (96-inch) diameter pipeline to carry outlet flows that was completed in 1984. The river is no longer visible in Figure 3-2, which indicates that it was taken after the 1980's improvements were completed.

Between 1992 and 1993, instrumentation consisting of seven inclinometers (labeled I-1 to I-7 in Figure 3-4) was installed (three along the crest, one over the buttress, and three downstream of the toe; Figure 3-6). Three of the four inclinometers installed on the buttress and downstream of the dam became inoperable within 10 years of their installation due to landslide movement. Although these inclinometers were not completely sheared by 2002, we understand that they currently are. Movement was reported to our team to have occurred at a depth of about 19 m (elevation 170 m), where a layer of green clay is present that slopes at an angle of about 4°. The piezometers do not appear to be present in Figure 3-2 and Figure 3-7, and their appearance suggests they are contemporaneous with the slope indicators, (i.e., installed in the early 1990's).

During Hurricane Maria, the spillway experienced significant damage (Figure 3-13), as described in a separate section below, which prompted emergency remedial measures, concerns voiced by authorities, and the evacuation of about 70,000 residents located downstream of the dam. The maximum reservoir elevation that resulted from Hurricane Maria is unknown.

3.2.2 Seepage and Internal Erosion

Aerial photographs taken during emergency repairs show circular features at the surface of the fill blanket located near the toe of the dam. These features have the distinct appearance of sand boils and suggest that subsurface materials were affected by internal erosion. Although the seepage path and source of the eroded materials are unknown, underseepage should be expected since the depth of embedment of the 1920's core/cutoff wall (shown in Figure 3-3) is extremely small, and the wall may have been affected locally by historical landslide movement in a differential manner.

The surface of fill blanket downstream of the dam is generally level, and surface water tended to accumulate within low spots during our visit. Although the piezometers had been covered, we observed water, soil, and other debris in the casings (Figure 3-10), which would be consistent with a recent spike in groundwater pressures. Furthermore, a large void, approximately 30 centimeters in diameter and located 10 m downstream of the toe and

directly downstream of the "A" of the AEE sign on the downstream slope, was noted during the team's visit. Note that excavations, structures, poles, and/or post were not reported or visible in aerial photographs at/near the location of the reported cavity. Hence, it is likely that the void was either created or exacerbated by underseepage resulting from the high hydraulic head caused by Hurricane Maria.

3.2.3 Spillway damage

Aerial photographs indicate that the spillway was apparently in good condition as of March 2017 (Figure 3-8) and suffered significant damage as a result of Hurricane Maria. Figure 3-8 shows that about 100 m (300 feet) of spillway was completely destroyed (roughly 40 m of concrete and 60 m of riprap), and that an additional 25 m of concrete spillway was significantly undermined and displaced (Figure 3-13). A siphon located under the spillway (Figure 3-4, Figure 3-11, and Figure 3-12) was also destroyed. Aerial photographs taken during the aftermath of Hurricane Maria show water spilling out of the upstream side of the siphon (on the north side of the spillway), indicating that the siphon was operational during Hurricane Maria. Scour depths below the spillway could not be measured since the area had already been partly filled, but the scour was massive.

The spillway was equipped with aeration pipes to mitigate cavitation damage of the concrete (Figure 3-14). The concrete and aeration pipes were observed to be in good condition in the upper 100 m of spillway. A section of the concrete spillway about 25 m long and located at a distance of about 100 m from the top of the spillway, was observed to have moved on the order of 1.5 m in the downstream direction and was severely undermined (Figure 3-13 and Figure 3-15). The small scarp shown in Figure 3-16 is consistent with local withdrawal of lateral support resulting from nearby scouring along the alignment of the spillway. A grab soil sample collected from the exposed scarp was found to have a USCS classification of GC (See Sample F in Appendix I). We did not observe movement consistent with the reactivation of the ancient landslide; instead, our observation strongly suggested that the failure of the spillway resulted from scour starting at the base of the spillway and progressing retrogressively upwards. We did not find indications that the aeration system contributed to the damage; however, it is likely that failure of the siphon provided an influx of water that exacerbated erosion in its vicinity. The presence of landslide materials under the spillway likely increased its vulnerability to scour.

3.2.4 Dam and Other Structures

During our site reconnaissance, a team of surveyors measured the alignment of the crest and reported that their measurements were roughly identical to those they had performed before Hurricane Maria. Although a crack was reported in the press (near the left abutment on the asphalt road along the crest of the dam), the team did not observe any indication of adverse movement along the crest of Guajataca Dam or along the top of the berm (Figure 3-17). Similarly, we did not observe adverse hurricane-related effects on the dam's auxiliary hydraulic structures.

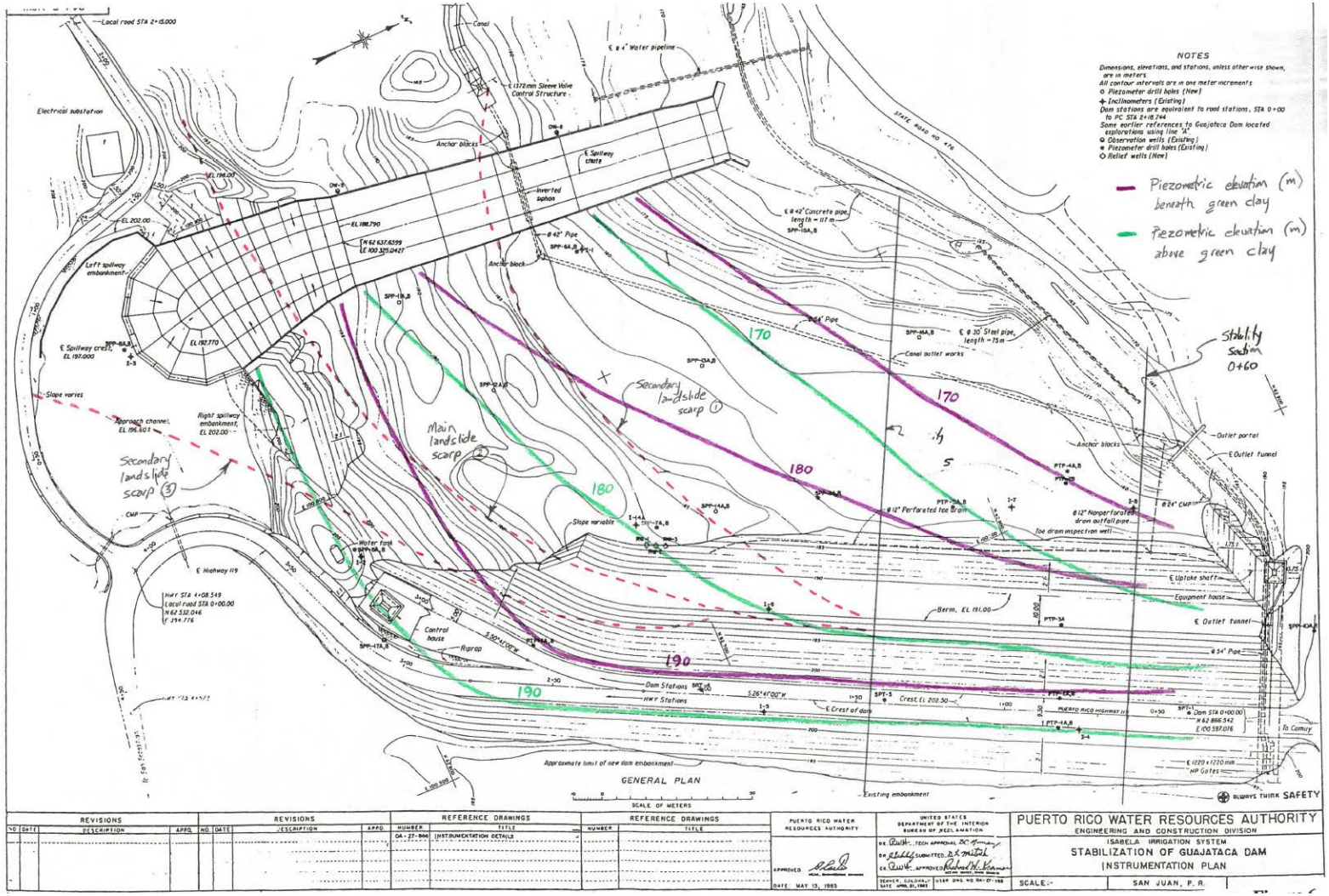

Figure 3-4: Landslide and outlet map from 1983.

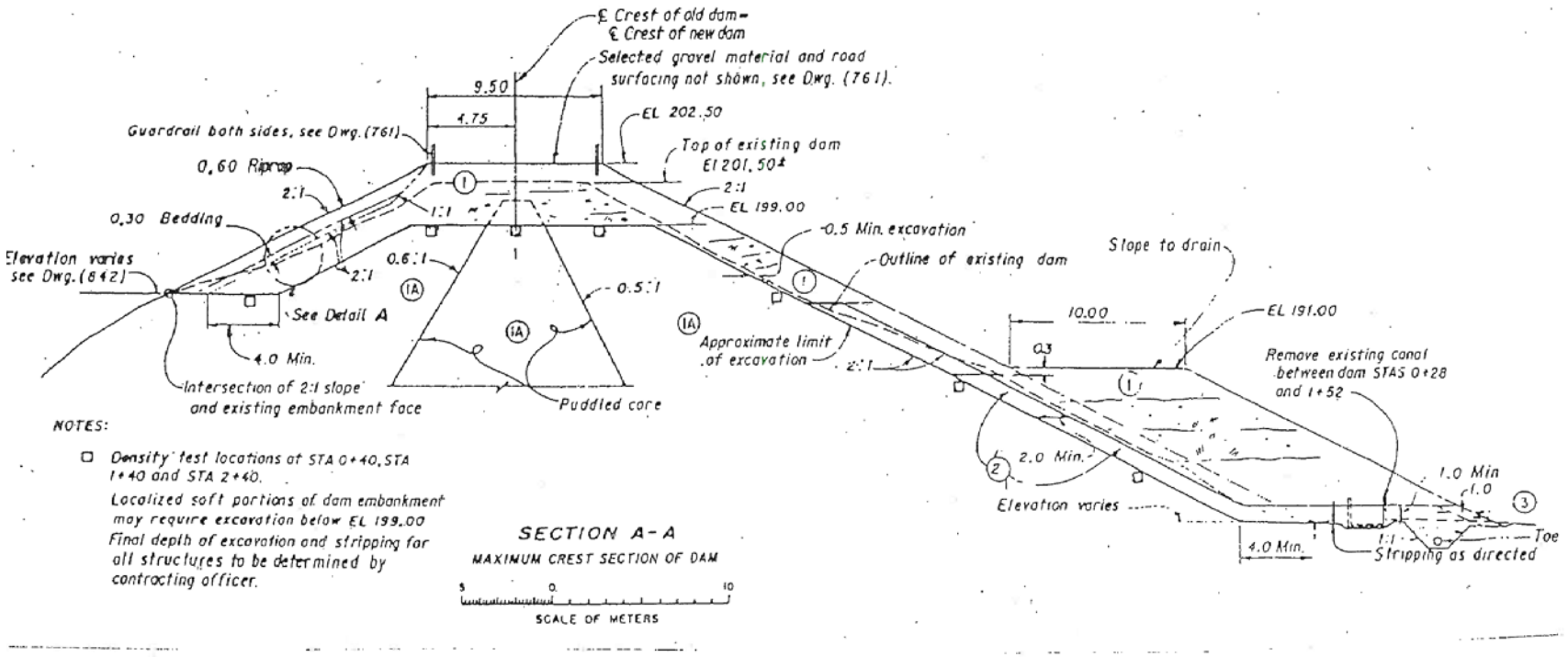

Figure 3-5: Cross-section of Guajataca Dam including 1980's remedial recommendations (date of drawing is unknown).

Figure 3-6: Instrumentation of Guajataca Dam (piezometers and slope inclinometers) (Lat: +18.39717, Lon: -66.92759).

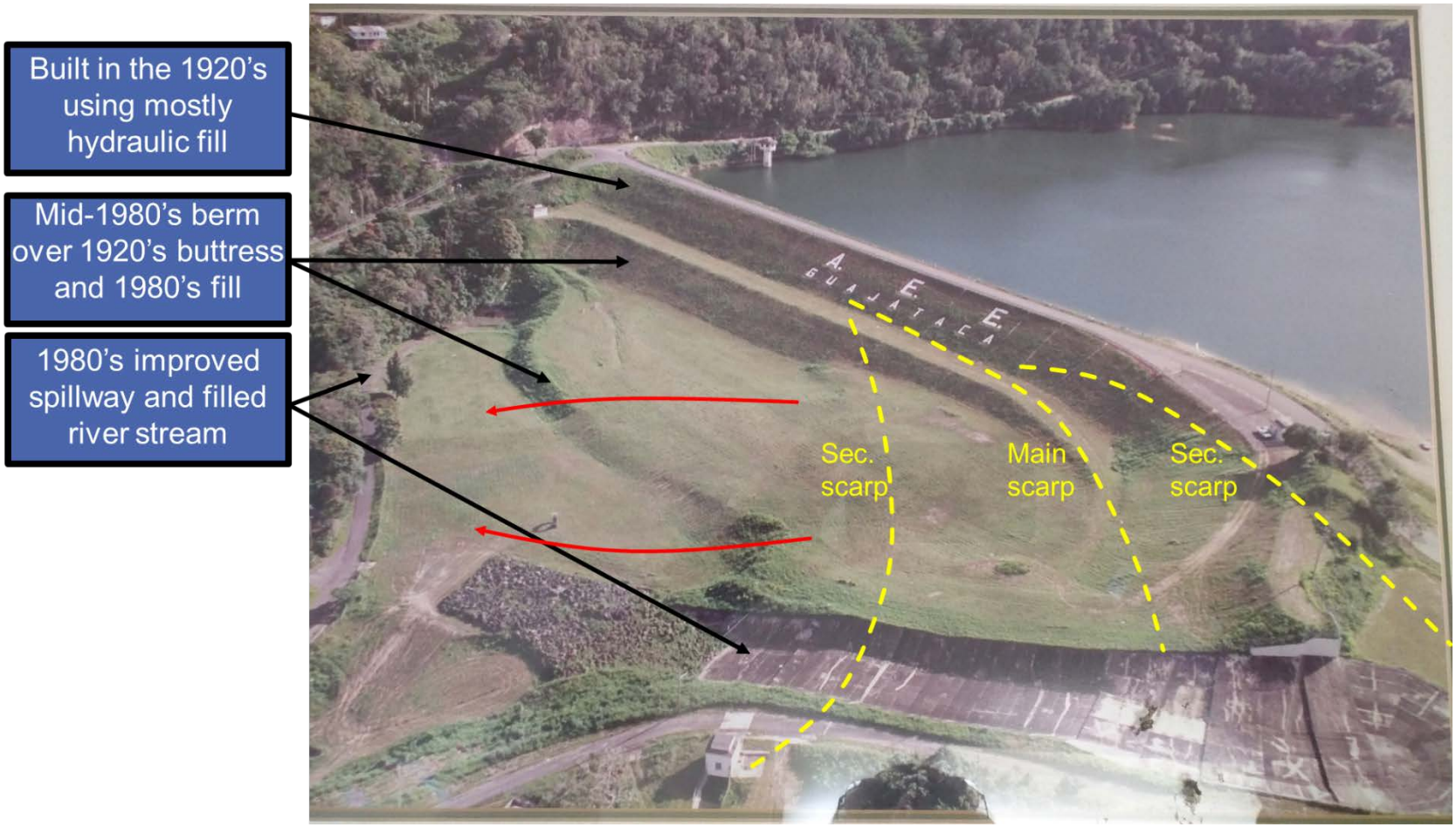

Figure 3-7: Oblique aerial photo with indication of historical and landslide features (Photo provided by AEEPR).

Figure 3-8: Comparison of condition between March and November 2017.

Note: Yellow arrows show location of sand boils downstream of the dam toe.

Figure 3-9: Sand boils downstream of the dam toe (photographs from the Pennsylvania National Guard).

Figure 3-10: Water and debris in piezometer (Lat: +18.397658, Lon: -66.924462).

Figure 3-11: Location of 54-inch water line and siphon structure under the spillway.

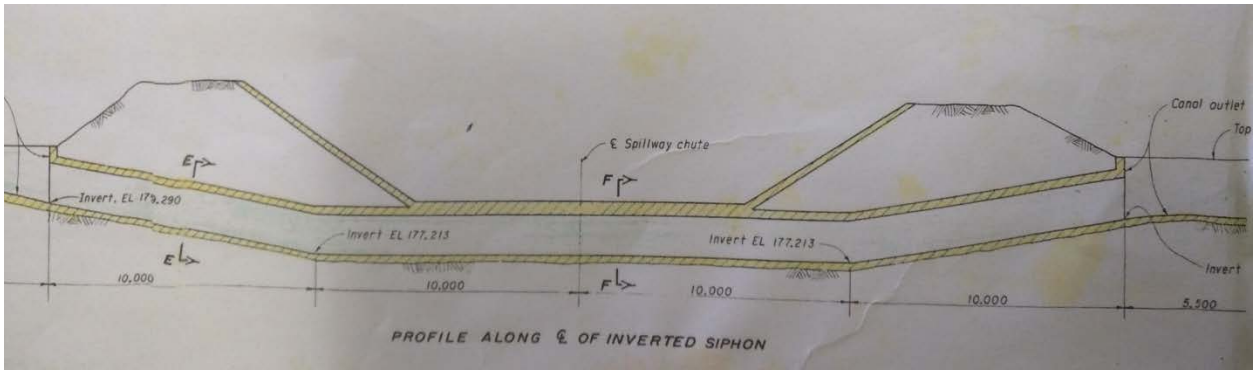

Figure 3-12: Siphon structure under the spillway.

Figure 3-13: Damaged spillway (Lat: +18.39724, Lon: -66.92554).

Figure 3-14: Spillway aeration pipes (Lat: +18.39684, Lon: -66.92561).

Figure 3-15: Displaced and damaged spillway (Lat: +18.39707, Lon: -66.92535).

Figure 3-16: Scarp adjacent to the spillway (Lat: +18.39702, Lon: -66.92540).

Figure 3-17: Dam crest (Lat: +18.39733, Lon: -66.92374).

4 COASTAL AND RIVER EROSION AND SCOUR

4.1 Coastal Erosion at Rincón, Puerto Rico

4.1.1 Introduction and Background

The beaches along the coastline near the town of Rincón have been affected by coastal erosion for decades (Thieler et al., 2007; Barreto et al., 2017). The town of Rincón is located on the west coast of Puerto Rico as shown in the highlighted area of the Puerto Rico map on Figure 4-1. It is located west of Añasco and Aguada, and it has approximately 13.26 km of total coastal length, of which 10.55 km is beach facing the Atlantic Ocean to the north and the Caribbean Sea to the south (Barreto et al., 2017). The major economy of Rincón is tourism-based, and the town is known for its beautiful beaches and as an international surfing destination. Hotel resorts, beach properties, vacation rentals, and regular housing can be found along the shoreline and at varying setback distances (from about 1 meter to 10 or more meters).

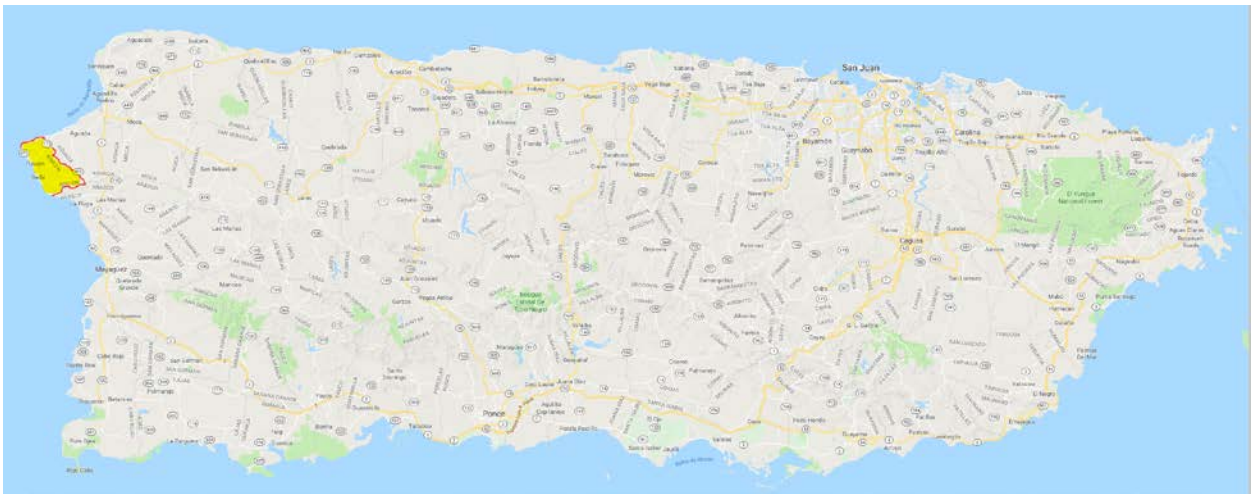

Figure 4-1: General location of town of Rincon.

Thieler et al. (2007) conducted a study to investigate the shoreline changes in Rincón between 1936 and 2006. The study included evaluation of approximately 8 km of shoreline divided into the four reaches shown on Figure 4-2. Rincón beaches are composed primarily of carbonates and marine deposit material. Thieler et al. (2007) reported that, in general, the study area shoreline that extends from Punta Higuero to Punta Cadena in Rincón is experiencing long-term erosion. The coast of Reach A, from Punta Higuero to the north end of the Balneario de Rincón, is fairly stable and has a long-term (70 year) average erosion rate of -0.2 ± 0.1 m/year (negative sign denotes loss of beach). The coast of Reach B, from the Balneario de Rincón to 500 m south of the mouth of Quebrada los Ramos, has an average long-term erosion rate of -1.1 ± 0.3

m/year with an observed increasing trend during 1977 to 1987. The coast of Reach C, from 500 m south of the mouth of Quebrada los Ramos to Córcega, has an average long-term erosion rate of -0.4 ± 0.2 m/year. Finally, the coast of Reach D, from Córcega to Punta Cadena, has an average long-term change rate of -0.2 ± 0.2 m/year. Thieler et al. (2007) suggested that there are several factors contributing to the observed high rates of erosion in Reach B including marina construction, complex wave patterns, and sand removal from the beach system. According to Thieler et al. (2007), the sea level rise, based on the simulation by the Intergovernmental Panel on Climate Change (IPCC) could be 0.6 m (Bindoff et al., 2007) or as high as 1 to 2 m (Overpeck et al., 2006; Hansen et al., 2007; Rahmstorf, 2007; Rahmstorf et al., 2007) by the year 2100. The projected sea level rise is expected to further increase the rate of erosion in the shoreline of Rincón.

The USGS conducted a number of measurements during and after Hurricane Maria (Figure 4-3). Several sensors were lost or damaged. There was no storm tide sensor available in Rincón as shown on Figure 4-3, and most of the storm tide sensors were located in the south or southeast of portion of PR or near San Juan. Table 4-1 lists data from the storm tide sensors available during Hurricane Maria. Figure 4-4 presents the maximum storm tidewater elevation above the datum of approximately 8 feet (2.44 m) recorded by the storm tide sensor located near San Juan. The only data available for Rincon is the high water elevation of 51.43 feet mark recorded at a local residential building located at latitude and longitude of 18.3155, -67.2246, respectively. The reported height of water above the ground surface at this location was 1.13 feet (0.34 m).

This report includes field observations conducted on November 3, 2017, at three sites in Rincón, shown on Figure 4-5. Site 1 is located within Reach D and Sites 2 and 3 are located within Reach C as defined in the Thieler et al. (2007) study.

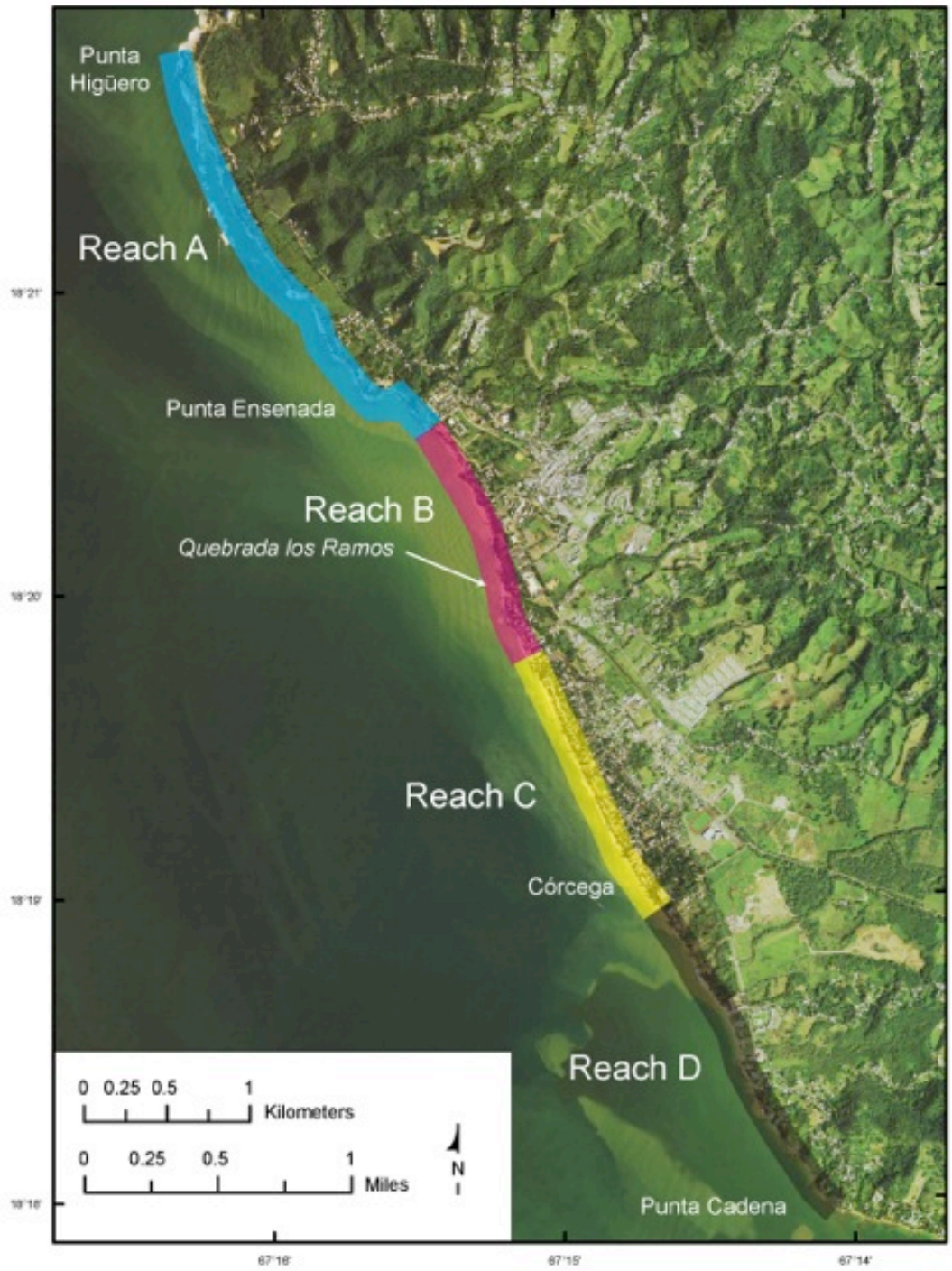

Figure 4-2: Rincon Shoreline Study Area by Thieler et al. (2007).

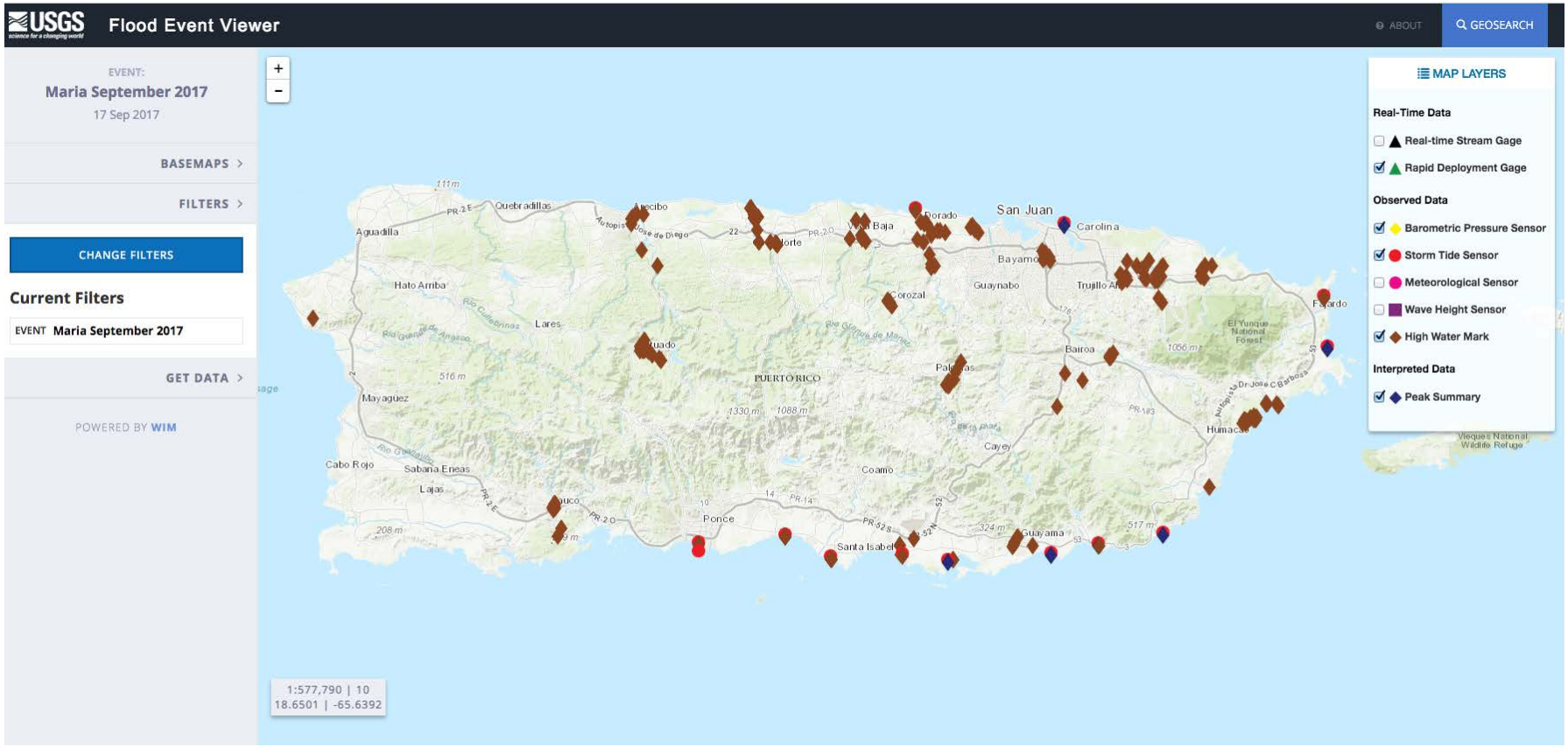

Note: USGS Flood Event Viewer for Hurricane Maria (https://stn.wim.usgs.gov/fev/#MariaSeptember2017). Link provides data shown for the only high water mark recorded near Rincón, PR (1.13 ft above ground) shown in Table 4 1.

Figure 4-3: USGS Flood Event Viewer for Hurricane Maria.

Table 4-1: High Water Mark Data, Rincón, PR.

HIGH WATER MARK | MARIA SEPTEMBER 2017	
STN Site No.:	PRRIN23799
Elevation(ft):	51.428
Datum:	PRVD02
Height Above Ground:	1.13
Approval status:	Approved
Type:	Seed line
Marker:	Marker
Quality:	Good: +/- 0.10 ft
Waterbody:	QUEBRADAS LARGAS DACHE
County:	Rincon Municipio
State:	PR
Latitude, Longitude (DD):	18.3155, -67.2246
Description:	INSIDE SMALL CONCRETE SHED LIKE STRUCTURE IN BACKYARD OF RESIDENCE OF HOUSE NUMBER 7 ON STREET
Full data link:	HWM data page

Note: Data from https://stn.wim.usgs.gov/fev/#MariaSeptember2017.

Table 4-2: Water elevation measurements during Hurricane Maria.

Site ID	Location (latitude, longitude)	Maximum Storm Tide Water Elevation (feet above datum)
PRJUA22307	17.9897, -66.4820	4.24
PRARR22313	17.6919, -66.0643	3.93
PRCEI22309	18.2702, -65.6304	4.21
PRDOR20633	18.4765, -66.2774	3.24
PRFAJ20587	18.3459, -65.6365	3.66
PRMAU22311	17.9913, -65.8889	4.26
PRPAT22312	17.9755, -65.9900	4.13
PRSAL22314	17.9515, -66.2264	3.84
PRSAN20648	18.4530, -66.0437	7.95

Note: Data from https://stn.wim.usgs.gov/fev/#MariaSeptember2017.

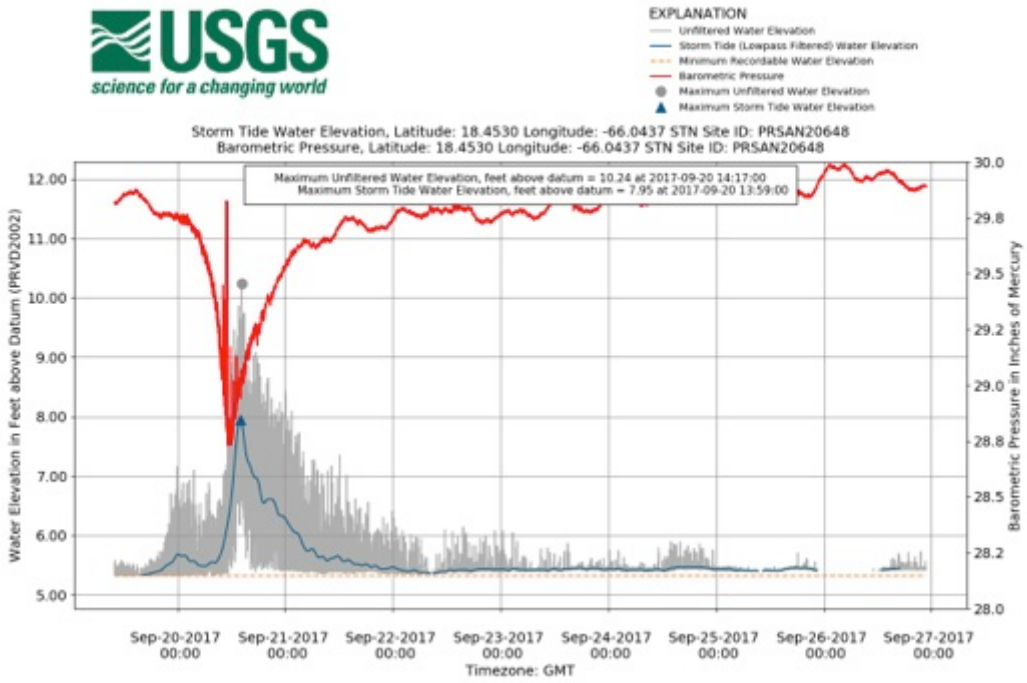

Figure 4-4: Storm Tide Sensor Near San Juan, PR (Lat: +18.4530, Lon: -66.0437).

4.2 Coastal Erosion Sites visited by the GEER team

The GEER team visited the six coastal erosion sites shown on Figure 4-5. These sites are labeled CE1 through CE6, and they are further described in the following subsections.

Figure 4-5: Location of coastal erosion sites visited by GEER team.

4.2.1 Coastal Erosion Site CE1: Punta Cadena

Two locations with evidence of coastal erosion associated to Hurricane Maria were found at Punta Cadena (Site CE1) in the municipality of Rincón. Site CE1 was visited by the GEER team on 11/3/17. The first location with coastal erosion of site CE1 is located at Punta Cadena in the south of Rincón near the old train tracks right-of-way. The site consists of a local one-lane asphalt pavement road supported by a seawall, which also serves as shoreline protection. An erosion scar approximately 167 feet long was observed behind the seawall (Figure 4-6). The slanted seawall, approximately 2 feet wide and 9 feet high, consists of cement/grout stabilized riprap rocks (Figure 4-7). Overall the wall had minor damage. The erosion behind the wall appeared to be caused by wave action, which also resulted in damage along the road shoulder.

Left photo (Lat: +18.30127, Lon: -67.23573, 2017.11.3, 08:04 AST); Right photo (Lat: +18.30155, Lon: -67.23589, 2017.11.3, 08:07 AST).

Figure 4-6: Erosion Scar at first location of Site CE1.

The second location with coastal erosion, within the general site CE1, is located approximately 300 meters north of the first location. At this second location, the coastal local one-lane road had a sinkhole-type failure as shown on Figure 4-8. The sinkhole resulted in road collapse parallel to the seawall and in front of a residential house. The dimensions of the void measured at the surface were approximately 7.01 meters (23 feet) long, 1.12 meters (3.7 feet) wide, and 1.83 meters (6 feet) deep. The height of the seawall at this location is about 2.74 meters (9 feet). Evidence of seepage through the seawall was observed at bottom of the sinkhole. It is likely that the storm surge or wave action caused the embankment material to wash out and erosion undermined the road.

Photo: Lat: +18.30167, Lon: -67.23601, 2017.11.3, 08:11 AST.

Figure 4-7: Seawall at first location of Site CE1.

Left photo: Lat: +18.30246, Lon: -67.23669, 2017.11.3, 08:22 AST; Right photo: Lat: +18.30254, Lon: -67.23678, 2017.11.3, 08:19 AST. Seepage through seawall observed at the bottom of the sinkhole.

Figure 4-8: Sinkhole and Road collapse at second location of Site CE1.

4.2.2 Coastal Erosion Site CE2: Calle Bastia Road

This site is located at the Córcega Beach in Rincón, and it is accessed by Calle Bastia. It consists of two buildings: one to the north and one to the south of the beach access as shown on Figure 4-9. The north building (Building A) is a residential apartment complex and the south building is a residential house. Severe damage of a perimeter wall including cracks of concrete/masonry portions and collapse of fence and gate access to the beach was observed on Building A, as presented on Figure 4-10. Based on the pre-storm aerial image, approximately 30 to 40 feet of beach was washed out during the hurricane. There was no overwash sand deposit on the shoreline at this site; therefore, the beach sand was most likely removed by the wave action to deeper depths offshore. As seen on Figure 4-11, the beach access ramp and seawall of Building B was damaged and displaced. Geotextile was left exposed near the damaged seawall. Based on visual observation, there was some minor damage to the building (e.g., broken balcony railing, damage to the walking path) but no cracks were observed on the building. Most of the damage appeared to be due to erosion on the ground surface.

Note: base image from Google Earth, n.d., accessed 3/6/2018.

Figure 4-9: Pre-storm aerial image of Site CE2.

Notes: Building A (Residential apartment complex “Pelican Reef”), top-left (Lat: +18.31623, Lon: -67.24442, 2017.11.3, 08:45 AST), top-right (Lat: +18.31629, Lon: -67.24444, 2017.11.3, 08:45 AST), bottom-left (Lat: +18.31625, Lon: -67.244442, 2017.11.3, 08:39 AST).

Figure 4-10: Photos of Residential apartment complex “Pelican Reef” (Building A) at Site CE2.

Notes: Building B, top (Lat: +18.31620, Lon: -67.24445, 2017.11.3, 08:38 AST), bottom-left (Lat: +18.31602, Lon: -67.24432, 2017.11.3, 08:41 AST), bottom-right (Lat: +18.31614, Lon: -67.24431, 2017.11.3, 08:40 AST).

Figure 4-11: Photos of Building B at Site CE2.

4.2.3 Coastal Erosion Site CE3: Rincón Ocean Club

Site CE3 is located within the Córcega Beach that can be accessed by Calle Pogio Doleta. As part of the reconnaissance of Site CE3, the GEER team visited the Rincón Ocean Club and a residence (Building A) located just south, as shown in Figure 4-12. The Rincón Ocean Club is an oceanfront condominium complex consisting of two building complexes: Rincón Ocean Club I and II, as shown in Figure 4-13 (pre-storm condition). Each complex has an oceanfront swimming pool. The extent of the beachfront at this site, before hurricane Maria, is shown in Figure 4-13 (a), where about 20 to 30 feet of beach can be seen.

Note: base image from Google Earth, n.d., accessed 3/6/2018.

Figure 4-12: Pre-storm aerial image of Site CE3.

(a)

(b)

(c)

(d)

Notes: (a) Beachfront, (b)Rincón Ocean Club I, (c) & (d) Rincón Ocean Club II.
Photos (a), (c), and (d): http://www.jmlandmarkpr.com/Listing/ViewListingPhotos.aspx?BackEmailTypeID=NONE&ListingID=42326131, Photo (b): https://hotpads.com/1-corcecega-beach-ocean-clbrincon-pr-00677-1scac7n/i/pad-for-sale.

Figure 4-13: Pre-storm condition of Rincón Ocean Club I and II (Site CE3).

After Hurricane Maria several buildings in the area of Site CE3 were damaged as shown in Figure 4-14.

Extensive damage of the three-story building, supported by shallow footings, of Rincón Ocean Club I, and the common areas of the terrace and swimming pool can be seen in Figure 4-14. A high volume of soil was eroded from the front of the buildings and from underneath the swimming pool. Footings and a connecting grade beams supporting the terrace were exposed and sheared off from the building foundation, as shown in Figure 4-15 (c) and Figure 4-15 (d).

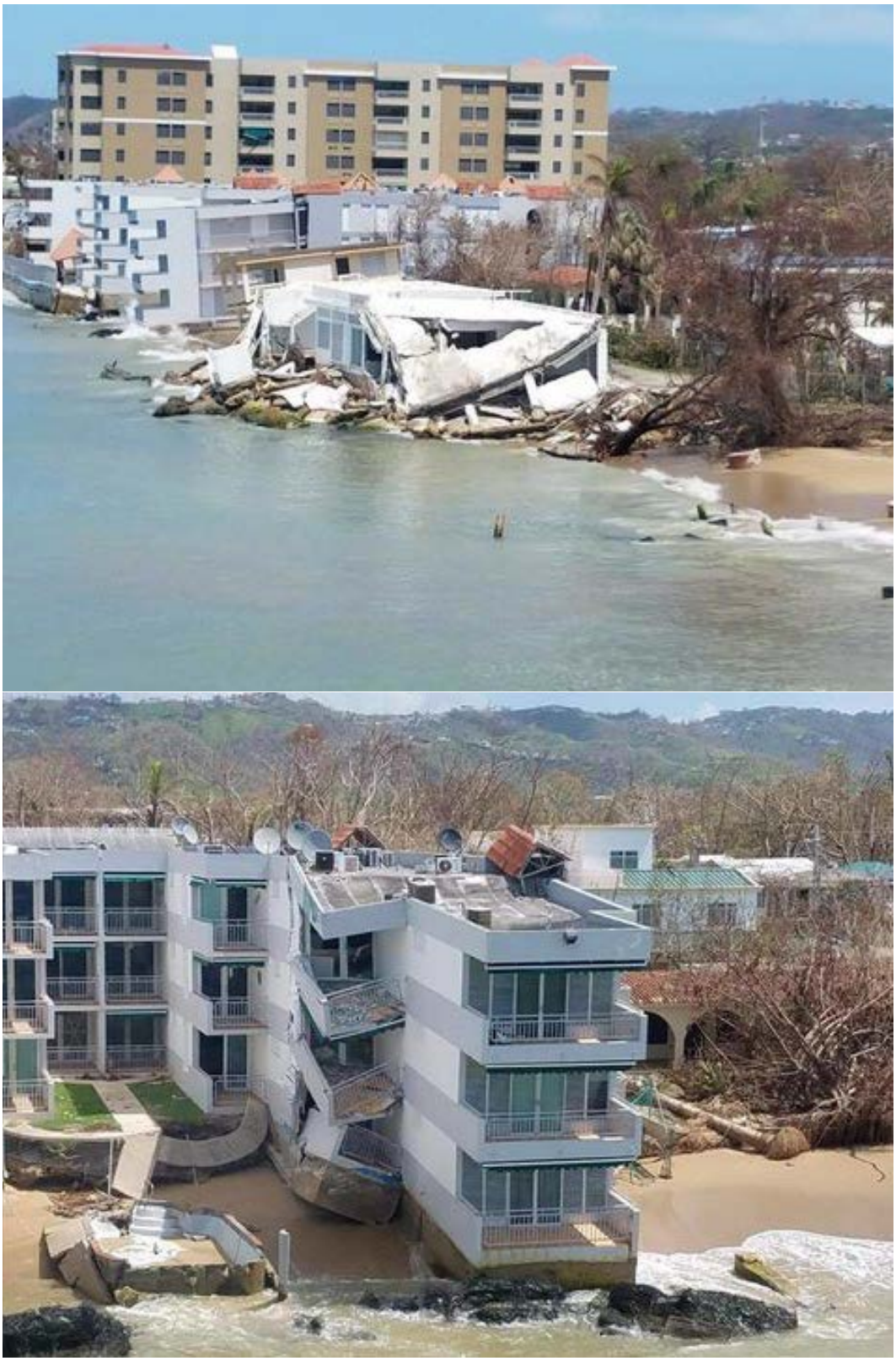

Notes: Top: multiple buildings damaged; Bottom: Rincón Ocean Club II (Source: http://www.noticel.com/english/condo-in-rincon-collapses-due-to-hurricane-maria/638463446)

Figure 4-14: Oceanfront damage in Corcega beach area (Site CE3).

(a) (b)

(c) (d)

Notes: (a) Damaged swimming pool, (Lat: +18.31820, Lon: -67.24583, 2017.11.3, 09:26 AST); (b) erosion in front of buildings (Lat: +18.31821, Lon: -67.24586, 2017.11.3, 09:26 AST); (c) (Lat: +18.31828, Lon: -67.24590, 2017.11.3, 09:21 AST) & (d) exposed footings (Lat: +18.31817, Lon: -67.24586, 2017.11.3, 09:32 AST).

Figure 4-15: Post-storm condition of Rincón Ocean Club I (Site CE3).

Damage of Rincón Ocean Club II, can be seen in the different images in Figure 4-16. Washout of the beach and soil foundation materials was also observed for the Club II complex contributing to the building collapse shown in Figure 4-16 (a) and Figure 4-16 (b). The courtyard swimming pool (shown in their pre-storm condition in Figure 4-13 (c) and Figure 4-13(d) appeared to have completely collapsed and washed away, as remnant materials of these areas were not observed during the field reconnaissance of Site CE3. Damage to the reinforced concrete beams and columns were observed along the side of the building as shown in in Figure 4-16 (c) and Figure 4-16 (d).

Damage to a residential house (Building A), at the location shown in Figure 4-12, is shown in Figure 4-16. Similar to the building of Rincón Ocean Club II, Building A collapsed into the ocean and the remaining structure was severely cracked.

The Victoria Del Mar Condominium, the tallest building in this area, located to the north of Rincón Ocean Club I as shown in Figure 4-15 (a), also suffered extensive damage associated to coastal erosion. The pre-storm condition of the pool and terrace area of the Victoria Del Mar Condominium is shown in Figure 4-18(a). The terrace and swimming pool area collapsed with the storm, as shown on Figure 4-18 (b) and Figure 4-18 (c).

In general, the beachfront in the Corcega beach (Site CE3) suffered extensive erosion. For example, the approximately 20 to 30 feet of beachfront shown in the pre-storm photo of Figure 4 13, was observed to be drastically reduced during the site reconnaissance. Sand washout deposits were not observed at the site. No shoreline erosion protection measures were observed during the field reconnaissance of Site CE3.

(a)

(b)

(c)

(d)

Damage, (a), Lat: +18.31776, Lon: -67.24546, 2017.11.3, 09:04 AST, (b) Lat: +18.31769, Lon: -67.24554, 2017.11.3, 09:09 AST, (c) Lat: +18.31791, Lon: -67.24554, 23017.11.3, 09:14 AST, (d) Lat: +18.31810, Lon: -67.24571, 2017.11.3, 09:18 AST.

Figure 4-16: Post-storm condition of Rincón Ocean Club II (Site CE3).

(a)

(b)

(c)

(d)

Notes: Photos of damage: (a) (Lat: +18.31792, Lon: -67.24552, 2017.11.3, 09:02 AST), (b) (Lat: +18.31779, Lon: -67.24540, 2017.11.3, 09:03 AST), (c) (Lat: +18.31769, Lon: -67.24549, 2017.11.3, 09:04 AST), (d) (Lat: +18.31768, Lon: -67.24549, 2017.11.3, 09:04 AST).

Figure 4-17: Post-storm condition of Building A (Site CE3).

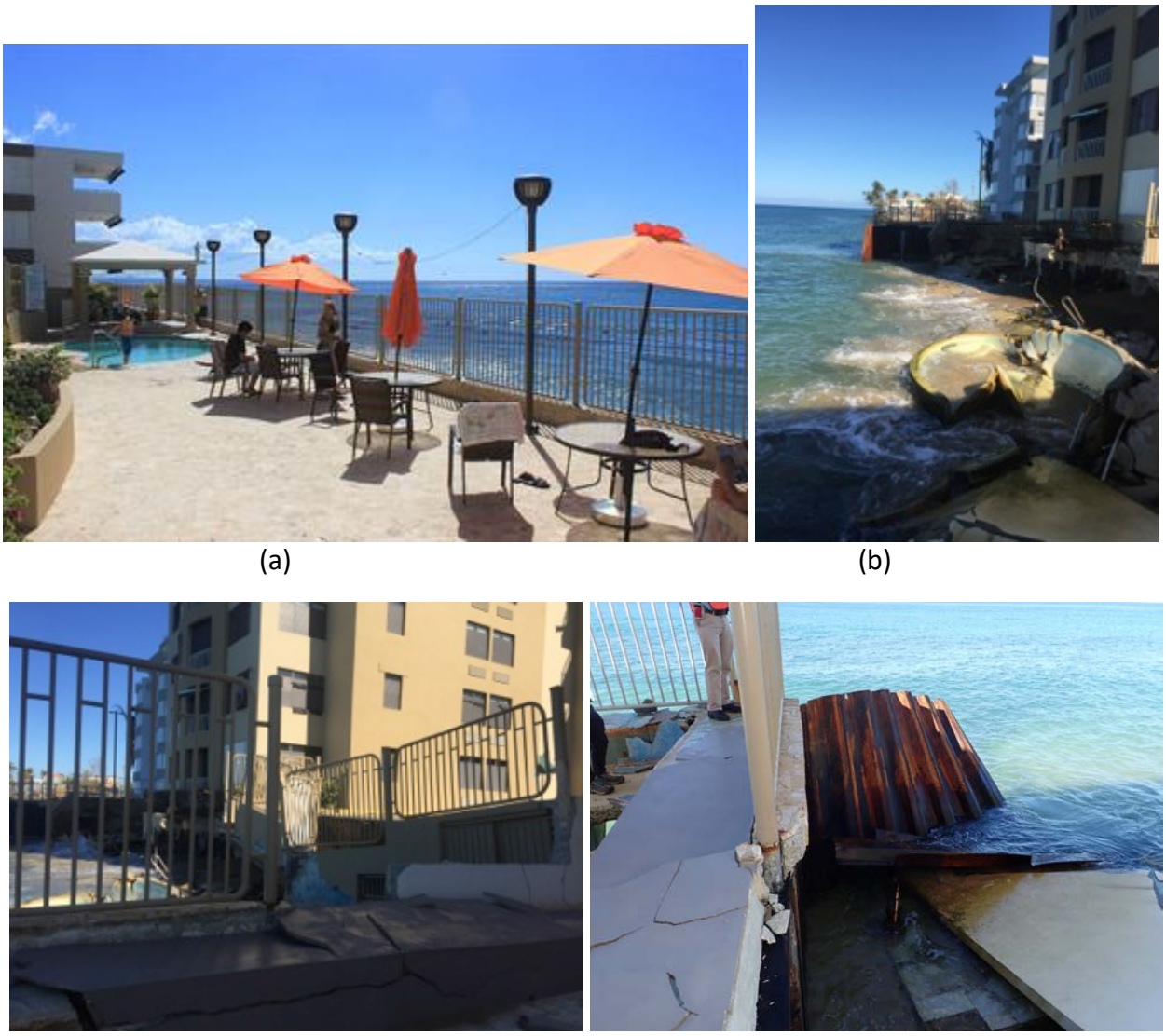

(a) (b)

(c) (d)

Notes: (a) Victoria Del Mar Condominium: top: pre-failure http://blog.realestaterinconpr.com/rentlease-dropped-on-1a-victoria-del-mar-in-victoria-del-mar-rincon/ (b) after failure (photo taken from Ocean Club I), (c) Lat: +18.31848, Lon: -67.24606, 2017.11.3, 09:25 AST (d) Lat: +18.31837, Lon: -67.24597, 2017.11.3, 09:22 AST).

Figure 4-18: Pre- and Post-storm damage at the Victoria Del Mar Condominium (Site CE3).

4.2.4 Coastal Erosion Site CE4: Crash Boat Beach, Aguadilla, PR

Site CE4 is located at Crash Boat Beach in Aguadilla, PR. It was visited by Drs. Silva-Tulla, Pando, and Bernal on Sunday, October 29, 2017. The top photo of Figure 4-19 illustrates the magnitude of coastal erosion at this site and scour of the foundation of the small fish store structure, where local fishermen used to sell their fish before the hurricane.

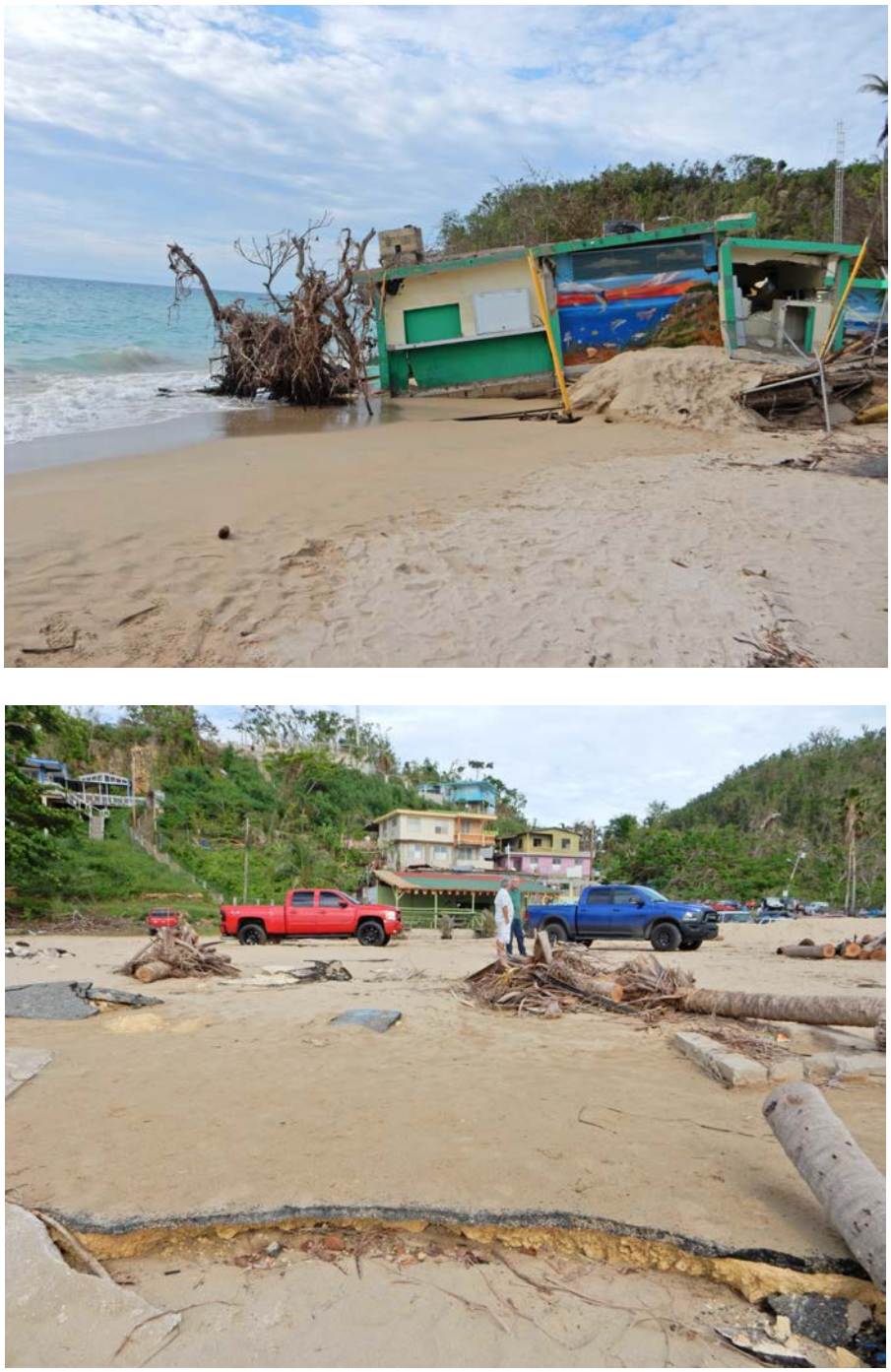

Figure 4-19: Coastal erosion at Site CE4 - Crash Boat Beach (Lat: +18.45878, Lon: -67.16413).

From the top photo of Figure 4-19, it is also possible to infer a considerable loss of sand, as shown from the elevation difference and rotation of the fish store structure. The lower photo of Figure 4.19 shows the parking area at this beach with considerable accumulation of sand.

4.2.5 Coastal Erosion Site CE5: Town center waterfront, Aguadilla

This site is located in the town center of Aguadilla along the coastal avenue that borders the west side of town. The site was visited by Drs. Silva-Tulla, Pando, and Bernal on Sunday, October 29, 2017. The photo in Figure 4-20 shows a collapse of the sidewalk. The reasons for the collapse of the sidewalk are difficult to determine. The edge of the guardrail structure shows some damage, likely related to weave action that could have overtopped and caused the sidewalk collapse. However, poor construction is also possible given the large cavity under the sidewalk still in place.

Figure 4-20: Coastal erosion Site CE5 – Collapse of sidewalk along coastal avenue in Aguadilla Town Center (Lat: +18.43159, Lon: -67.15529).

4.2.6 Coastal Erosion Site CE6: Playa El Maní, Mayagüez, Puerto Rico

The shoreline of the beach of El Maní in Mayagüez, PR was greatly affected by Hurricane Maria due to heavy flooding and severe coastal erosion. This site was visited by GEER members Drs. Silva-Tulla, Pando, and Park on November 4, 2017. Evidence of coastal erosion can be seen on Figure 4-21 through Figure 4-25.

Note: Photo location: Lat: +18.24749, Lon: -67.17513, 11/04/17.

Figure 4-21: Coastal erosion at Site CE6 - beachfront house at Playa El Maní, Mayagüez, PR.

Note: Photo location: Lat: +18.24732, Lon: -67.17516xx, 11/04/17.

Figure 4-22: Coastal erosion at Site CE6 - beachfront house at Playa El Maní, Mayagüez, PR.

Note: Photo location: Lat: +18.233271, Lon: -67.172661, 11/04/17.

Figure 4-23: Coastal erosion at Site CE6 - Playa El Maní, Mayagüez, PR.

Note: Photo location: Lat: +18.233328, Lon: -67.172646, 11/04/17.

Figure 4-24: Coastal erosion at Site CE6 - Playa El Maní, Mayagüez, PR.

Note: Photo location: Lat: +18.233271, Lon: -67.172661, 11/04/17.

Figure 4-25: Coastal erosion at Site CE6 - Playa El Maní, Mayagüez, PR.

4.2.7 Coastal Erosion Site CE7: Playas del Yunque, Rio Grande, PR

Some beach erosion was observed at Playas el Yunque in Rio Grande, PR (lat:+18.39770, lon:-65.76260). This site was visited by GEER members Drs. Silva-Tulla and Pando on October 28, 2017. Photos showing the coastal erosion can be seen on Figure 4-26 through Figure 4-29.

Figure 4-26: Coastal erosion at Site CE7 - Playas del Yunque, Rio Grande, PR (Lat: +18.39821, Lon: -65.76466).

Figure 4-27: Coastal erosion site CE7: Playas del Yunque, Rio Grande, PR (Lat: +18.39823, Lon: -65.76483).

Figure 4-28: Coastal erosion site CE7: Playas del Yunque, Rio Grande, PR (Lat: +18.39754, Lon: -65.76246).

Figure 4-29: Coastal erosion site CE7: Playas del Yunque, Rio Grande, PR (Lat: +18.39754, Lon: -65.76246).

4.3 River Erosion Sites visited by the GEER team

The GEER team documented river erosion at the sites labeled as RE1 through RE3 shown on Figure 4-30. These sites are described in the following subsections.

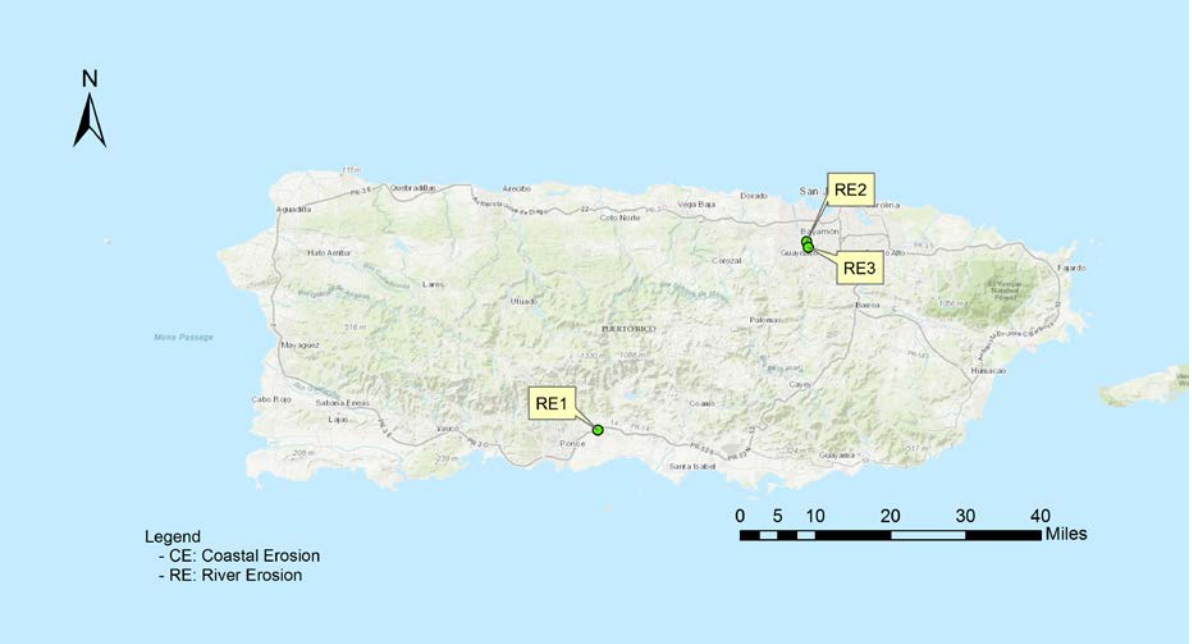

Figure 4-30: Location of river erosion sites documented by the GEER team.

4.3.1 River Erosion Site RE1: Erosion at Highway 52 bridges over the Inabón River

On October 31, 2017, the GEER team visited a river erosion site involving scour and erosion of a pier and abutment foundations of the bridges of Highway 52 over the Inabón River. This bridge is just east of the city of Ponce. Select photos of the site visit are shown on Figure 4-31 through Figure 4-34. These photos show ongoing work to repair the abutment. Figure 4-31 shows several exposed abutment H-piles and ongoing emergency work including erection of formwork for abutment repair and a temporary protection gabion wall; the gabion wall is to protect the abutment and reinforced concrete that will be installed in the area where the original piles are exposed. Additional photos appear in Appendix C. Figure 4-33 shows erosion that exposed several original abutment H-piles and the ongoing emergency repair works.

Figure 4-31: West abutment of westbound Highway 52 bridge over the Inabón River (Lat: +18.04003, Lon: -66.53795, October 31, 2017).

Figure 4-32: West abutment of westbound Highway 52 bridge over Inabón river (October 31, 2017). Photo shows erosion along this abutment and ongoing emergency repair work (Lat: +18.03967, Lon: -66.53764).

Figure 4-33: Erosion damage at west abutment of westbound Highway 52 bridge over the Inabón River (Lat: +18.03962, Lon: -66.53767, October 31, 2017).

Figure 4-34: Erosion along pier foundation of westbound Highway 52 bridge over the Inabón River (Lat: +18.03992, Lon: -66.53754, October 31, 2017).

4.3.2 River Erosion Site RE2: PR-177 in near Costco of Bayamón, PR

This site was not visited by the GEER team because it was repaired during the emergency recovery efforts by the PR government. The repairs we carried out by Del Valle Group for the Puerto Rico Highways and Transportation Authority (PRHTA). The photos in Figure 4-35 through Figure 4-38 were provided by GeoCim with authorization from PRHTA and show the extent of the scour erosion at this bridge site.

Figure 4-35: Erosion along pier foundation of bridges of Highway PR-177 in Bayamón, PR (Photo by Geo-Cim) (Lat: +18.38384, Lon: -66.13571).

Figure 4-36: Erosion along pier foundation of bridges of Highway PR-177 in Bayamón, PR (Photo by Geo-Cim) (Lat: +18.3838, Lon: -66.13557).

Figure 4-37: Erosion along pier foundation of bridges of Highway PR-177 in Bayamón, PR (Photo by Geo-Cim) (Lat: +18.38389, Lon: -66.135562).

Figure 4-38: Erosion along pier foundation of bridges of Highway PR-177 in Bayamón, PR (Photo by Geo-Cim) (Lat: +18.38392, Lon: -66.13581).

4.3.3 River Erosion Site RE3: River bank erosion near Guaynabo, PR

Photos of river erosion site RE3 are shown on Figure 4-39 through Figure 4-41. These photos show river bank erosion at the Guaynabo River, a tributary of the Bayamón river. Photos for this site were provided by Luis Garcia of GeoCim. The river erosion resulted in a bank failure upstream of the bridge near the offices of Villavicencio & Associates. The Guaynabo River tributary joins Río Bayamon a few hundred meters downstream from this site.

Figure 4-39: River bank erosion failure of Guaynabo River at Site RE3 (Photo by Geo-Cim) (Lat: +18.37306, Lon: -66.13248).

Figure 4-40: River bank erosion failure of Guaynabo River at Site RE3 (Photo by Geo-Cim) (Lat: +18.37307, Lon: -66.13248).

Figure 4-41: River bank erosion failure of Guaynabo Riverat Site RE3 (Photo by Geo-Cim) (Lat: +18.37356, Lon: -66.13253).

5 ROAD AND BRIDGE FAILURES

5.1 Introduction

Hurricane Maria triggered many road failures and damage to several bridges. The GEER team visited several sites; this section describes failures for ten sites that represent the main modes of failure observed. The locations of the ten representative sites are shown on Figure 5-1. Information and select photos for the remainder of the road and bridge failure sites visited appears in Appendix D.

Figure 5-1: Map showing location of ten road and bridge failure sites.

The road and bridge failures have been categorized in five different sub-sections: road failures associated to partial or total culvert blockage; road failure sites with downslope slope failures; road failure sites with slope failures on the upslope side (road blockage); road failure sites with complete road failure cut-off; and bridge failure. Most road failures were at locations where the section was built on a fill bench, as shown in Figure 5-2(a). Some road embankment failures were on the downslope side (Figure 5-2(b)), other failures were uphill (Figure 5-2(c)), and some were deep -seated involving both sides of the road (Figure 5-2(d)). In addition to these failure mechanisms, a large number of the road failures involved blockage (total or partial) of the culvert beneath the road.

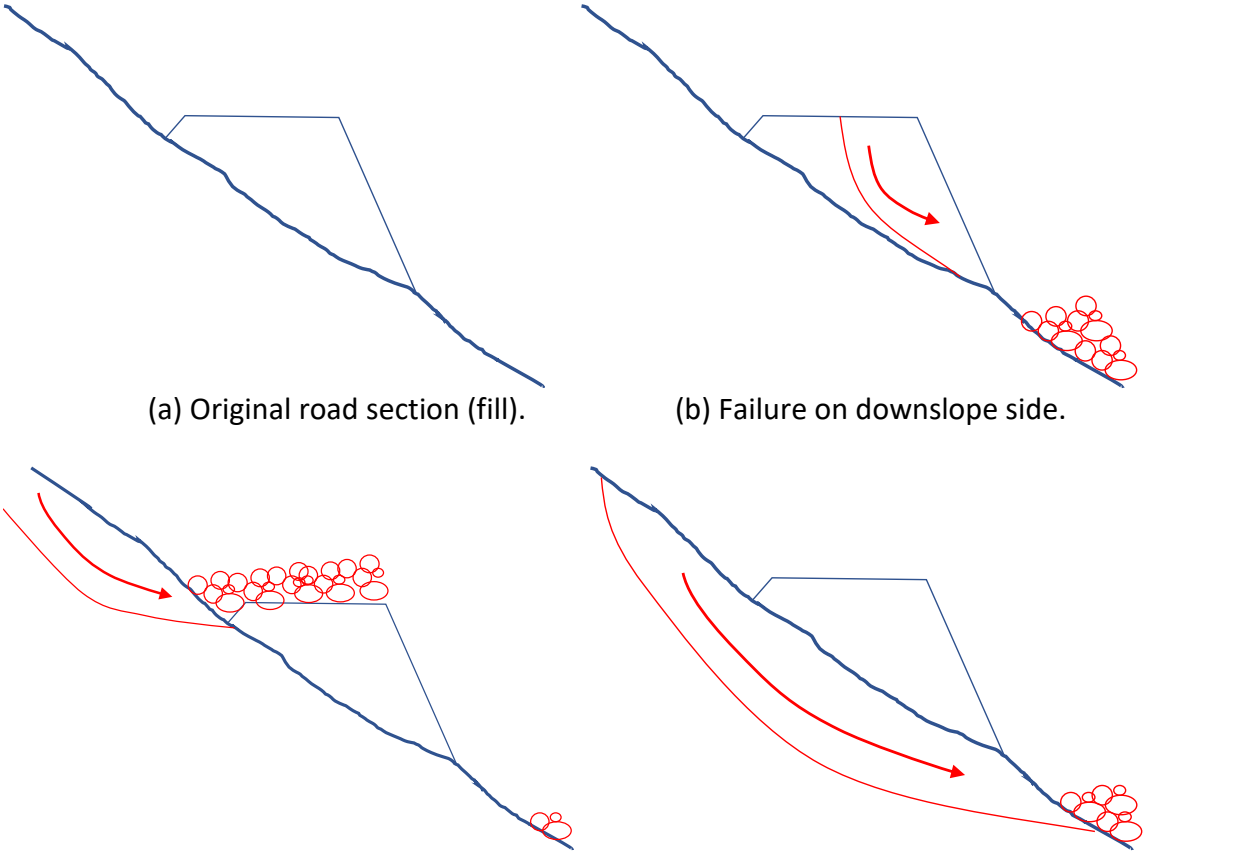

(a) Original road section (fill). (b) Failure on downslope side.

(c) Failure affecting upslope side. (d) Deep seated failure affecting both sides.

Figure 5-2: Schematic failure types for road sections on fill embankments.

In terms of bridge damage, including partial or total failure, the GEER team visited several bridge sites where damage was related to the large hydrodynamic forces from the increased volume and flow speeds associated with Hurricane Maria. The large magnitude of these hydrodynamic forces is illustrated in Figure 5-3; this figure shows a satellite image from NOAA of the induced curvature of a bridge in Yauco.

Figure 5-3: Images showing induced curvature on bridges near Yauco, PR, due to heavy river flows during Hurricane Maria (images from NOAA taken a few days after Maria).

The hurricane-induced loading demand on bridges was not only related to the large hydrodynamic forces, but also related to drag and impact forces associated with large amounts of trees and debris materials transported by the rivers, as illustrated in the images shown on Figure 5-4.

(a) Lat: +18.28686, Lon: -67.1062 (11/03/17)

(b) Lat: +18.28683, Lon: -67.10610 (11/03/17)

Figure 5-4: Photos showing large accumulation of debris under bridge.

5.2 Road failures associated with partial to total culvert blockage

Road failures associated with partial or total culvert blockage was identified at several sites visited by the GEER team. This section describes this type of road failures for two sites.

5.2.1 Road & Bridge Site 1

The site location is shown on the map and photo shown on Figure 5-5(a) and Figure 5-5 (b). The red marker shown on Figure 5-5(b) represents the approximate location of a corrugate pipe culvert under the road (PR-555), and the red arrow indicates the direction of the water flow. Figure 5-6 shows photos of the road failure associated with clogging of the corrugated pipe culvert under the road.

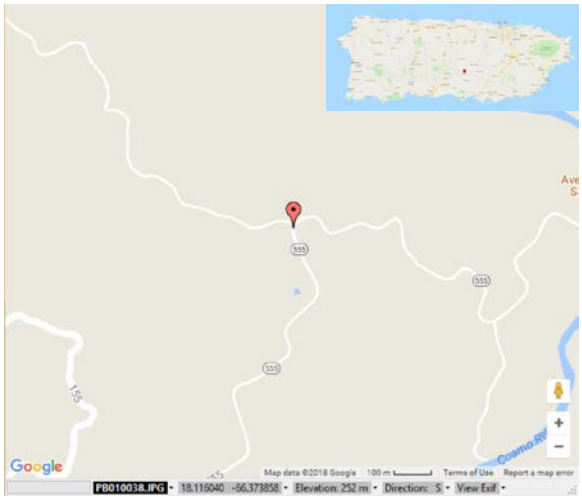

(a)

(b)

Note: Lat: +18.116040°, Lon: -66.373858°; Date: 11/01/17.

Figure 5-5: General location of Road & Bridge Site 1.

Figure 5-6(a) and Figure 5-6(b) show the subsided road surface above the culvert. Many cracks developed on the road pavement. The subsided length across the road was almost 13 feet, about half of the road width.

The culvert conditions were shown on Figure 5-6(c) and Figure 5-6(d). While most of the debris in the culvert was gone, many trees and other debris remained on the upstream side of culvert.

(a) (b)

(c) (d)

Note: Lat: +18.116040°, Lon: -66.373858°; Date: 11/01/17 09:55 EDT.

Figure 5-6: Photos of Road and Bridge Site 1 associated to culvert clogging.

5.2.2 Road & Bridge Site 2

The location of this site is at Marker km 4.2 of PR-555, that is about 1.9 km East of Site 1 described above. Figure 5-7 shows the location map and a photo showing the location of the culvert and direction of water flow. This failure site involved a corrugated pipe culvert with a diameter of about five feet that crossed under the road. The red circle in the photo shown on Figure 5-8(a) marks the downstream outlet of the culvert. Photos on Figure 5-8(b) and Figure 5-8(c) show the extent of road width loss and the presence of large longitudinal cracks.

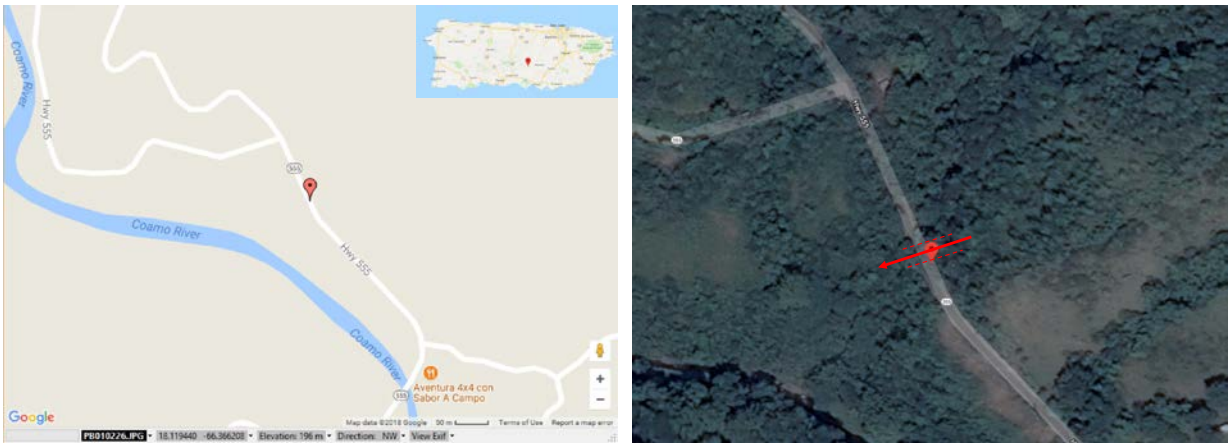

(a) (b)

Note: Lat: +18.11944°, Lon: -66.36624°; Date: 11/01/17 10:31 EDT.

Figure 5-7: Location of Road & Bridge Site 2 at km 4.2 of PR-555.

A grab soil sample collected from the exposed scarp was found to have a USCS classification of SM-SC (See Sample A in Table I-1 of Appendix I).

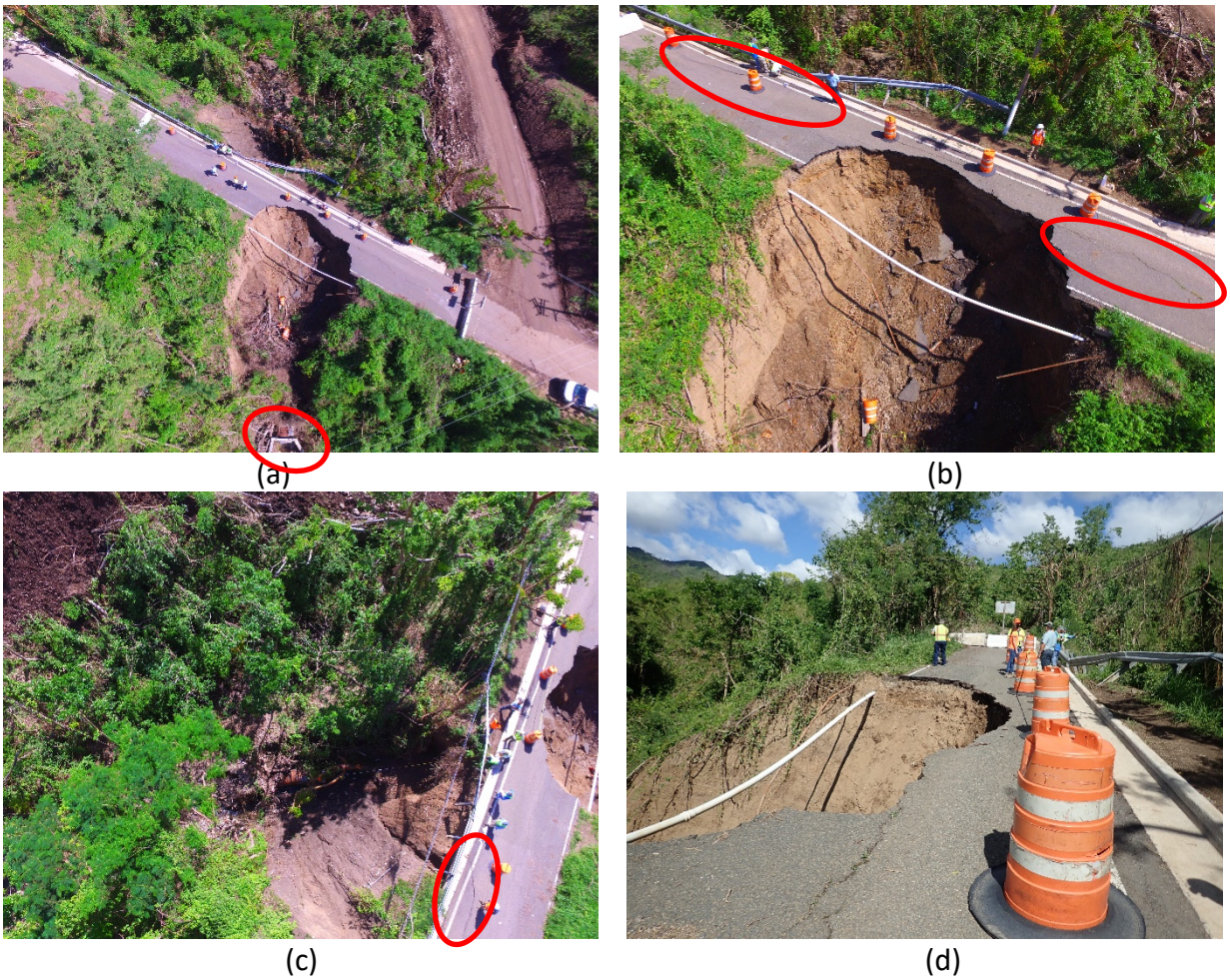

(a) (b)

(c) (d)

Note: Lat: +18.11944°, Lon: -66.36624°, Time: 11/01/17 10:21 EDT.

Figure 5-8: Photos of Road & Bridge Site 2 related to culvert clogging at km 4.2 of PR-555.

5.3 Road failure sites with downslope slope failures

5.3.1 Road & Bridge Site 3

The site was visited by the GEER team on 11/1/17. The location of this road failure site is shown on Figure 5-9. At this site, the road failure was observed on the downslope side of the road, as shown on Note: Lat: +18.172445°, Lon: -66.377797°, Date: 11/01/17 12:57 EDT. Figure 5-10 via the drone photos. However, a tension cracks and a scarp were observed on the upslope side, as shown in the red circle on Figure 5-10(c). A photo showing the loss of the upper slope side of the lane is shown on Figure 5-10 (d), but it was not considered significant.

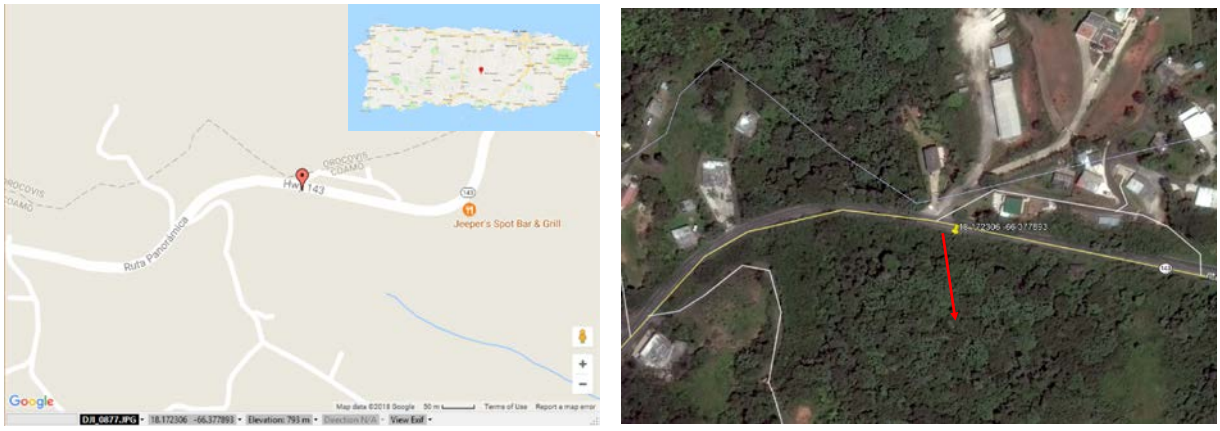

(a) (b)

Note: Lat: +18.172445°, Lon: -66.377797°, Date: 11/1/17.

Figure 5-9: Location of Road & Bridge Site 3 at km 50.7 of PR-143.

Three shear vane tests were performed by the GEER team at a location along the exposed scar near the lower right corner of photo in Figure 5-10(b). Tests involved use of a Humboldt Geovane with the small vane attachment (19 mm blade). Two of the Geovane tests were performed with the vane axis pushed vertically into the ground about 4 inches and yielded peak shear strength values of 43 and 62 kPa. Results of a Geovane tests pushed horizontally into a vertical face of the scar yielded a peak and residual shear strength of 70 and 14 kPa, respectively.

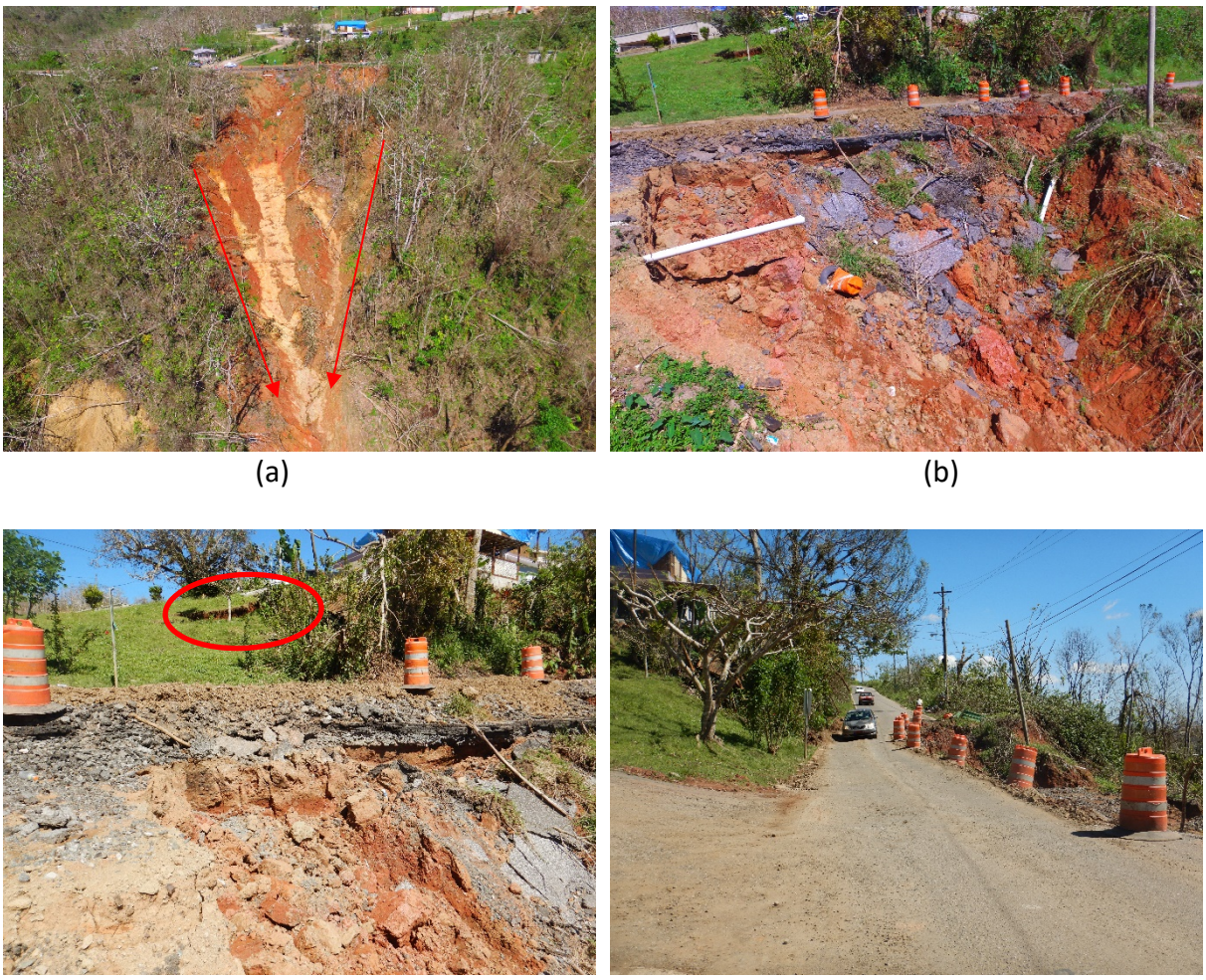

(a) (b)

(c) (d)

Note: Lat: +18.172445°, Lon: -66.377797°, Date: 11/01/17 12:57 EDT.

Figure 5-10: Select photos of Road & Bridge Site 3 involving primarily road damage associated to downslope slope failure.

5.3.2 Road & Bridge Site 4

The general location of the road failure Site 4 is shown on Figure 5-11. The downslope side of this road site was lost as shown on Figure 5-12. The road lost almost a half its width. To widen the remaining access and maintain two-way traffic, the upload side was excavated.

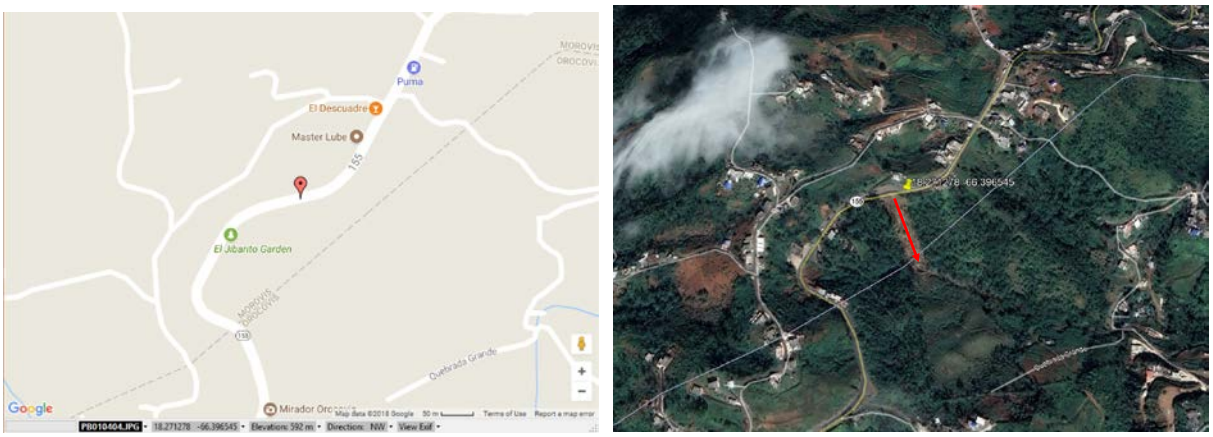

(a) (b)

Note: Lat: +18.271278°, Lon: -66.396545°.

Figure 5-11: Location of Road & Bridge Site 4.

(a) (b)

(c) (d)

Note: Lat: +18.271278°, Lon: -66.396545°, Time: 11/01/17 13:41 EDT

Figure 5-12: Road & Bridge Site 4 - Road Damage by Lower Slope Failure.

5.4 Road failure sites with slope failures on the upslope side (road blockage)

This category represents sites where a debris flow occurred on the upslope side of the road, resulting in road blockage from the failed soil mass. The following subsections describe two sites with this type of failure.

5.4.1 Road & Bridge Site 5

The location of Site 5 is shown on Figure 5-13. A large boulder, as well as other debris, blocked about half of the road.

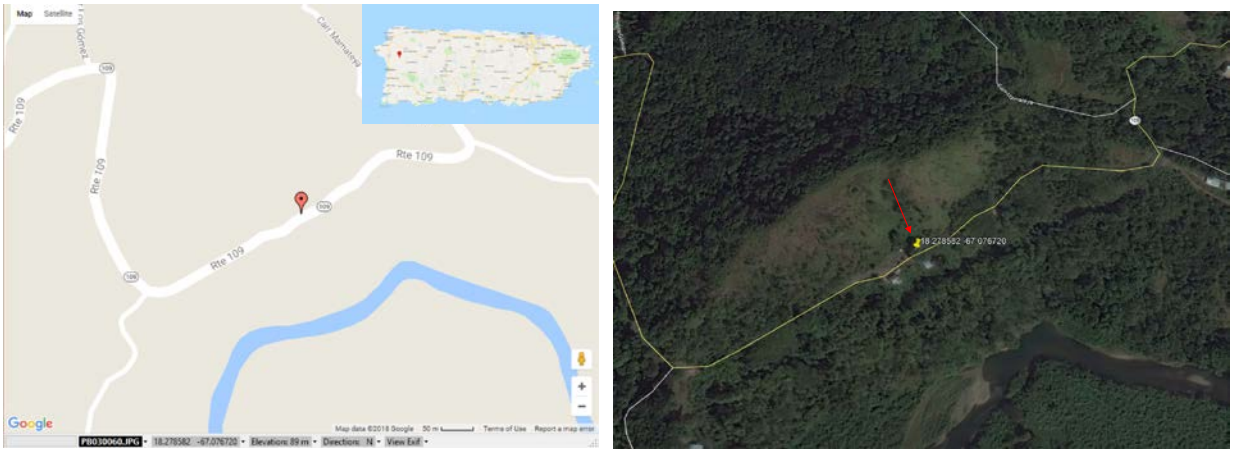

(a) (b)

Note: Lat: +18.278582°, Lon: -67.076720°

Figure 5-13: Location of Road & Bridge Site 5.

(a) (b)

(c) (d)

Note: Lat: +18.278582°, Lon: -67.076720°, Date: 11/01/17 13:41 EDT.

Figure 5-14: Photos of Road & Bridge Site 4 showing upslope side failure and road blockage.

5.4.2 Road & Bridge Site 6

The location of the Site 6 road failure is shown on Figure 5-15. About 30 feet of the road was covered by red clay, and at the time of our visit, construction crews had opened only one lane.

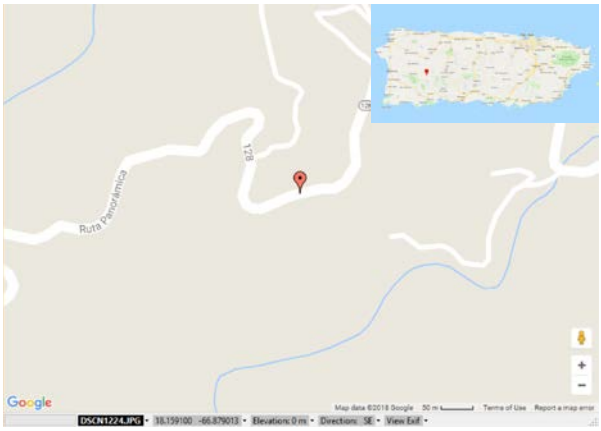

(a)

(b)

Note: Lat: +18.159100°, Lon: -66.879013°

Figure 5-15: Location of Road & Bridge Site 6.

(a)

(b)

(c)

(d)

Note: Lat: +18.159100°, Lon: -66.879013°, Date: 11/03/17 13:32 EDT.

Figure 5-16: Photos of Road & Bridge Site 4 showing surficial slope failure on the upslope side of the road.

5.5 Road failure sites with complete cut-off

5.5.1 Road & Bridge Site 7 - Road damage with complete cut-off

The location of the Road & Bridge Site 7 is shown in Figure 5-17. The site is located on the northwest side of the island along road PR-186 road near the west boundary of the El Yunque National Forest. The failure affected the full width of the PR-186 road and the entrance driveway of a residence on the west side of the road (upslope side). The arrows shown on Figure 5-17(b) point towards the slope failure direction (southeast).

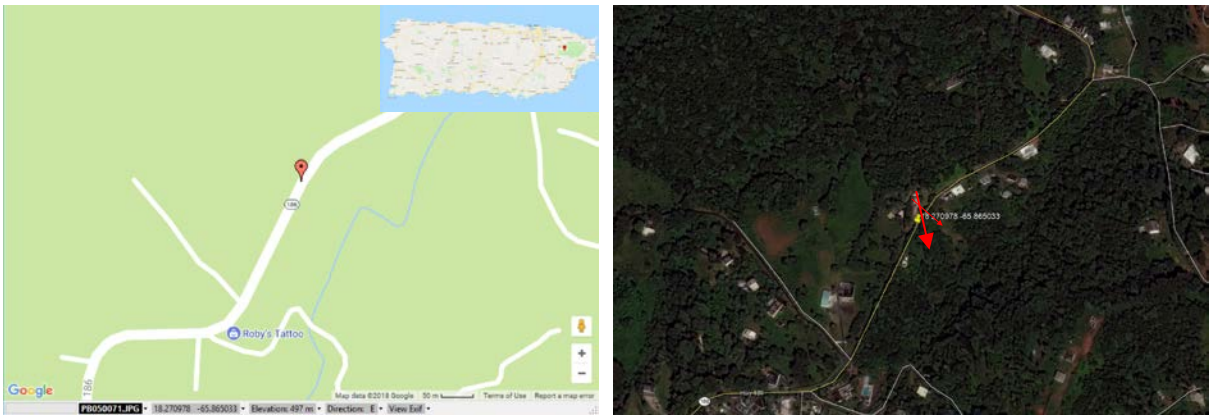

(a) (b)

Note: Lat: +18.270978°, Lon: -65.865033°

Figure 5-17: Location of Road & Bridge Site 7.

Figure 5-18(a) shows the upper portion of the failure resulted in a complete cut-off of PR-186. This figure also shows a portion of the concrete pavement driveway of a residence to the left of the image (residence not shown). The final position of the piece of concrete driveway is shown inside the red circle. The arrow on Figure 5-18(d) points toward the slope failure direction (southeast).

(a) (b)

(c) (d)

Note: Lat: +18.270978°, Lon: -65.865033°, Date: 11/05/17 08:52 EDT

Figure 5-18: Photos of Road & Bridge Site 7 affecting PR-186.

5.5.2 Road & Bridge Site 8 - complete cut-off of PR-431

Site 8 involved a complete cut-off failure along road PR-431 in the municipality of Lares. Details of the location of this road failure site are provided in Figure 5-19. As shown in Figure 5-19(b), the failure affected two locations on parallel portions of the same windy PR-431 road. The complete cut-off occurred along the upper site, and soil and boulders from the failure debris blocked the lower site of the road.

(a) (b)

Note: Lat: +18.250348°, Lon: -66.884155°.

Figure 5-19: Road & Bridge Site 8 - Complete cut-off failure along PR-431 in Lares.

Figure 5-20(a) shows the whole slope failure from a photo taken from the opposite side of the mountain. Figure 5-20(b) shows the lower site of the road partially blocked by a large boulder. The upper portion of PR-431 was destroyed by the failure (see Figure 5-20(c) and Figure 5-20(d)).

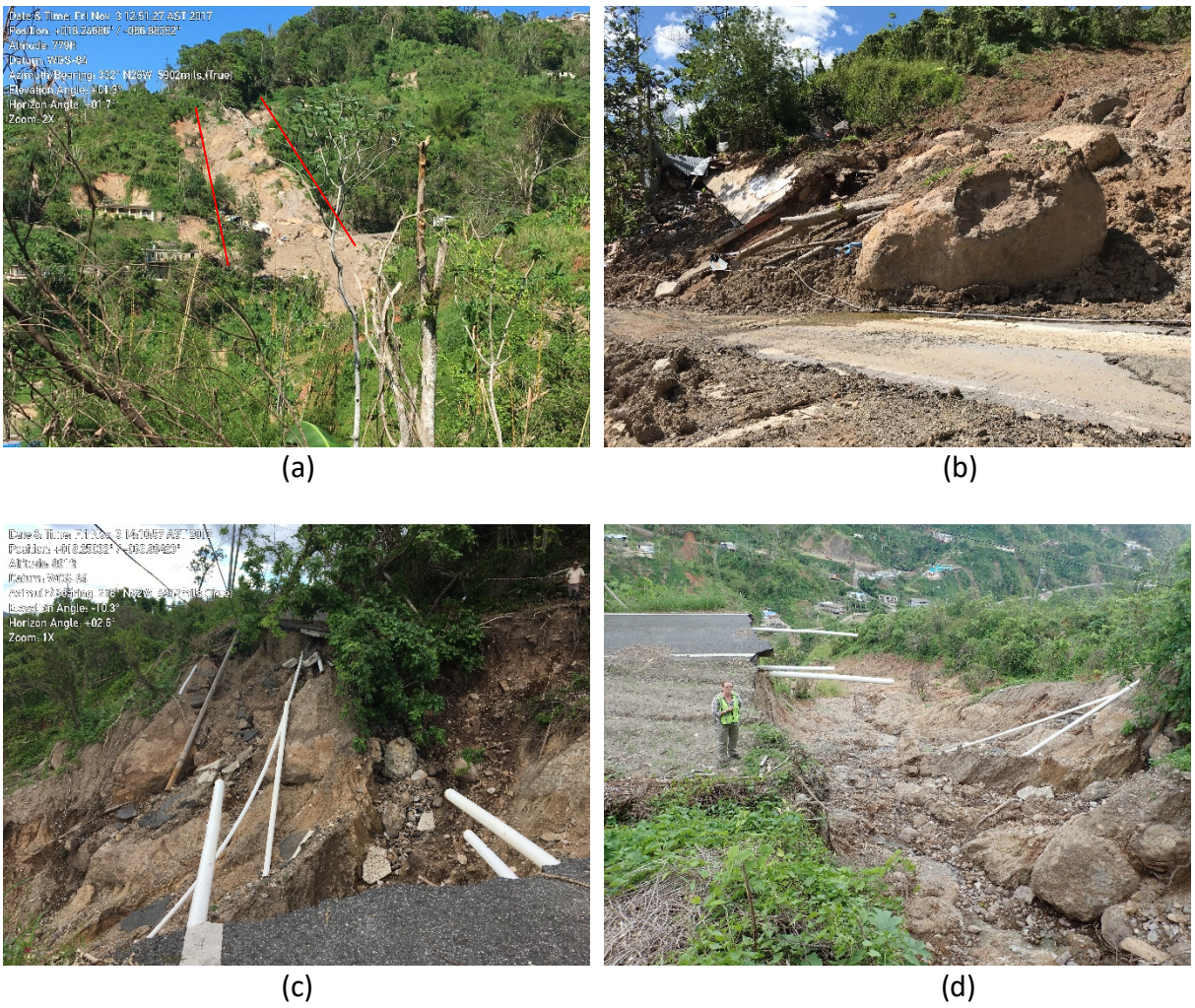

(a) (b)

(c) (d)

Note: Lat: +18.250348°, Lon: -66.884155°, Time: 11/03/17 13:08 EDT

Figure 5-20: Photos of Road & Bridge Site 8 - Road damage with complete cut-off at PR-431 in Lares.

5.6 Bridge failures

5.6.1 Road & Bridge Site 9 – Washed away bridge failure

Site 9 involved a bridge failure located in the eastern side of Ciales. The bridge spans over the Río Grande de Manati river and connected road PR-6632 on the west bank and PR-145 on the east side, as shown in Figure 5-21. The bridge was completely washed away, as shown in Figure 5-22. Figure 5-22(a) shows a photo of the site taken from PR-145. The red circle on Figure 5-22(b) is a photo taken looking north that shows part of the failed bridge deck resting several hundred feet downstream. Figure 5-22(c) and Figure 5-22(d) show the extent of the damage of the east bridge abutment.

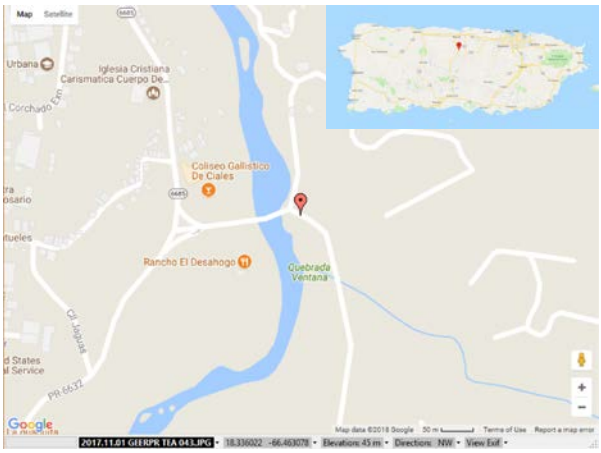

(a)

(b)

Note: Lat: +18.336022°, Lon: -66.463078°,

Figure 5-21: Road & Bridge Site 9 - Washed away bridge failure in Ciales.

(a)

(b)

(c)

(d)

Notes: Lat: +18.336022°, Lon: -66.463078°, Date: 11/01/17 16:07 EDT

Figure 5-22: Road & Bridge Site 9 - Failure of Bridge over the Río Grande de Manati river in Ciales.

5.6.2 Road & Bridge Site 10

Site 10 involved the failure of the bridge along PR-123 ((also known as the old PR-10) that spans over the Río Grande de Arecibo river as shown on Figure 5-23. This bridge is located about 2.7 miles north of Utuado. The bridge of PR-123 was completely washed away as shown in Figure 5-24. The GEER team was only able to reach the west abutment of the PR-123 bridge.

(a) (b)

Note: Lat: +18.301439°, Lon: -66.698319°, 11/02/17 10:58 EDT

Figure 5-23: Road & Bridge Site 10: PR-123 bridge over Río Grande de Arecibo.

After hurricane Maria people living in communities on the east side of the bridge could not be reached by first responders. Videos and photos showing the ingenuity of locals that rigged a system using an old supermarket cart and zip lines to pass water and food from the west side to inaccessible communities in the east side became viral. Figure 4-24(b) shows the part of the system used to send supplies to the east side of the washed away bridge. The red circle on Figure 5-24 (c) and (d) show debris under the bridge.

(a)

(b)

(c)

(d)

Notes: Photos (a) and (b) taken from west abutment at Lat: +18.301439°, Lon: -66.698319°, Date: 11/02/17 10:58 EDT. River flows from right to left in photos (a) and (b), as shown by deposition of debris on the left side of the remaining pier. (d) shows bridge remains downstream of the east abutment.

Figure 5-24: Road & Bridge Site 10 - Failure of PR 123 Bridge failure.

6 FOUNDATION FAILURES

6.1 Introduction

The previous section presented foundation failures of bridges. These failures were primarily related to scour and hydrodynamic forces due to the increased flow volume and velocities of many of the rivers. This section presents a summary of foundation forces related to wind forces and their effects on structures such as traffic signs and towers. The GEER team visited three cantilevered traffic sign structures and one stadium illumination tower where foundation failures were observed. The locations are shown on Figure 6-1, and the coordinates provided in Table 6-1.

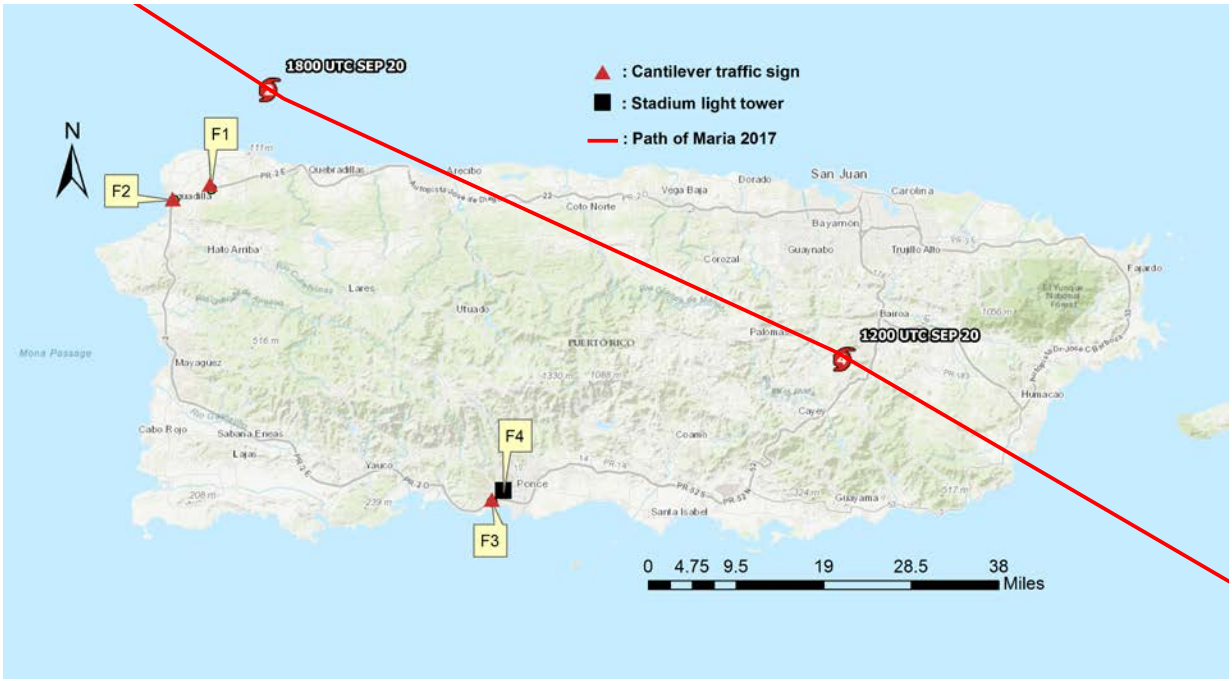

Figure 6-1: Foundation failures visited by 2017 GEER Team.

Table 6-1: Coordinates of foundation failure sites visited by 2017 GEER Team

Site ID	Latitude	Longitude	Location Information
F1	18.45360°	-67.08921 °	Near Aguadilla. Cantilevered traffic sign on drilled shaft on Southbound PR-2 highway.
F2	18.43662 °	-67.14799 °	Near the baseball stadium of Aguadilla. Cantilevered traffic sign on drilled shaft on Northbound PR-2 highway.
F3	17.98795 °	-66.64882 °	Near Exit 224 of PR-2 highway (eastbound). Square pedestal over drilled shaft.
F4	18.00209 °	-66.63100 °	Guy-supported light tower bearing capacity failure at Francisco Montaner Stadium in Ponce. Square shallow foundation.

6.2 Cantilevered traffic sign foundation failures

After Hurricane Maria, several cantilevered traffic sign structures were reported as having a rotational failure, meaning the sign rotated out of position by more than 90 degrees. Additional to rotation of the sign structure and foundation, all cantilevered sign structures visited showed small degrees of tilting. According to the PRHA, a single drilled shaft supports the majority of these type of structures. This section describes the reconnaissance observation made at three locations shown on Figure 6-1 above as F1 through F3.

6.2.1 Cantilevered Sign Site F1

The first site is located along the southbound lane of Highway PR-2 in Aguadilla. The photo of the traffic sign structure is shown on Figure 6-2. The final position of the traffic signal is rotated about 100 degrees (positive using the right-hand sign convention with respect to a vertical Zenith axis) with respect to the original installation position. The diameter of the drilled shaft that supports this structure was measured to be 30 inches (0.76 m).

Note: Lat: +18.453627°, Lon: -67.089248°; Date: October 30, 2017.

Figure 6-2: Photo of Cantilevered sign foundation failure at Site F1.

The high wind loading on the superstructure is complex in nature, and the resulting foundation loading involves torsion, axial and lateral loading, and bending. Furthermore, the dynamic wind load contains wide ranges of amplitude and frequency. Figure 6-2 shows some tilting of the superstructure with respect to the Zenith. The visual inspection revealed a deep gap around most of the perimeter circumference between the drilled shaft and the ground. Figure 6-3 and Figure 6-4 show photos of the top of the drilled shaft foundation where the gap formation can be observed. The gap, which likely formed due to the large bending and lateral forces transmitted to the drilled shafts, reduced the contact area between soil and foundation, and thus, the torsional resistance of the drilled shafts.

Note: Lat: +18.453627°, Lon: -67.089248°; photo taken October 30, 2017.

Figure 6-3: Photo of drilled shaft foundation of traffic sign at Site F1.

Note: Photo location: Lat: +18.453627°, Lon: -67.089212°; Date: October 30, 2017.

Figure 6-4: Photo of drilled shaft foundation of traffic sign at Site F1.

6.2.2 Cantilevered sign Site F2

The second cantilevered sign site is located at the southwest corner of the Luis A. Canena Marquez Stadium in Aguadilla. The sign is located along the northbound lane of Highway PR-2. A photo of the rotated mast-arm traffic sign is shown on Figure 6-5. The diameter of the drilled shaft was approximately 30 inches (0.76 m). The field reconnaissance also revealed a near continuous gap around the circumference of the drilled shaft. In some locations, the gap was as wide as 10 inches. The observed depth of the gap was about 18 inches, as shown in Figure 6-6; however, the bottom of the gap had loose soils, which suggest that minor caving may have filled some of the gap. The superstructure also experienced some tilt as shown on Figure 6-6. The traffic sign experienced a rotation of about -100 degrees with respect to the zenith and using the right-hand rule sign convention.

Note: Photo location: Lat: +18.436633°, Lon: -67.147746°; Date: October 30, 2017.

Figure 6-5: Photo of Cantilevered sign foundation failure at Site F2.

Note: Lat: +18.436633°, Lon: -67.147746°; photo taken 10/30/2017

Figure 6-6: Photo of drilled shaft foundation of traffic sign at Site F2.

6.2.3 Cantilevered sign Site F3

The third cantilevered sign showing a rotational failure of the drilled shaft foundation is located just north of the city of Ponce along the southbound lanes of Highway PR-2. A photo of the rotated state of this structure is shown on Figure 6-7. The foundation system at this site was not confirmed, as it was only possible to see a square pedestal, as shown in Figure 6-8. The sign was severely rotated (by about 12°) and a gap between the top pedestal and the surrounding ground was observed, as shown on Figure 6-8(a) and Figure 6-8(b). Neither the depth of the pedestal, nor the presence of a drilled shaft foundation could be confirmed. Because of the severe rotation shown on Figure 6-10, a structural foundation failure could not be excluded.

Note: Lat: +017.98789°, Lon: -066.64900°; photo taken November 1, 2017

Figure 6-7: Photo of cantilevered sign foundation failure at Site F3.

(a) **(b)**

Note: Lat: +017.98789°, Lon: -066.64900°; photo taken November 1, 2017

Figure 6-8: Photos of foundation pedestal of traffic sign at Site F3.

Note: Lat: +017.98789°, Lon: -066.64900°; photo taken November 1, 2017.

Figure 6-9: Photo showing the rotation of the traffic sign at Site F3.

6.3 Foundation failure of a light tower at baseball stadium in Ponce, Site F4

The fourth foundation failure (Site F4) was located at the baseball stadium, "Estadio Francisco 'Paquito' Montaner", in the city of Ponce. The structure is an illumination tower with cable guys and a shallow square foundation. Bearing capacity failure was observed at this site, as shown on Figure 6-10 and Figure 6-11. The team visited the site on 10/31/17.

Note: Lat: +18.002077°, Lon: -066.630990°; Date: October 31, 2017.

Figure 6-10: Photo of foundation failure of illumination tower at Site F4 in Ponce.

The light tower height above the ground is estimated to be 30 meters. It was supported by four guy wires and the foundation consisted of a 2.1 meter square concrete footing with a height of 1.25 meters. The rotation of the footing base was measured to be 40 degrees with respect to the horizontal plane. A grab sample was collected from the exposed soil under the shallow footing and consisted of a clayey sand (See Appendix I for index test results for grab sample ID E). Additional photos of this foundation failure are provided in Appendix E.

Figure 6-11: Photo of failed tower published by El Vocero 9/27/17 (Photo from Bartolomei, 2017) (Lat: +18.002275, Lon: -66.630714).

7 OTHER IMPACTS

Hurricanes Irma and Maria not only impacted the performance of geotechnical facilities and components including those described in detail throughout this document, but severe wind damages were also observed through the island of PR. A team of professors from the UPRM and local meterologist Ada Monzón visited the town of Cayey for a structural site reconnaissance on 10/27/17. During that visit, they found the NEXTRAD NOAA Doppler radar completely destroyed. As shown on Figure 7-1, the shell of the dome covering the radar was completely blown away from the tower, resulting in limited reliable weather data in PR during the passage of the storm. Ada Monzón stated that this is an unprecedented case history because the National Weather Center and other federal and local agencies were left without access to the valuable data recorded by this radar.

Figure 7-1: Before and after pictures of the NEXTRAD NOAA Doppler radar in Cayey, PR. (photo credit: Dr. Luis Suarez) (Lat: +18.115483, Lon: -66.077978).

Wind farms and solar farms also suffered extensive damage. The Punta Lima wind farm located on the east side of PR near Playa Húcares, where the strongest winds from Hurricane Maria were felt, was destroyed as shown in Figure 7-2. Almost every turbine was damaged after the passage of Hurricane Maria, and many were completely destroyed. The Santa Isabel wind farm, located on the south side of PR did not suffer significant damage, and officials reported that they were ready to produce energy immediately after the hurricane.

Figure 7-2: Destroyed wind turbine at Punta Lima Wind Farm, PR (Lat: +18.181809, Lon: -65.694291).

The second largest solar farm in PR, located on the east side of the island in the town of Humacao, was also almost completely destroyed by Hurricane Maria. This solar farm used to produce approximately 40% of the solar-generated electricity in PR. Significant numbers of solar panels were torn from their foundations.

Another solar farm, which was considered the largest in the Caribbean when built in 2012, also suffered damages. This farm, Ilumina Project, is located in Guayama, PR. Pictures are shown in Figure 7-3. Also the Humacao Solar Project, LLC, a small-scale solar farm, located in Humacao, PR, was nearly completely destroyed during Hurricane Maria. This small solar farm was designed and built to provide up to 60% energy to Humacao's sewage treatment facility. Before and after pictures are shown in Figure 7-4. The TSK solar farm, located in Loiza, PR, survived the strong wind and rains of Hurricane Maria. This design by TSK was developed for harsh weather, with panels mounted on structures 2 to 4 ms above ground level capable of withstanding winds of up to 160 miles per hour (mph). Additionally, a 645-kilowatt (kW) rooftop solar panel array in the Veterans Affairs Hospital in San Juan, PR, which was installed in 2015, was fully operational after the hurricanes. NOAA estimated winds of 180 mph in this area. According to Rothschild (2017) in an article for PV Magazine, "the array was installed with a combination of ballasts and mechanical anchors. It's a pliant racking system that is polymer based, and injection molded from galls-reinforced nylon. This gives the array the ability to flex in multiple directions without breaking – the main reason it's still on the roof".

Figure 7-3: Before and after pictures of Ilumina Project Farm in Guayama, PR (Lat: +17.947233, Lon: -66.156011).

Figure 7-4: Before and after pictures of the Humacao's sewage treatment facility solar farm (Lat: +18.130247, Lon: -65.789883).

REFERENCES

Barreto M., 2017, Assessment of beach morphology at Puerto Rico Island, Department of Natural Resources Puerto Rico Report no. 2015-000101, p58. (Available online at: http://drna.pr.gov/wp-content/uploads/2017/05/Geomorphic-Assessment-of-Puerto-Rico-1977-to-2016.pdf; accessed February 2018).

Bartolomei, J. (2017). "Estocada al deporte ponceño", El Vocero, 9/27/17. Photo of failed illumination tower at Paquito Montaner baseball stadium. https://www.elvocero.com/deportes/estocada-al-deporte-ponce-o/article_d58450ba-a3e0-11e7-a075-738eb4a93d59.html (accessed 2/18/18).

Bawiec, W.J., ed., 1999, Geology, geochemistry, geophysics, mineral occurrences and mineral resource assessment for the Commonwealth of Puerto Rico: U.S. Geological Survey Open-File Report 98-038, available online only (https://pubs.usgs.gov/of/1998/of98-038/).

Beauchamp, S.F., 2018, Planificación y Logistica ante Catástrofes, Semana de la Transportación, Department of Civil Engineering and Surveying, University of Puerto Rico at Mayagüez.

Bessette-Kirton, E.K., Coe, J.A., Godt, J.W., Kean, J.W., Rengers, F.K., Schulz, W.H., Baum, R.L., Jones, E.S., and Staley, D.M., 2017, Map data showing concentration of landslides caused by Hurricane Maria in Puerto Rico: U.S. Geological Survey data release, https://doi.org/10.5066/F7JD4VRF.

Bindoff, N.L., Willebrand, J., Artale, V., Cazenave, A., Gregory, J., Gulev, S., Hanawa, K., Le Quéré, C., Levitus, S., Nojiri, Y., Shum, C.K., Talley, L.D., and Unnikrishnan, A., 2007, Observations: Oceanic climate change and sea level, in Solomon, S., Qin, D., Manning, M., Chen, Z., Marquis, M., Averyt, K.B., Tignor, M., and Miller, H.L., eds., Climate change 2007: The physical science basis: Contribution of Working Group I to the Fourth Assessment Report of the Intergovernmental Panel on Climate Change, Cambridge, United Kingdom and New York Cambridge University Press, p. 385-432.

Boose, E.R., Serrano, M. I. & Foster, D.R. 2004. Landscape and regional impacts of hurricanes in Puerto Rico. Ecological Monographs, Vol. 74(2), 335-352.

Briggs, R.P. & Akers, J.P. 1965. Hydrogeologic map of Puerto Rico and adjacent islands. U.S. Geological Survey Hydrologic Investigations Atlas HA-197.

Caine, N. (1980). "The rainfall intensity-duration control of shallow landslides and debris flows." Geografiska Annaler. Vol. 62A, 23-27.

Calvesbert, R.J. 1970. Climate of Puerto Rico and the U.S. Virgin Islands. U. S. Department of Commerce, Climatography of the States, no. 60-52, 29p.

CNN (2018). https://www.cnn.com/2017/12/18/health/puerto-rico-maria-death-count-review/index.html (accessed March 2018).

Deere, D.U. & Patton, F.D. 1971. Slope stability in residual soils. In Proceedings: Panamerican Conference on Soil Mechanics and Foundation Engineering, American Society of Civil Engineers, Vol. 1, 87-170.

Deere, D.U. 1955. Engineering properties of the Pleistocene and recent sediments of the San Juan bay area, Puerto Rico. Ph.D. Thesis, University of Illinois, Urbana, Illinois.

Feng, Y., Negron-Juarez, R.I., Patricola, C.M., Collins, W.D., Uriarte, M., Hall, J.S., Clinton, N., and Chambers, J.Q. (2018). "Rapid remote sensing assessment of impacts from Hurricane Maria on forests of Puerto Rico", PEERJ Preprints, https://doi.org/10.7287/peerj.preprints.26597v1 (Accessed March 2018).

Hansen, J., Sato, M., Kharecha, P., Russell, G., Lea, D.W., and Siddall, M., 2007, Climate change and trace gases: Philosophical Transactions of the Royal Society A: Mathematical, Physical and Engineering Sciences, v. 365, no. 1856, p. 1925-1954.

https://www.accuweather.com/en/weather-blogs/weathermatrix/nexrad-radar-wind-turbines-solar-farms-destroyed-in-puerto-rico/70002879

https://www.metro.pr/pr/noticias/2017/10/13/finca-viento-santa-isabel-lista-dar-energia-electrica-30-mil-hogares.html

http://www.theweatherjunkies.com/single-post/2017/09/28/Puerto-Rican-Solar-Farms-Heavily-Damaged-By-Hurricane-Maria

https://cleantechnica.com/2012/10/03/puerto-rico-solar-power-plant-built-to-withstand-hurricanes-deliver-power-reliably-in-all-types-of-weather/

Hughes, K.S., and Morales Vélez, A.C., 2018, Personal Communicatios.

Hughes, K.S., and Morales Vélez, A.C., 2017, Characterization of Landslide Sites in Puerto Rico after Hurricanes Irma and María, American Geophysical Union Annual Conference, Abstract NH23E-2859.

Jibson, R. W. (1986). "Evaluation of landslide hazards resulting from the 5-8 October 1985 storm in Puerto Rico." U. S. Geological Survey Open-File Report 86-26.

Jibson, R.W. (1987). "Landslide hazards of Puerto Rico." In Proceedings: Assessment of Geologic Hazards and Risk in Puerto Rico, U.S. Geological Survey Open-File Report 87-008, Editors W.W. Hays and P. L. Gori, 183-188.

Jibson, R.W. (1989). "Debris flows in Southern Puerto Rico." In Proceedings: Landslide Processes of Eastern United States and Puerto Rico, Editors A.P. Schultz and R.W. Jibson, Geological Society of America Special Paper No. 236, 29-55.

Lan, HX, Zhou, CH, Lee, CF, Wang, Sijing, Wu, FQ (2003). "Rainfall-induced landslide stability analysis in response to transient pore pressure-A case study of natural terrain landslide in Hong Kong", Science in China Ser. E Technological Sciences, Vol. 46, pp. 52-68.

Larsen, M.C. and Santiago-Román, A., (2001). "Mass wasting and sediment storage in a small mountain watershed: An extreme case of anthropogenic disturbance in the humid tropics in Dorava, J. M., Palcsak, B.B., Fitzpatrick, F. and Montgomery", D.eds., American Geophysical Union Water Science & Application Volume 4, Geomorphic Processes and Riverine Habitat, 119-138.

Larsen, M.C., and Simon, A. (1993). "Rainfall-threshold conditions for landslides in a humid-tropical system, Puerto Rico." Geografiska Annaler, Vol. 75A (1-2), 13-23.

Larsen, M.C., and Torres-Sánchez, A. J. (1995). "Geographic relations of landslide distribution and assessment of landslide hazards in the Blanco, Cibuco, and Coamo river basins, Puerto Rico." U.S. Geological Survey Water Resources Investigations Report 95-4029, 56 p.

Lepore, C., Kumal, S.A., Shananhan, P., and Bras, R.L. (2012) "Rainfall-induced landslide susceptibility zonation of Puerto Rico", Environmental Earth Sciences, 66, 1667-1681.

Monroe, W.H. (1979). “Map Showing Landslides and Areas of Susceptibility to Landsliding in Puerto Rico.” U.S. Geological Survey Miscellaneous Investigations, USGS Map No. I-1148, 1 sheet.

Neumann, C.J., Jarvinen, B.R. & Pike, A.C. 1987. Tropical cyclones of the North Atlantic Ocean 1871-1986. . Third revised edition. NOAA-National Climatic Data Center, Asheville, North Carolina, USA.

NRC (National Research Council). 2004. Partnerships for Reducing Landslide Risk: Assessment of the National Landslide Mitigation Strategy. National Academy Press, Washington, D.C., 131 pp.

Overpeck, J.T., Otto-Bliesner, B.L., Miller, G.H., Muhs, D.R., Alley, R.B., and Kiehl, J.T., 2006, Paleoclimatic Evidence for future ice-sheet instability and rapid sea-level rise: Science, v. 311, no. 5768, p. 1747-1750.

Pando, M.A., Ruiz, M.E. & Larsen, M.C. 2005. Rainfall-induced landslides in Puerto Rico: An Overview, ASCE, Geotechnical Special Publication No. 140: Slopes and Retaining Structures under Seismic and Static Conditions , 15 p.

Pando, M.A., Ruiz, M.E., and Larsen, M.C., (2005) “Rainfall-Induced Landslides in Puerto Rico: An Overview”, ASCE Geo-Frontiers Congress, ASCE GSP No. 140, pp. 1-15.

Rahmstorf, S., 2007, A semi-empirical approach to projecting future sea-level rise: Science, v. 315, p.368-370.

Rahmstorf, S., Cazenave, A., Church, J.A., Hansen, J.E., Keeling, R.F., Parker, D.E., and Somerville, R.C.J., 2007, Recent climate observations compared to projections: Science, v. 316, no. 5825, p. 709.

Rothschild, E. (2017). “Solar survives the storms in Puerto Rico”, PV Magazine, November 7, 2017, https://pv-magazine-usa.com/2017/11/07/solar-survives-the-storms-in-puerto-rico/ (accessed 3/15/18).

Segoni, S., Piciullo, L. & Gariano, S.L. (2018). “A review of the recent literature on rainfall thresholds for landslide occurrence” Landslides, https://doi.org/10.1007/s10346-018-0966-4

Silva-Tulla, F., 1986, The October 1985 Landslide at Barrio Mameyes, Ponce, Puerto Rico, Committee on Natural Disasters, Commission on Engineering and Technical Systems, National Research Council, National Academy Press, Washington, D.C.

Sowers, G.G. 1971. Landslides in Weathered Volcanic Soil in Puerto Rico. In Proceedings: 4th Panamerican Conference of Soil Mechanics and Foundation Engineering, Vol. 1, 105-115.

ST. John, B.J., Sowers, G.F. & Weaver, C.E. 1969. Slickensides in Residual Soils and their Engineering Significance. 7th International Conference on Soil Mechanics and Foundation Engineering, Mexico, Proceedings. Sociedad Mexicana de Mecánica de Suelos 2:591-597.

Terzaghi, Peck, and Mesri (1996) “Soil Mechanics in Engineering Practice”, 3rd Ed., Prentice-Hall, 546 p.

Thieler, E. R., Rodríguez, R. W., and Himmelstoss, E.A., 2007, Historical Shoreline Changes at Rincón, Puerto Rico, 1936-2006: U.S. Geological Survey Open-File Report 2007-1017, 32 p.

Wieczorek GF, and Glade T (2005) Climatic factors influencing occurrence of debris flows. In: Jakob, M, Hungr, O (eds) Debris flow hazards and related phenomena. Springer, Berlin, Heidelberg, pp 325–362.

Wu, T. H., McKinnell III, W.P., and, Swanston, D.N. (1979). “Strength of tree roots and landslides on Prince of Wales Island, Alaska”, Canadian Geotechnical Journal, 16(1), pp. 19-33.
USGS (2018). “Historical hurricanes in Puerto Rico”, https://www.usgs.gov/media/images/puerto-rico-hurricanes-map, accessed March 2018.

APPENDICES

Appendix A Supplementary Information, Section 2 – Landslides and Debris Flows A-1
Appendix B Supplementary Information, Section 3 – Dams B-1
Appendix C Supplementary Information, Section 4 – Coastal Erosion C-1
Appendix D Supplementary Information, Section 5 – Roads and Bridges D-1
Appendix E Supplementary Information, Section 6 – Foundations E-1
Appendix F Supplementary Information, Section 7 – Other Impacts F-1
Appendix G LIDAR Data G-1
Appendix H NOAA Graphics and Data H-1
Appendix I Index test results and locations of collected grab samples. I-1
Appendix J GEER – PR Team Resumes J-1

Appendix A

Supplementary Information, Section 2 – Landslides and Debris Flows

Figure A-1: Lat: +18.25123, Lon: -65.79661; 2017.10.28; #3252.

Figure A-2: Lat: +18.25313, Lon: -65.79734; 2017.10.28; #3253.

Figure A-3: Lat: +18.25308, Lon: -65.79735; 2017.10.28; #3259.

Figure A-4: Lat: +18.25398, Lon: -65.79531; 2017.10.28; #3262.

Figure A-5 : Lat: +18.25455, Lon: -65.79176; 2017.10.28; #3266.

Figure A-6: Moca, PR-110; Lat: +18.40492, Lon: -67.11142; 2017.10.29; #3287.

Figure A-7: Moca, PR-110; Lat: +18.40493, Lon: -67.11146; 2017.10.29; #3289.

Figure A-8: Moca, PR-110; Lat: +18.40490, Lon: -67.11138; 2017.10.29; #3292.

Figure A-9: Moca, PR-110 failures from a distance; Lat: +18.38861, Lon: -67.07504; 2017.10.29; #3305.

Figure A-10: Moca; Lat: +18.38864, Lon: -67.07502; 2017.10.29; #3308.

Figure A-11: Moca; Lat: +18.39792, Lon: -67.06614; 2017.10.29; #3316.

Figure A-12: Moca; Lat: +18.39803, Lon: -67.06618; 2017.10.29; #3319.

Figure A-13: Moca; Lat: +18.39766, Lon: -67.06626; 2017.10.29; #3324.

Figure A-14: Raw water line severed by debris flow, Carillo, Villalba, PR-149, Km 59.1; Lat: +18.15855, Lon: -66.49808; 2017.10.31; #3500.

Figure A-15: Raw water lines, rectangular section about 100 years old; Lat: +18.15848, Lon: -66.49798; 2017.10.31; #3503.

Figure A-16: Temporary repairs; Lat: +18.15865, Lon: -66.49810; 2017.10.31; #3506.

Figure A-17: Downstream of raw water line break, Carillo, Villalba, PR-149, Km 59.1; Lat: +18.15849, Lon: -66.49821; 2017.10.31; #3515.

Figure A-18: Lat: +18.13924, Lon: -66.32987; 2017.11.01; #3673.

Figure A-19: Lat: +18.17465, Lon: -66.37314; 2017.11.01; #3678.

Figure A-20: Lat: +18.27130, Lon: -66.39671; 2017.11.01; #3685.

Figure A-21: Debris Flows; Lat: +18.28422, Lon: -66.40087; 2017.11.01; #3700.

Figure A-22: Debris Flows; Lat: +18.28414, Lon: -66.40093; 2017.11.01: #3706.

Figure A-23: Lat: +18.29063, Lon: -66.40768; 2017.11.01; #3727.

Figure A-24: Debris flow; Lat: +18.28397, Lon: -66.40132; 2017.11.01; #3710.

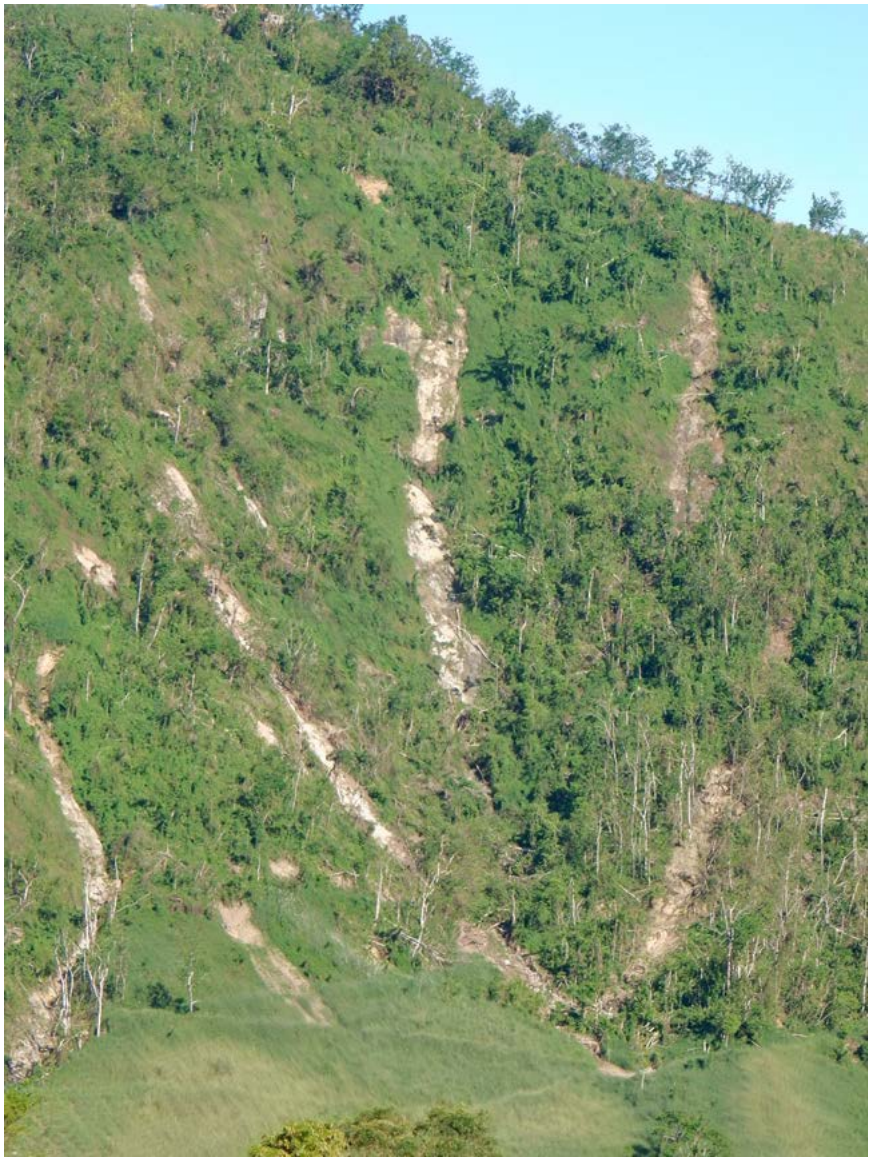

Figure A-25: Lat: +18.29061, Lon: -66.40769; 2017.11.01; #3729.

Figure A-26: Utuado, C-24 San Miguel St.; Lat: +18.26427667, Lon: - 66.698025, 2001-11-02; #3851.

Figure A-27: Utuado, C-24 San Miguel St.; Lat: +18.26427667, Lon: - 66.698025, 2001-11-02; #3851.

Figure A-28: Utuado, PR-140, Km 26.1, rusty cast iron pipe at head scarp; Lat: +18.26700333, Lon: -66.66004833; 2017.11.02; #3876.

Figure A-29: Utuado, Caonillas Lake; Lat: +18.26701, Lon: -66.66009667; 2017.11.02; #3889.

Figure A-30: Utuado, PR-140, Km 30.4; Lat: +18.284865, Lon: -66.63693333; 2017.11.02; #3902.

Figure A-31: Utuado, PR-146, Km 9.3, Rio Limón Slide, Head Scarp; Lat: +18.32294444, Lon: -66.599125; 2017.11.02; #3929.

Figure A-32: Utuado, PR-146, Km 9.3, Rio Limón Slide, Toe; Lat: +18.32237833, Lon: -66.59932833; 2017.11.02; #3931.

Figure A-33: Utuado, PR-146, Km 9.3, Rio Limón Slide, Toe; Lat: +18.32237833, Lon: -66.59932833; 2017.11.02; #3934.

Figure A-34: PR-106, Km 6.4; Lat: +18.21036833, Lon: - 67.08635333; 2017.11.04; #4197.

Figure A-35: PR-106, Km 6.4; Lat: +18.21036833, Lon: - 67.08635333; 2017.11.04; #4198.

Figure A-36: Lat: +18.18079, Lon: - 66.96581167; 2017.11.04; #4203.

Figure A-37: PR 424, Km 1.0; Lat: +18.291862, Lon: -67.007809; 2017.11.03; #4089. Gently sloped hillside shows evidence of sliding on three sides. According to geologist Alejandro E. Soto, it has always been that way.

Figure A-38: Lat: +18.29314, Lon: -67.00574; 2017.11.03; #4090.

Figure A-39: Debris flow; Lat: +18.309755, Lon: - 65.89074333; 2017.11.05; #4231.

Figure A-40: Canóvanas, PR-186; Lat: +18.27966, Lon: - 65.87966; 2017.11.05; #4247.

Figure A-41: Canóvanas, PR-186; Lat: +18.27966, Lon: - 65.87966; 2017.11.05; #4252.

Figure A-42: Canóvanas, PR-186; Lat: +18.270945, Lon: - 65.86504667; 2017.11.05; #4255.

Figure A-43: Canóvanas, PR-186; Lat: +18.270945, Lon: - 65.86504667; 2017.11.05; #4256.

Appendix B

Supplementary Information, Section 3 – Dams

Figure B-1: Guajataca Dam; Lat: +18.39878, Lon: -66.92330; 2017.10.30; #1159.

Figure B-2: Guajataca Dam; Lat: +18.39642, Lon: -66.92497; 2017.10.30; #2707.

Figure B-3: Lago Guayabal Dam; Lat: +18.08582, Lon: -66.50480; 2017.10.31; #3550.

Figure B-4: Lago Guayabal Dam; Lat: +18.08618, Lon: -66.50519; 2017.10.31; #3551.

Figure B-5: Lago Guayabal Dam; Lat: +18.08591, Lon: -66.50520; 2017.10.31; #3552.

Figure B-6: Lago Guayabal Dam; Lat: +18.08733, Lon: -66.50503; 2017.10.31; #3564.

Figure B-7: Lago Caonillas dam; LAT18.27703, lon-66.65593; 2017.11.02; #1234.

Figure B-8: Lat: +18.27733, Lon: -66.65520; 2017.11.02: #1235.

Figure B-9: Utuado, Dos Bocas Dam, Surficial slide near trasformer's yard; Lat: +18.33541333, Lon: -66.66602664; 2017.11.02; #3940.

Figure B-10: Utuado, Dos Bocas Dam; Lat: +18.33570, Lon: -66.66798; 2017.11.02; #3941.

Appendix C

Supplementary information, Section 4 – Coastal and River Erosion and Scour

Figure C-1: Coastal Erosion, Yunque Mar, Rio Grande, PR; Lat: +18.39770, Lon: -65.76260; 2017.10.28; #3209.

Figure C-2: Coastal Erosion, Yunque Mar, Rio Grande, PR; Lat: +18.39774, Lon: -65.76471; 2017.10.28; #3211.

Figure C-3: Crash Boat Beach, Aguadilla; Lat: +18.45878 Lon: -67.16413: 2017.10.29; #3274.

Figure C-4:; Aguadilla waterfront; Lat: +18.43159, Lon: -67.15529; 2017.10.29; #3279.

Figure C-5: Aguadilla waterfront; Lat: +18.43168, Lon: -67.15523; 2017.10.29; #3280.

Figure C-6: Cidra; Lat: +18.33613, Lon: -66.46309; 2017.11.01; #3740.

Figure C-7: Cidra; Lat: +18.33613, Lon: -66.46309; 2017.11.01; #3749.

Figure C-8: Coastal erosion at El Maní, Mayagüez; Lat: +18.24457, Lon: -67.17390; 2017.11.04; #4151.

Figure C-9: Coastal erosion at El Maní, Mayagüez; Lat: +18.23323, Lon: -67.17270; 2017.11.04; #4180.

Figure C-10: Coastal erosion at El Maní, Mayagüez; Lat: +18.24732, Lon: -67.17516; 2017.11.04; #4176. Previously grassy area after Hurricane María.

Figure C-11: Coastal erosion at El Maní, Mayagüez; Lat: +18.24732, Lon: -67.17516; 2017.11.04; #4175.

Appendix D

Supplementary information, Section 5 – Roads and Bridges

Figure D-1: Lat: +18.12974, Lon: -66.31595 2017.11.01.

Figure D-2: Lat: +18.13669, Lon: -66.32568 2017.11.01.

Figure D-3: Lat: +18.13924, Lon: -66.32990 2017.11.01.

Figure D-4: Lat: +18.27847, Lon: -66.40490 2017.11.01.

Figure D-5: Lat: +18.24980, Lon: -66.66157 2017.11.02.

Figure D-6: Lat: +18.24990, Lon: -66.66179 2017.11.02.

Figure D-7: Lat: +18.26704, Lon: -66.66018 2017.11.02.

Figure D-8: Lat: +18.26702, Lon: -66.66017 2017.11.02.

Figure D-9: Lat: +18.32304, Lon: -66.59955 2017.11.02.

Figure D-10: Lat: +18.322735, Lon: -66.599739 2017.11.02.

Figure D-11: Lat: +18.322939, Lon: -66.599655 2017.11.02.

Figure D-12: Lat: +18.21036, Lon: -67.08735 2017.11.04.

Figure D-13: Lat: +18.21035, Lon: -67.08734 2017.11.04.

Figure D-14: Lat: +18.21084, Lon: -67.09095 2017.11.04.

Figure D-15: Lat: +18.18081, Lon: -66.96496 2017.11.04.

Figure D-16: Lat: +18.18072, Lon: -66.96581 2017.11.04.

Figure D-17: Lat: +18.14245, Lon: -66.09301 2017.11.04.

Figure D-18: Lat: +18.18212, Lon: -66.93215 2017.11.04.

Figure D-19: Lat: +18.16288, Lon: -66.90378 2017.11.04.

Figure D-20: Lat: +18.17829, Lon: -66.85580 2017.11.04.

Figure D-21: Lat: +18.18317, Lon: -66.93352 2017.11.04.

Figure D-22: Lat: +18.19949, Lon: -66.98711 2017.11.04.

Figure D-23: Lat: +18.32651, Lon: -65.88905 2017.11.05.

Figure D-24: Lat: +18.32651, Lon: -65.88905 2017.11.05.

Figure D-25: Lat: +18.288, Lon: -65.894 2017.11.05.

Figure D-26: Lat: +18.2879, Lon: -65.8941 2017.11.05.

Figure D-27: Lat: +18.2879, Lon: -65.8941 2017.11.05.

Figure D-28: Lat: +18.2873, Lon: -65.8874 2017.11.05.

Figure D-29: Lat: +18.2872, Lon: -65.8876 2017.11.05.

Figure D-30: Lat: +18.2872, Lon: -65.8876 2017.11.05.

Figure D-31: Lat: +18.2717, Lon: -65.8798 2017.11.05.

Figure D-32: Lat: +18.2719, Lon: -65.8799 2017.11.05.

Figure D-33: Lat: +18.2719, Lon: -65.8799, 2017.11.05.

Figure D-34: Lat: +18.27186, Lon: -65.87985 2017.11.05.

Appendix E

Supplementary information, Section 6 – Foundation Failures

Figure E-1: Photo looking south of Site F2 (Lat: +18.43681, Lon: -67.14776; 2017.10.30).

Figure E-2: Photo of drilled shaft of cantilevered traffic sign at Site F2 (Lat: +18.43681, Lon: -67.14776; 2017.10.30).

Figure E-3: Photo of cantilevered traffic sign at Site F3 (Lat: +17.987991, Lon: -66.648788; 2017.11.1).

Figure E-4: Photo of foundation failure of illumination tower at Site F4 (Lat: +18.00207, Lon: -66.63098; 2017.10.31).

Figure E-5: Photo of illumination tower foundation pedestal at Site F4 (Lat: +18.00207, Lon: -66.63098; 2017.10.31).

A grab sample was collected 10/31/17 from the exposed foundation soil. Atterberg limits for this sample yielded a LL = 47.5%, and a PI = 29.8%. Grain size distribution tests for this sample resulted in 29.8% of gravel sizes, 20.7% of sands fraction, and 49.5% of fines. A shear vane test carried out on exposed foundation (See Figure E-6) yielded a shear strength (affected by failure mechanism) of about 54 kPa.

Figure E-6: Shear vane test on exposed foundation soil. Photo also shows location of grab sample (Lat: +18.00207, Lon: -66.63098; 2017.10.31).

Figure E-7: Photo of the foundation spot of the tower (Lat: +18.00207, Lon: -66.63098; 2017.10.31).

Figure E-8: Photo of portion of the structure of the failed illumination tower (Lat: +18.00207, Lon: -66.63098; 2017.10.31).

Figure E-9: Photo of adjacent illumination tower with similar height and design at the same stadium shown in Figures E-4 and 5 (Lat: +18.00207, Lon: -66.63098; 2017.10.31).

Appendix F

Supplementary information, Section 7 – Other Impacts

Figure F-1: Lar: +18.21429, Lon: -65.70233; 2017.10.28; #3236.

Figure F-2: Lar: +18.21091, Lon: -65.70574; 2017.10.28; #3240.

Figure F-3: LAT18.21090, Lon: -65.70574; 2017.10.28; #3242.

Figure F-4: Interim water supply; Lat: +18.30687, Lon: -66.71299; 2017.11.02; #3755.

Figure F-5: New growth in devastated State Forest; Lat: +18.12358, Lon: - 66.079185.

Appendix G

LIDAR Data

HYBRID SFM-LIDAR MODEL OF GUAJATACA DAM SPILLWAY

Geomatic-reconnaissance of damage primarily to Guajataca Dam spillway following Hurricane Maria consisted of two principal elements: [1] Observations of damage to the spillway through the use of unmanned aerial systems (UAS) and [2] terrestrial laser scanning, also by GEER. This reconnaissance effort took advantages of these two technologies in order to [1] merge the data sets, [2] provide quality control on the Structure from Motion (SFM) data sets using Terrestrial Laser Scanning (TLS) data as the control, assign UTM coordinates to the TLS LIDAR data that were internally registered in an arbitrary project coordinate system, and [4] provide a means for coloring TLS data using the orthomosaic imagery and colored point cloud of the SFM data. Most importantly, the hybrid model used TLS data to validated the quality of the aggregated effects of calculations to align SFM target points through a projective matrix that preserves target intersection and tangency, a Euclidean scaling matrix that preserves angles and lengths, an affinity matrix that computes best-fit volume ratios and parallelism, and a similarity matrix that corrects for model skew, and proportions angles and unscaled lengths of the SFM data. Coordinates in UTM are marked on Figure G-1. Overall length of the damaged spillway is about 119m. Guajataca is located at 18.396910°, -66.925822°.

Figure G-1: The orthomosaic of the damaged spillway at Guajataca dam from a hybridized model of SFM imagery analysis and TLS LIDAR data.

SFM and TLS methodology

Computational imaging methods using unmanned-aerial-systems (UAS), Structure-from Motion (SFM) matrix methods, and LIDAR-based terrestrial laser scanning (TLS) were used to conduct mapping, and to compare remotely sensed imagery with direct physical measurements. The

GEER geomatics team collected new SFM photogrammetric data with DJI Mavic Pro drone equipped with a 20-megapixel lens. These data were collected at low elevations of less than 50 m, and high elevations of 75 m over the spillway. Flying the UAS closely over the steeply sloping embankment required operator care.

Terrestrial laser scan data was collected over the entire spillway in 6 separate scan locations. The GEER TLS system is based on a near-infrared laser transceiver manufactured by Riegl (http://www.rieglusa.com/). The system is portable and designed for the rapid acquisition of high-resolution three-dimensional imagery under outdoor conditions. The maximum distance to targets the laser can detect is 1000m for an object with 80% reflectance under the best atmospheric conditions. The minimum target distance is 2 m. The range accuracy is consistently 0.4cm. TLS systems also have the ability to collect real color object data. Lidar data was collected using the terrestrial laser scanning method. The scanner was placed on a tripod, and its GPS location was recorded. A point cloud of coordinates visible to the scanner is collected and registered with the other scans in the same area where overlapping data exists.

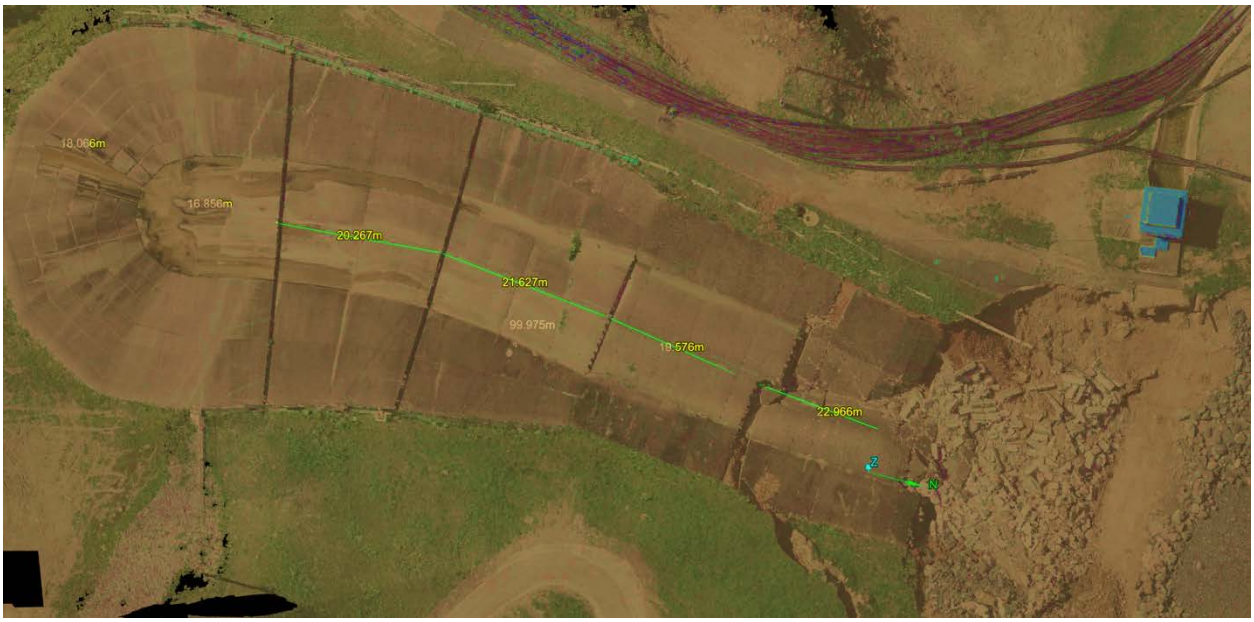

Figure G-2: Hybrid SFM-TLS model of Guajataca spillway with length measurements of individual panel segments.

Point cloud data from the UAS are processed through a computationally-intensive multi-stage process. First, a flight plan is written to overfly the spillway and collect downward looking photographs using the Mavic Pro UAS quad-copter. These images were collected with a minimum of 80% overlap and 80% side-lap coverage to ensure that there are common features in adjacent images in the central portion of the camera lens where spherical aberrations are minimal. Using cloud computing software from 'Dronedeploy,' and workstation-based software 'ContextCapture' from Bentley Software, all of the downward-looking images were aligned using hard features that were common to multiple photographs. Images were first aligned crudely, and then a sequence of higher level alignments improved the model and established a

tight relationship between adjacent images. The structure-from-motion method computes angular separations between objects visible in overlapping images. The scale and location of the objects are determined by knowing the location of each photograph from the photo metadata GPS-location. That is, the autonomous GPS-tagged photographs from the drone provided the Euclidean scaling of the model.

Aligned drone imagery was used to process a dense point cloud and a 3-D mesh triangular irregular network surface. The same aligned imagery was used to construct a precise orthomosaic of the scanned area. Once the UAS model was constructed, the point cloud from the UAS data can be merged with the point cloud from the Lidar scanner. UAS and LiDAR datasets are merged using the software ISITE-Studio (Maptek company). The advantage of merging data is that the Lidar data-set is presumably more precise regarding pixel location, whereas the UAS data have a more accurate color representation for each pixel because of the direct relationship between the point cloud and the orthomosaic image.

The six individual scans of the TLS data set were registered initially in the field using the target reflector registration technique of Riegl RiScan-Pro. Post processing involved breaking the registration links made in the field and slightly adjusting individual scans to through a global TLS point matching algorithm to find the best-fit minimum error model. Final registration of the TLS data was performed in Maptek I-Site Studio. Then these data were translated and rotated into UTM global georeferenced coordinates to best fit the SFM model.

The TLS LIDAR point cloud data are not colored, and so we took advantage of the natural color and light of the SFM imagery to assign colors to co-located points in the laser data. To colorize the terrestrial lidar data, the co-registered SFM and TLS data were brought into the software 'CLOUDCOMPARE' and color for the TLS was interpolated from the independent SFM point cloud entity.

Results

The spillway design is segmented into 5 sections. A steeply sloped apron at head of the concrete spillway is 19 m in horizontal length with a slope of 11 degrees. The spillway transitions to flatter slopes in four segments. Segment A (the highest elevation) is 17 horizontal meters in length with a slope of 2.2 degrees. The second segment B is 19 horizontal meters in length with a slope of 3.5 degrees. The third segment C is 20 horizontal meters in length with a slope of 3.0 degrees. The failed fourth segment D was approximately 22 horizontal meters in length with a slope of 10 degrees.

Damage to the spillway occurred exclusively to section D. Discussion with engineers of the site indicate that cracks in the spillway concrete facing allowed for water to seep into the underlying so well and undermine the bottom of the spillway structure. A large cavity formed beneath the last 30 meters of the spillway. From the terrestrial laser scanning data (structure from motion data could not see into the void) The depth of the void varies and approximately 2 meters deep at the greatest depth.

Undermining of the spillway structure triggered a slide of the concrete facing. The section that slid 2.4 meters down slope (2.3 horizontal, 0.75m vertical) included the entire lower 23-meter potion of section D. On Spillway right, a small slump occurred on the north eastern side of the spillway. The concrete facing failure slid downslope and impacted into a rip rap toe at the transition zone beneath the concrete spillway.

Emergency repair and maintenance work can be seen in the hybrid model. New rip rap is being placed at the base of the damaged concrete spillway to provide a Erosion protection. Hydraulic pumps in the reservoir are diverting water past the spillway into the water canal to the west, and creek that is fed at the small concrete bridge beneath the spillway. New concrete riprap can be seen at the toe of the spillway (see from Figure G-3 to Figure G-6). Bypass flexible hydraulic pipes can be seen west of the spillway, diverting water released from the reservoir.

Figure G-3: Plan view of the damaged section D of the spillway.

Figure G-4: Oblique view of the damaged section D of the spillway.

Figure G-5: Oblique view of the damaged section D of the spillway.

Figure G-6: Oblique view of the damaged section D of the spillway.

Figure G-7: Figure 7. Hybrid SFM-TLS model of the upper apron of the spillway, above section A. Reservoir waters pass over a soil bench before plunging done the apron when entering the spillway.

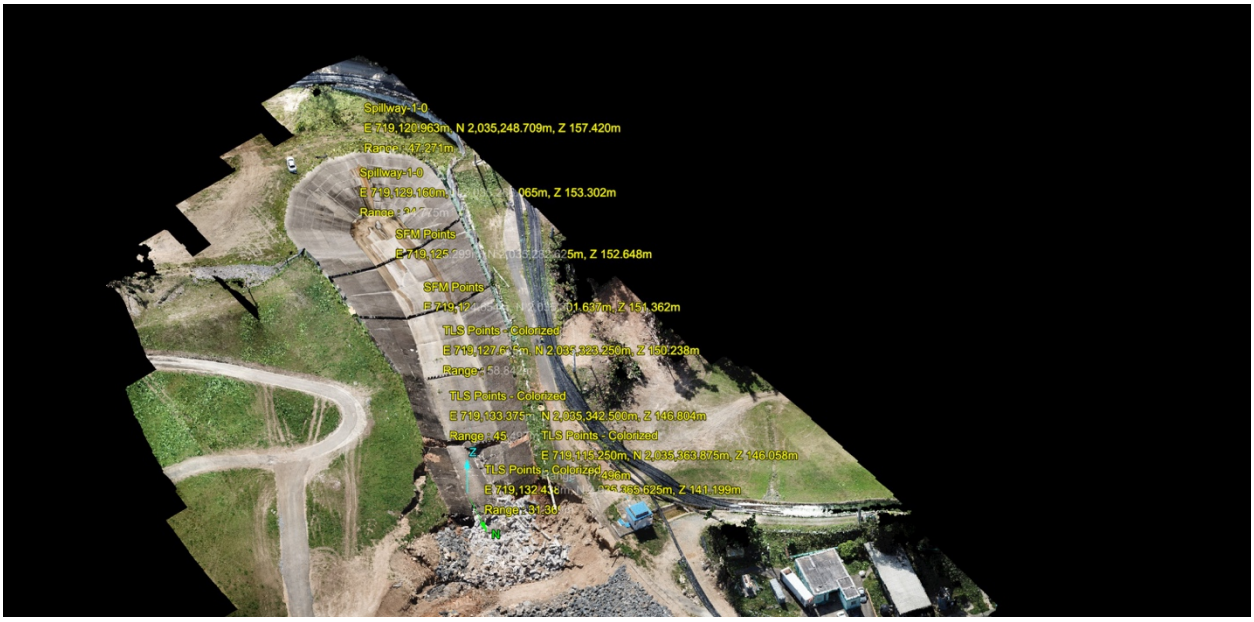

Figure G-8: Oblique hybrid SFM-TLS model of the entire concrete and riprap spillway at Guajataca dam with UTM-based coordinates used for project measurements.

LiDAR data file

The LiDAR data files will be available in the DesignSafe Data Depot (https://www.designsafe-ci.org/).

Appendix H

NOAA Graphics and Data

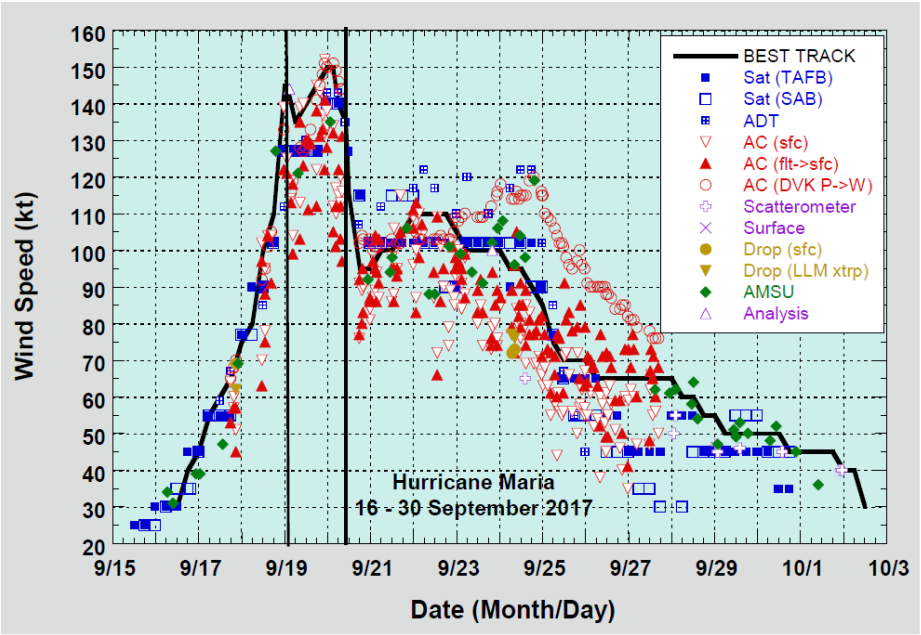

Figure 2. Selected wind observations and best track maximum sustained surface wind speed curve for Hurricane Maria, 16–30 September 2017. Aircraft observations have been adjusted for elevation using 90%, 80%, and 80% adjustment factors for observations from 700 mb, 850 mb, and 1500 ft, respectively. Dropwindsonde observations include actual 10 m winds (sfc), as well as surface estimates derived from the mean wind over the lowest 150 m of the wind sounding (LLM). Advanced Dvorak Technique estimates represent the Current Intensity at the nominal observation time. AMSU intensity estimates are from the Cooperative Institute for Meteorological Satellite Studies technique. Dashed vertical lines correspond to 0000 UTC, and solid vertical lines correspond to landfalls.

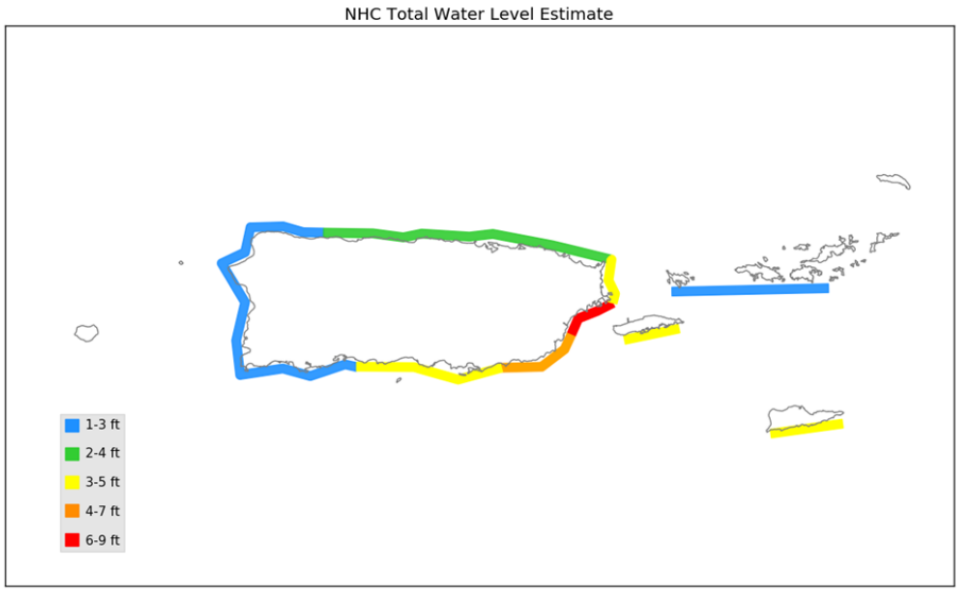

Figure 5. Estimated storm surge inundation (feet above ground level) based on an analysis of water level observations along the coasts of Puerto Rico and the U.S. Virgin Islands from Hurricane Maria. Image courtesy of the NHC Storm Surge Unit.

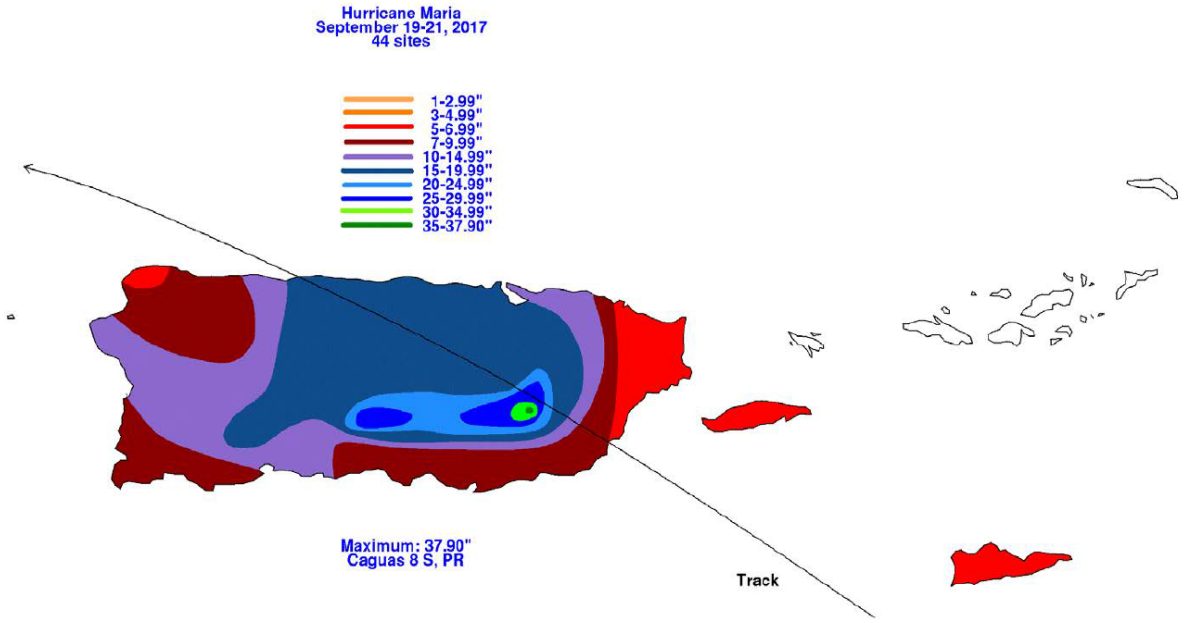

Figure 8. Storm total rainfall (inches) from Hurricane Maria. Figure courtesy of David Roth, NOAA Weather Prediction Center.

Figure 10. The remnants of the San Juan WSR-88D radar after its destruction by Hurricane Maria. Photo credit: WFO San Juan.

Appendix I

Index test results and locations of collected grab samples.

Table I-1: Summary of information of six grab samples[1]

Sample ID	Sampled Date	Atterberg Limits			Grain size distribution			USCS	Location	Coordinates	Notes
		LL (%)	PL (%)	PI	% Gravel	% Sands	% Fines (Silts + clays)				
A	11/1/17	20.7	14.6	6.1	41.9	37.1	21.0	SM-SC	PR-555 GO to MO, km. 4.2	Lat: +18.11959, Lon: -66.3662	Site 2 in Chapter 5
B	11/2/17	22.7	18.0	4.7	3.3	61.0	35.7	SM-SC	Calle San Miguel, Utuado	Lat: +18.26430, Lon: -66.69787	Appendix A, Figure A-26 & A-27
C	11/1/17	44.0	33.3	10.7	11.0	35.8	53.2	ML	PR 723, km 4.95	Lat: +18.13924, Lon: -66.32990	Appendix A Figure A-18, Appendix D Figure D-3
D	11/1/17	104.1	65.9	38.2	16.5	7.8	75.7	MH	PR 569, km 6.6	Lat: +18.17485, LON -66.3731	Appendix I, Figure I-4
E	10/31/17	47.5	25.6	21.9	29.8	20.7	49.5	SC	Stadium Paquito Montaner, Ponce	Lat: +18.00207, Lon: -66.63098	Chapter 6, Figure 6-10
F	10/30/17	59.0	24.4	34.6	60.3	14.6	25.1	GC	Guajataca dam	Lat: +18.39852, Lon: -66.92329	Chapter 3

Note: Please see following figures showing sampling location for the above grab samples.

[1] Index tests performed at the geotechnical laboratory of UPR Mayaguez

Figure I-1: Sample A; Lat: +18.11959, Lon: -66.3662; 2017.11.1.

Figure I-2: Sample B; Lat: +18.26430, Lon: -66.69787; 2017.11.2.

Figure I-3: Sample C; Lat: +18.13924, Lon: -66.32990; 2017.11.1.

Figure I-4: Sample D; Lat: +18.17485, LON -66.3731; 2017.11.1.

Figure I-5: Sample E; Lat: +18.00207, Lon: -66.63098; 2017.10.31.

Figure I-6: Sample F; Lat: +18.39740, Lon: -66.92603; 2017.10.30.

Appendix J

GEER – PR Team Resumes

Figure J-1: Team Photo, Carillo, Villalba, PR-149, Km 59.1; Lat: + 18.14923, LON -66.49350; 2017.10.31; #3476.

Figure J-2: Team Photo; Lat: + 18.08576, LON -66.50481; 2017.10.31; #3536.

Figure J-3: Team Photo, Rincón; Lat: + 18.31776833, LON - 67.245475; 2017.11.03; #3997.

Name	Last Name	Team Role	Organization	Discipline	Base
Francisco	Silva-Tulla	Leader*	Consulting Civil Engineer	Geotechnical Engineering, earth structures	MA
Miguel A.	Pando	Co-Leader*	University of NC, Charlotte	Geotechnical Engineering	NC
Tiffany	Adams	Member*	AECOM	Geotechnical Engineering	CO
Juan R.	Bernal Vera	Member	University of PR, Mayagüez	Geotechnical Engineering	PR
Luis Oscar	García	Member	GeoCim	Geotechnical Engineering	PR
Carlos	García Echevarría	Member	GeoCim	Geotechnical Engineering	PR
Stephen	Hughes	Member*	University of PR, Mayagüez	Geology of PR, UAV	PR
Gokhan	Inci	Member*	FEMA	Civil Engineer, National Dam Safety Program	DC
Robert	Kayen	Member*	USGS	Geometry determination, UAV, LIDAR	CA
Alesandra Cristina	Morales Velez	Member*	University of PR, Mayagüez	Geotechnical Engineering	PR
Youngjin	Park	Member*	University of NC, Charlotte	Geotechnical Engineering	NC
Daniel	Pradel	Member*	The Ohio State University	Geotechnical Engineering	OH
Inthuorn	Sasanakul	Member*	University of SC	Geotechnical Engineering, erosion and scour	SC
Alex	Soto	Member*	GeoCim	Geology of PR, landslides	PR

EDUCATION:

Sc.D., Civil Engineering, Massachusetts Institute of Technology, Cambridge, MA, 1977
M.S., Civil Engineering, Massachusetts Institute of Technology, Cambridge, MA, 1975
B.S. with high honors, Civil Engineering, University of Illinois, Champaign - Urbana, Illinois, 1971

CERTIFICATIONS AND TRAINING

Registered Professional Engineer, Alabama, Florida, and Puerto Rico
Certified U.S. Navy Diver (not current); Certified NAUI Diver
Public Works Management, U.S. Navy Civil Engineer Corps Officer School, 1971
OSHA 40-Hour Hazardous Waste Site Health & Safety (HAZWOPER) Training, OSHA Supervisory Training

EXPERIENCE OVERVIEW

Dr. Silva has 47 years of professional experience including 43 years as a consulting engineer, participating on engineering projects and studies in roles ranging from complete responsibility (program or project management, design, plans and specifications, budget control, construction supervision, quality control, and long-term surveillance) to specialized services (supervision of work performed by other engineering firms; guidance to groups of consultants; quality assurance; value engineering; expert witness and litigation support; soil and groundwater exploration, sampling, analysis and characterization; and environmental assessments and impact studies). He currently serves on the National Dam Safety Review Board (Dam Safety Training Workgroup) and has served as chairman of the Embankment, Dams and Slopes Technical Committee of the Geo-Institute of the American Society of Civil Engineers. For U.S. Government agencies and private corporations, Dr. Silva has performed engineering and environmental work linked to Superfund- (CERCLA-, RCRA-), Clean Water Act-, Clean Air Act-, and National Environmental Policy Act- related projects. Dr. Silva's experience includes work for the mining, construction, chemical, petrochemical, petroleum, power, transportation, manufacturing, and waste disposal industries as well as U.S. and foreign government agencies. A large part of his professional experience relates to earth structures (especially embankments, dams, levees, dikes, slopes, landfills, and excavations) and the safety of constructed facilities (including probabilistic risk assessments and dam safety). Dr. Silva also has corporate management experience at the operating group level in consulting organizations with up to US$700MM annual revenues. Dr. Silva is the author or co-author of numerous technical papers and reports on geotechnical and geo-environmental subjects. He is the author of the Soil Mechanics article in the McGraw-Hill Encyclopedia of Science and Technology and co-editor of ASCE's "Judgment and Innovation: The Heritage and Future of the Geotechnical Engineering Profession" and "Embankments, Dams, and Slopes – Lessons from the New Orleans levee failures and other current issues".

EMPLOYMENT HISTORY

GeoEngineering and Environment, Lexington, MA	Consulting Civil Engineer, Owner	2005 – Pres.
Isaiah Engineering Inc., Mobile, AL	Vice President of Engineering	2016 – Pres
ICF Consulting, Fairfax, VA and Lexington, MA[2]	Senior Vice President and Distinguished Consultant[3]	2002-2005
Arthur D. Little, Inc., Cambridge, MA	Vice President and Director	1993-2002
T. William Lambe and Associates, FL / Geotechnics, Inc., MA	Associate / President, Owner	1975-1993
Massachusetts Institute of Technology, Department of Civil Engineering, Cambridge, MA	Research Assistant	1973-1975
U.S. Navy, Inter-American Naval Training Center, Civic Action and Rural Development Department, Key West, FL	Assistant Director	1972-1973
U.S. Navy, Naval Station, Key West, FL	Activity Civil Engineer	1971-1972

[2] ICF Consulting acquired the Global Environment and Risk (Americas) division of Arthur D. Little Inc. in April 2002

[3] Appointed *ICF Distinguished Consultant* in 2003. ICF recognizes individuals who have set themselves apart as leaders in their chosen consulting discipline. Selection as a Distinguished Consultant is the highest company honor that can be bestowed upon a consultant and is recognition of the significant and sustained substantive accomplishments of the awardees. This permanent honor is limited to six individuals among 1,500 employees.

Miguel A. Pando, Ph.D., P. Eng. Resume

EDUCATION:

Ph.D., Civil Engineering, Virginia Tech, Blacksburg, VA, 2003
M.S., Civil Engineering, University of Alberta, Edmonton, Alberta, Canada, 1995
B.S., Civil Engineering (5 year program), Javeriana University, Bogota, Colombia, 1991
BSCE general science and engineering courses, National University of Asuncion, Paraguay, 1985-1988

CERTIFICATIONS

Registered Professional Civil Engineer, Ontario, Canada (P.Eng.)
Registered Engineer, Colombia

EXPERIENCE OVERVIEW

Dr. Miguel Pando is an Associate Professor at the University of North Carolina at Charlotte in Geotechnical Engineering. Previously he was a geotechnical engineering faculty (Assistant and the Associate Professor) at the University of Puerto Rico at Mayaguez, in Mayaguez, PR. Dr. Pando has more than 10 years of industry and consulting experience in geotechnical engineering in Canada, US (mainland and PR), and Colombia. He has been involved in tailings dams projects. Large transportation projects, slope stability assessment and landslide stabilization, and foundation engineering. He has performed post-disaster reconnaissance visits after major natural hazard events such as the 2005 Katrina in Louisiana, Mississippi and Alabama, 2008 ICA Earthquake in Peru, 2005 and the 2017 Hurricane Maria in Puerto Rico. He is a member of several ASCE-Geo-Institute technical committees including Embankments, Dams and Slopes, and Retaining Structures. He is also active in the ASTM and Transportation Research Board. He is an editorial board member in several journal in geotechnical engineering and has been co-editor for the 2013 ASCE Geo-Congress (with Pradel and Meehan) and served as reviewer for multiple journals and conferences. Dr. Pando is the author or co-author of more than 100 technical journal and conference papers on geotechnical engineering subjects. In addition to his research in Geotechnical Engineering on the topics of soil-structure interaction and engineering characterization of geomaterials, Dr. Pando is active in engineering education through teaching and mentoring students at both UPRM and UNCC, as the Assistant Director of Education and Outreach for the CAMMSE USDOT Transportation Center, and through recent and ongoing engineering education research projects that include the development of a Bridge to the Doctoral Program to attract Latinos to geotechnical earthquake engineering (NSF-NEES), use of a multi-institutional classroom learning environment for remote geotechnical engineering education (NSF-TUES), as well as a mixed methods study of the role of student–faculty relationships in the persistence and retention of underrepresented minority students in engineering (NSF-RIGEE). He has also organized several editions of the summer study abroad course “Engineering for Development Workers”, focused on undertaking Civil Engineering projects in rural communities in Andean Peru.

EMPLOYMENT HISTORY

Department of Civil and Environmental Engineering University of North Carolina at Charlotte, Charlotte, NC	Associate Professor	2010 – Pres.
CAMMSE Tier 1 University Transportation Center, University of North Carolina at Charlotte, Charlotte, NC	Assistant Director of Education and Outreach	2016 – Pres
Department of Civil Engineering and Survey, University of Puerto Rico, Mayagüez, PR	Associate Professor	2006 – 2010
Department of Civil Engineering and Survey, University of Puerto Rico, Mayagüez, PR	Assistant Professor	2003 – 2006
Geopier Foundation Co, Blacksburg, VA	Project Engineer (Part-time)	2000 – 2002
Thurber Engineering, Toronto, Canada	Project Engineer	1997 – 1998
AMEC Earth & Environmental, Edmonton, Canada	Assistant Project Engineer	1994 – 1997
EM Modular Structures, Bogota, Colombia	Junior Engineer	1991 – 1992

EDUCATION:
Virginia Tech, Ph.D. in Civil Engineering, 2010.
Virginia Tech, M.S. in Civil Engineering, 2006.
Oregon State University, 1995.

CERTIFICATIONS AND TRAINING
Registered Professional Civil Engineer, Colorado

EXPERIENCE OVERVIEW
Dr. Tiffany Adams is a Geotechnical Engineer at AECOM, Denver, CO where she works primarily on design of earth dams. She has over 20 years of consulting experience in geotechnical engineering. Dr. Adams has worked on large consulting projects in the US and worldwide, including large dams and multibillion transportation projects. She has also designed numerous landslide stabilizations, worked on levees, and performed numerous geotechnical investigations and designs for residential and commercial buildings. Her main areas of professional expertise are in Slope Stability, Geotechnical Earthquake Engineering, and Goetechnical Numerical Modeling. She was one of the main instructors of the 2018 ASDSO short course on Stability Analysis of Embankment Dams. She actively publishes in geotechnical journals and conferences.

EMPLOYMENT HISTORY

AECOM, Denver, CO	Geotechnical Engineer	2010– Pres.
United States Bureau of Reclamation	Student Intern	2010
PanGEO, Inc.	Project Geotechnical Engineer	2001– 2005
URS Greiner Woodward Clyde, Denver, CO	Senior Staff Engineer	1997– 2001

K. Stephen Hughes, Ph.D. Resume

POSITION:
Assistant Professor, Department of Geology, University of Puerto Rico at Mayagüez, 2014-present

EDUCATION:
Ph.D., Geology, North Carolina State University, 2014
B.S., Geology, University of North Carolina at Chapel Hill, 2009

RESEARCH FUNDING:
2015: University of Puerto Rico at Mayagüez Seed Money Grant ($5,000)
Age of the Elk Hill Volcanic Complex, central Virginia Piedmont
2017: Puerto Rico Science, Technology, and Research Trust Small Research Grant ($70,000)
Timing and Style of Fault Development in Western Puerto Rico
2017: NSF HSI Conference ($99,999)
Accelerating the Impact of HSI STEM Education and Research on Innovation Ecosystems (PI: Rodlofo Romañach; co-PIs: Alesandra Morales Vélez, Jose Lugo, Ubaldo Córdova, and K. Stephen Hughes)
2018: NSF CMMI (in review; $193,068)
Testing and Calibrating Frequency Ratio Landslide Hazard Susceptibility Mapping in the Tropics: Mass Wasting Characterization after Hurricane María in Puerto Rico

EXPERIENCE OVERVIEW
Dr. Hughes is an Assistant Professor in the Department of Geology at the University of Puerto Rico. He has active research projects in Puerto Rico and currently supervises 4 MS students and over 10 undergraduate research students. His expertise lies in geomorphology, landscape change, active tectonics, structural geology, photogrammetry, and geochronology. He has published peer-reviewed scientific articles in journals such as the American Journal of Science, Geological Society of America, and Geoscience Canada. He frequently presents active research projects at conferences inside Puerto Rico and throughout the remainder of the United States. Dr. Hughes is an expert on the geologic and geomorphic situation of Puerto Rico and has active funding from the Puerto Rico Science, Technology, and Research Trust in addition to grant proposals in review by both the National Science Foundation Civil, Mechanical, and Manufacturing Program and the Federal Emergency Management Agency Hazard Mitigation Grant Program.

EMPLOYMENT HISTORY

Department of Geology, University of Puerto Rico, Mayagüez, PR	Assistant Professor	2014 – Pres.
Marine, Earth, and Atmospheric Sciences Department, North Carolina State University, Raleigh, NC	Research Assistant	2010 – 2014
Department of Geosciences, University of North Carolina, Chapel Hill, NC	Radiogenic Isotope Laboratory Assistant	2008 – 2010
BI-LO Grocery Store Marion, NC / Chesnee, SC	Inventory Replacement Expert/Coordinator	2008 – 2010

AFFILIATIONS:
American Association of Petroleum Geologists
Geological Society of America
P.R. Louis Stokes Alliance Minority Participation
CienciaPR

UNIVERSITY POSITIONS HELD:
Department Assessment Coordinator
President, Graduate Committee
Member, Field Trip Committee
Faculty Advisor, Sociedad Geológical Estudiantil

EDUCATION:

PhD., Geotechnical and Environmental Engineering, Wayne State University, Detroit, MI, 2001
M.Eng.Sc., Geotechnical Engineering, University of New South Wales, Sydney, NSW, Australia, 1998
M.S., Geotechnical Engineering, The Ohio State University, Columbus, OH, 1997 (transferred to UNSW)
B.S. with honors, Civil Engineering, Bosphorus University, Istanbul, Turkey, 1996

CERTIFICATIONS AND TRAINING

Registered Professional Engineer, Michigan, Colorado, Nevada, Wyoming, Alaska
Professional Engineer, Alberta
Emergency Manager, 2017
Project Management Certification (PMP), 2015
24-Hour MSHA New Miner Training, 2006
Potential Failure Mode Analysis (PFMA) Facilitator, 2004

EXPERIENCE OVERVIEW

Dr. Inci has 22 years of professional experience including 17 years as a consulting engineer. He has been responsible for conceptual level planning, feasibility level design, final design, construction oversight, independent external peer review of world-class infrastructure and mining projects. Infrastructure projects included hydropower dams, lined/unlined zoned/homogeneous embankment dams, levees, waterfront structures, ponds, foundation work for buildings and industrial plants, deep excavations, tunnels, pavements, and other civil/structural projects. Mining projects included tailings and waste storage facilities for gold, silver, copper, uranium and other metals, heap leach pads, water dams, surface water diversion designs, ponds, stockpiles, roads, foundation work for processing plants and other facilities. Dr. Inci has analized, inspected or designed more than 70 water and waste retaining dams, including large international projects. Select projects include coal combustion residual groundwater monitoring systems certification and coal ash basin management projects; Los Chancas copper mine project feasibility level design for 500m high comingled tailings/waste rockfill and internal storage heap leach facility; Livengood gold mine project feasibility level design for tailings, waste rock and water storage facilities over permafrost, Kearl oil sands project west ETA detailed design and construction; New Orleans East-hurricane protection levees analysis and design; and Cerro Verde dynamic deformation, stability and seepage analysis for a 260m high tailings dam. His work experience includes most states of US and most provinces of Canada. His countries of work experience include Australia, Canada, Ghana, Honduras, India, Indonesia, Italy, Jordan, Kuwait, Mexico, Panama, Papua New Guinea, Peru, Romania, Russia, Saudi Arabia, Suriname, Taiwan, Turkey, United States, and Venezuela. Dr. Inci has contributed to literature with more than 20 technical publications. Dr. Inci has been a registered professional engineer since 2003 with licenses in Michigan, Colorado, Nevada, Wyoming, Alaska, Alberta; PMP certified since 2015; and an emergency manager since 2017.

EMPLOYMENT HISTORY

FEMA, National Dam Safety Program, Washington, DC	Civil Engineer, Research Lead, Haz. Mit. Eng. And Arch. Specialist	2017 – Pres.
HDR Inc., Denver, CO	Dams and Civil Works Project Manager	2015 – 2017
Amec Foster Wheeler Inc., Denver, CO	Senior Project Manager and Principal Geotechnical Engineer	2008-2015
URS Corporation, Denver, CO	Senior Project Engineer	2006-2008
MWH Global Inc., Chicago, IL	Geotechnical Engineer	2002-2005
SOMAT Engineering Inc., Detroit, MI	Field/Staff Engineer	2001-2002
Wayne State University, Detroit, MI	Research Assistant	1998-2001
The Ohio State University, Columbus, OH	Research Assistant	1996-1997

EDUCATION:
University of California, Berkeley, California, Ph.D. in Civil Engineering, 1993.
Dissertation Title: Accelerogram-energy approach for prediction of earthquake-induced ground liquefaction
Graduate Advisor: James K. Mitchell
University of California, Berkeley, California, M.S. in Civil Engineering, 1989.
California State University, East Bay, California, M.S. in Geology, 1988
Tufts University, Medford, Massachussetts, B.S.C.E. Double Major Civil Engineering & Geology, 1981.

CERTIFICATIONS AND TRAINING
Registered Professional Civil Engineer, California

EXPERIENCE OVERVIEW
Dr. Robert Kayen is an Adjunct Professor at The University of California Berkeley in Geosystems Civil Engineering and is a Senior Research Civil Engineer at the United States Geological Survey, Pacific Science Center, Menlo Park, CA where he has worked for nearly three decades. He also serves as an Adjunct Professor in the Department of Civil and Environmental engineering at UCLA, and previously was a Visiting Professor and Visiting Scholar at Kobe University, Japan.

Kayen has authored over 350 research publications in the fields of earthquake geotechnical engineering, TLS-LIDAR, Structure-From-Motion geomatics, engineering geophysics, marine-geotechnics, and marine methane hydrate stability. He is one of the founders and a long-time steering committee member of the National Science Foundation (NSF) sponsored Geotechnical Extreme Events Reconnaissance. Dr. Kayen has received honors that include the Middlebrooks Award from ASCE, United States Department of Justice Commendation awarded by the Environmental Division, and the NASA-Ames Honor Award. In 2017, he was an SFGI-U.C. Berkeley Distinguished Lecturer. He is the current Vice-Chairman of the Marine Engineering Geology Commission of the IAEG. He was the editor of a multi-volume U.S. Geological Survey Professional Paper Series on 'Earthquake Hazards of the Pacific Northwest Coastal and Marine Regions'.

EMPLOYMENT HISTORY

University of California, Berkeley, California	Professor of Practice	2017 – Pres.
University of California, Los Angeles, California	Professor of Practice	2008 – Pres.
United States Geological Survey, Menlo Park, CA	Research Civil Engineer	1983 – Pres.

POSITION:
Assistant Professor, Department of Civil Engineering and Survey, University of Puerto Rico at Mayagüez, 2015-present

EDUCATION:
Ph.D., Civil and Environmental Engineering, University of Rhode Island, 2015
M.S.C.E., Civil Engineering and Survey, University of Puerto Rico at Mayaguez, 2010
B.S.C.E., Civil Engineering and Survey, University of Puerto Rico at Mayaguez, 2007

RESEARCH FUNDING:
2015: University of Puerto Rico at Mayagüez Seed Money Grant ($10,000)
Cyclic Resistance of Calcareous Sands
2017: NSF HSI Conference ($99,999)
Accelerating the Impact of HSI STEM Education and Research on Innovation Ecosystems (PI: Rodlofo Romañach; co-PIs: Alesandra C. Morales Vélez, José Lugo, Ubaldo Córdova, and K. Stephen Hughes)
2018: NSF CMMI (in review; $193,068)
Testing and Calibrating Frequency Ratio Landslide Hazard Susceptibility Mapping in the Tropics: Mass Wasting Characterization after Hurricane María in Puerto Rico

EXPERIENCE OVERVIEW
Dr. Alesandra C. Morales-Velez obtained a PhD in Civil and Environmental Engineering (2015) from the University of Rhode Island and a Master of Science (2010) and Bachelor of Science in Civil Engineering (2007) from the University of Puerto Rico at Mayaguez (UPRM). She joined the University of Puerto Rico at Mayaguez in March 2015 as the new faculty member of the Geotechnical Engineering Group at the Department of Civil Engineering and Survey. Her main research interests are liquefaction of unique soils such as calcareous sands and non-plastic dilatant silts, short-and-long-term durability properties of crushed limestone aggregate and linking laboratory and field behavior of soils using shear wave velocity. Dr. Morales-Vélez is the Civil Engineering Geotechnical Engineering Undergraduate and Graduate Laboratories Coordinator and HEDGE's Co- PI. She is currently working with students and industry partners in the design and implementation of low impact green infrastructure that could potentially help minimize and prevent flooding in Puerto Rico. She currently supervises one PhD student and is the co-advisor of one Master of Science student. She is very active in the Geotechnical Engineering community; she participates in GEER reconnaissance teams, international conference and is an active speaker in different organizations in PR. Dra. Morales-Vélez has active funding with the National Science Foundation and has a grant proposal in review by the National Science Foundation Civil, Mechanical, and Manufacturing Program and the Federal Emergency Management Agency Hazard Mitigation Grant Program.

EMPLOYMENT HISTORY

Department of Civil Engineering and Survey, University of Puerto Rico, Mayagüez, PR	Assistant Professor	2015 – Pres.
Department of Civil/Ocean Engineering, University of Rhode Island, Kingston, RI	Research Assistant/Instructor	2010 – 2014
Department of Civil Engineering and Survey, University of Puerto Rico, Mayagüez, PR	Instructor	2007 – 2009

AFFILIATIONS:
GEER
Colegio de Ingenieros y Agrimensores de PR
Geotechnical Engineering Women Faculty Group

UNIVERSITY POSITIONS HELD:
Associate Director of Graduate Studies
Geotechnical Engineering Laboratories Coordinator

EDUCATION:
Ph.D., Civil Engineering, Virginia Polytechnic Institute and State University, Blacksburg, VA, 2003
M.S.C.E., Civil Engineering, Pusan National University, Busan, South Korea, 1997
B.S., Civil Engineering, Pusan National University, Busan, South Korea, 1991

AFFILIATION
American Society of Civil Engineer (ASCE), Member
Geotechnical Extreme Events Reconnaissance (GEER), Regular Member
American Institute of Steel Construction (AISC), Member
University of North Carolina at Charlotte, Graduate Faculty

EXPERIENCE OVERVIEW
Dr. Park's expertise is geotechnical engineering with emphasis on laboratory and field experimentation, sensors and instrumentation for short- and long-term monitoring. As the research manager of the Energy Production and Infrastructure Center (EPIC) at the University of North Carolina at Charlotte, Dr. Park is responsible for managing a 5,000 square feet research facility with about two-million-dollars of structural and geotechnical equipment. Since 2011, he has managed and supervised several energy-industry-related research projects and soil-structure interaction projects. As part of his duties, he also coordinates and manage safety, security plans, training of students, faculties, staffs, and researchers in the EPIC Highbay. As a faculty associate of the Civil and Environmental Engineering department in the UNC Charlotte, he participates in graduate committees of students that have an experimental component as part of their research and provides support in the design phase of the experiments and geotechnical testing advice. Also related to laboratory experimentation, he had 6 years of experience working at Geocomp Corp. At this company, he worked in the R&D department helping with the design of new geotechnical laboratory devices and providing training for the use of geotechnical equipment while traveling around the world.

EMPLOYMENT HISTORY

University of North Carolina at Charlotte, Charlotte, NC	EPIC HighBay Manager	2011-Pres.
Geocomp Corp., Acton, MA	Project Geotechnical Engineer and R&D Geotechnical Testing Device	2005-2011
Virginia Polytechnic Institute and State University, Blacksburg, VA	Post-Doctoral Researcher	2003-2005
Virginia Polytechnic Institute and State University, Blacksburg, VA	Ph.D. Student and Graduate Research Assistant	1997-2003
Pusan National University, Busan, South Korea	Graduate Research Assistant	1995-1997
Republic of Korea Army	Combat Engineer	1991-1993

EDUCATION:

Certificate of Postdoctoral Studies in Geotechnical Engineering, University of California, Los Angeles, CA, 1989
Doctor of Engineering in Civil Engineering, University of Tokyo, Japan, 1987
Diploma of Civil Engineer, Swiss Institute of Technology in Lausanne, Switzerland, 1982

CERTIFICATIONS AND TRAINING

Registered Professional Civil Engineer, California, Nevada, Utah, Hawaii
Registered Professional Geotechnical Engineer, California
Registered Engineer, Switzerland
Post-Disaster Safety Assessment Program Evaluator, State of California Governor's Office of Emergency Services

EXPERIENCE OVERVIEW

Dr. Daniel Pradel is Professor of Practice at The Ohio State University in Geotechnical Engineering. Previously he was Vice-President of Shannon & Wilson in Glendale, California, and an Adjunct Associate Professor in the Department of Civil & Environmental Engineering at UCLA, where he was teaching since 1988. Before joining OSU, Dr. Pradel was in industry for about 30 years and worked on projects located in four continents, including large dams (El Cajon in Honduras, Paute Mazar in Ecuador, Yuracmayo in Peru, Emosson in Switzerland) and multibillion transportation projects (Silicon Valley Rapid Transit, Los Angeles Metro). He has also designed numerous landslide stabilizations, worked on levees for the US Army Corps of Engineers, and performed numerous geotechnical investigations and designs for residential and commercial buildings. His main areas of professional expertise are in Slope Stability, Geotechnical Earthquake Engineering and Geomechanical Numerical Modeling. He has performed numerous reconnaissance visits after major natural hazard events such as Earthquakes (e.g., 2015 Gorkha Earthquake in Nepal, 2011 Tohoku Earthquake and Tsunami in Japan), Landslides (e.g., 2005 La Conchita in California, 2014 Oso in Washington) and Hurricanes (2017 Puerto Rico).

He is a Fellow of the American Society of Civil Engineers, and a Diplomate of the Academy of Geo-Professionals. He is a member of several ASCE-GeoIntitute committees, including Embankments, Dams and Slopes, Computational Methods, Awards, and the AGP Examination committees. In the Deep Foundation Institute, he is a member of the Slope Stabilization and Foundation Testing committees. He is a member of the ASCE Committee on Accreditation Operations, and a Commisioner of ABET. Since 2007, he serves on the board of the ASCE Journal of Geotechnical Engineering and Geo-Environmental Engineering where he is currently Associate Editor.

Dr. Pradel is the author or co-author of more than 50 technical papers on geotechnical subjects. His manuscripts have appeared in journals, such as, Soils & Foundations and the ASCE Journal of Geotechnical Engineering and Geo-Environmental Engineering, and in conferences such as the ASCE Geo-Congress, DFI Specialty Conferences, and the International Conference of Soil Mechanics and Foundation Engineering.

EMPLOYMENT HISTORY

The Ohio State University, Columbus, OH	Professor of Practice	2016 – Pres.
Shannon & Wilson, Glendale, CA	Vice President	2015 – Pres
University of California, Los Angeles, CA	Adjunct Associate Professor	1997-2016
Group Delta Consultants, Torrance, CA	Principal Engineer	2011-2015
Praad Geotechnical, Los Angeles, CA	Chief Engineer and Owner	1997-2011
University of California, Los Angeles, CA	Lecturer	1988-1997
Lockwood-Singh, Los Angeles, CA	Senior to Chief Engineer	1988-1997
Motor Columbus, Baden, Switzerland	Civil Engineer (dams)	1982-1984

EDUCATION:
Ph.D., Civil Engineering, Utah State University, Logan, UT, 2005
M.E., Civil Engineering, Asian Institute of Technology, Bangkok, Thailand, 2000
B.S., Civil Engineering, Thammasat University, Bangkok, Thailand, 1998

CERTIFICATIONS AND TRAINING
Registered Professional Engineer, New York

EXPERIENCE OVERVIEW
Dr. Inthuorn Sasanakul is an assistant professor of the Civil and Environmental Engineering Department at the University of South Carolina. She was formerly a research assistant professor and technical manager of the National Science Foundation (NSF) Network for Earthquake Engineering Simulation (NEES) Facility at Rensselaer Polytechnic Institute. She currently serves on the United States Society of Dam (USSD) Embankment Dams and Foundation committee, ASCE Geo-Institute Earthquake Engineering and Soil Dynamics, and Erosion committee; and Transportation Research Board AF20, Geotechnical Modeling and Instrumentation committee. Dr. Sasanakul has expertise in geotechnical centrifuge modeling, specializing in soil dynamics, soil characterization, instrumentations, and behavior of soils and soil-structure systems that are subjected to natural hazards. Dr. Sasanakul's research includes work on advance soil testing using resonant column and torsional shear devices, triaxial testing on unsaturated soils, and centrifuge modeling studies of mine tailings, internal erosion, contaminant transport, New Orleans levees and T-walls system. Dr. Sasanakul was a recipient of "ASTM Hogentogler Award of 2012" presented to the author(s) of an ASTM paper of outstanding merit on soil and rock. She also received the "Commander's Award of Public Service" with accompanying medal from the Chief of U.S. Army Corps of Engineers in appreciation for the support of New Orleans Recovery after Hurricane Katrina.

EMPLOYMENT HISTORY

University of South Carolina	Assistant Professor	2014 – Pres.
Rensselaer Polytechnic Institute/Center for Earthquake Engineering Simulation	Research Assistant Professor Technical Manager	2005-2014
Utah State University, Department of Civil and Environmental Engineering	Research Assistant	2000-2005
University of Texas at Austin, Department of Civil, Architectural and Environmental Engineering	Research Assistant	2002
Asian Center of Soil Improvement and Geosynthetics	Project Assistant	1998-2000

Alejandro E. Soto, MS, PG — Resume

EDUCATION:
BS, Geology, University of Puerto Rico-Mayagüez, 1973
MS, Engineering Geology-Stanford University, 1975

CERTIFICATIONS AND TRAINING
Registered Professional Geologist, Puerto Rico; Lic. # GP-002
OSHA 40-Hour Hazardous Waste Site Health & Safety (HAZWOPER) Training

EXPERIENCE OVERVIEW
Alex has close to 40 years of professional experience working with and promoting the study of Puerto Rico geology, beginning with a summer job between college and graduate school when he worked as a PRDNER field assistant to Dick Krushensky who was then mapping the geology of the Yauco 7.5' Quadrangle for the USGS. His involvement resumed in 1979 when he joined the then fledgling Geology Department of UPRM as an Instructor. He would leave academia 13 years later a tenured Assistant Professor proud of having contributed to the education of a generation of UPRM geologists and civil engineers, and to the development of what is today a top-notch geology program. Leaving Mayagüez was not easy, as he loved the Department, working long hours to meet his academic commitments, while at the same time providing consulting services in geology and hydrogeology to clients that included geotechnical consulting firms, state and municipal government entities, design and architect firms, private industries including several pharmaceutical companies, and a variety of parties involved in litigation. When the "offer you can't refuse" came he joined the San Juan office of what was then one of the nation's leading groundwater consulting firms. Three years later he moved to Geo Cim, at the time and continuing until today, one of the island's leading geotechnical-geologic consulting firms, where as Chief Geologist and Associate he specializes in site characterization with geotechnical and/or environmental goals, and in the identification and analysis of geologic hazards, with extensive experience with landsliding and sinkhole collapse. He continued to promote the use of geology after academia, becoming active with, and on several occasions leading the Puerto Rico Geological Society. He also presided the Puerto Rico Board of Geology Examiners for 6 years following its inception in 1996, and has participated in numerous other activities promoting geology and its application including providing testimony to the Puerto Rico legislature and participating in a variety of professional gatherings, most recently serving on the Organizing Committee for the 2013 meeting of the Southeast Section of the Geological Society of America held in San Juan.

EMPLOYMENT HISTORY

Geo Cim, Inc., Geotechnical Testing Services	Engineering Geology Consultant, Associate	1995 – Pres
Geraghty and Miller, Inc., San Juan, Puerto Rico	Principal Scientist and Project Manager	1992-1995
Department of Geology, University of Puerto Rico-Mayagüez	Assistant Professor	1983-1992
	Instructor	1979-1983
Geo-Caribe, Inc., Earth-Ocean Services; Mayagüez, Puerto Rico	President and Senior Geologist	1989-1992
Private Earth Science Consultant, Mayagüez, Puerto Rico	Engineering and Environmental Geology Consultant	1979-1989